Development and evaluation of thermal imaging techniques for non-contact respiration monitoring.

AL-KHALIDI, Farah Qais.

REFERENCE

r^-> Sheffield
* Hallam University
SHARPENS YOUR THINKING

Development and Evaluation of Thermal Imaging Techniques for Non-Contact Respiration Monitoring

Farah Qais AL-khalidi

A thesis submitted in partial fulfilment of the requirements of Sheffield Hallam University
for the degree of Doctor of Philosophy

^ 5 R S

^ RESEARCH **INSTITUTE** ^

Materials & Engineering Research Institute

November 2011

DECLARATION

This is to certify that I am responsible for the work submitted in the thesis, and that neither the thesis nor the original work contained therein has been submitted to this or any institution for a higher degree.

Signed..

Date.....*I. l.rr. /J. 7.*

Allah will exalt in degree those of you who believe and those who have been granted knowledge. And Allah is well-acquainted with what you do"

Holy Quran

Sura AL–Mujadila , number 58,part 28 Verse 11

List of abbreviations:

BR_t	Respiration rate using thermal methods
BR_c	Respiration rate using contact methods
CCD	Charge-Coupled Device
CO_2	Carbon dioxide
CP	Control points
dB	Decibel
DER	ECG-Derived respiration
DFT	Discrete Fourier transform
ECG	Electrocardiogram
FFT	Fast Fourier transform
FG	Fibre grating
FIR	Far wave infrared
FLIR	Forward of view
FOV	Field of view
FPA	Focal plan array
FPN	Fixed pattern noise
GTRI	Georgia tech research institute
H2O	Water
HPFs	High-pass filters
Hz	Hertz
IP	Impedance pneumography
IR	Infrared
LPFs	Low-pass filters
LWIR	Long wave infrared
Min	Minute
MWIR	Middle wave infrared
NIR	Near infrared
NUC	Non-uniformity correction
O3	Ozone
PPG	Photoplethysmogram
R	Radius
RGB	(red, green, blue)
ROI	Region of interest
RVSM	Radar vital signs monitor
Sec	Seconds
SpO_2	Saturation of Oxygen in the Blood
SWIR	Short wave infrared
T	Temperature
ε	Emissivity
λ	Wavelength
μm	Micrometers

Abstract

Respiration rate is one of the main indicators of an individual's health and therefore it requires accurate quantification. Its value can be used to predict life threatening conditions such as the child death syndrome and heart attacks. The current respiration rate monitoring methods are contact based, i.e. a sensing device needs to be attached to the person's body. Physically constraining infants and young children by a sensing device can be stressful to the individuals which in turn affects their respiration rate. Therefore, measuring respiration rate in a non-contact manner (i.e. without attaching the sensing device to the subject) has distinct benefits. Currently there is not any non-contact respiration rate monitoring available for use in medical field.

The aim of this study was to investigate thermal imaging as a means for non-contact respiration rate monitoring. Thermal imaging is safe and easy to deploy. Twenty children were enrolled for the study at Sheffield Children Hospital; the children were from 6 month to 17 years old. They slept comfortably in a bed during the recordings. A high resolution high sensitivity (0.08 degree Kelvin) thermal camera (Flir A40) was used for the recordings. The image capture rate was 50 frames per second and its recording duration per subject was two minutes (i.e. 6000 image frames)

A median digital lowpass filter was used to remove unwanted frequency spectrum of the images. An important issue was to localize and track the area centered on the tip of the nose (i.e. respiration region of interest, ROI). A number of approaches were developed for this purpose. The most effective approach was to identify use the warmest facial point (i.e. the point where the bridge of the nose meets the corner of one of the eyes). A novel method to analyse the selected ROI was devised. This involved segmenting the ROI into eight equal segments centred on the tip of nose. A respiration signal was produced for each segment across the 6000 recorded images from each subject. The study demonstrated that the process of dividing the ROI into eight segments improves determination of respiration rate. The respiration signals were processed both in the time and frequency domains to determine respiration rates for the 20 subjects included in the study. The respiration values obtained from the two domains were close. During each recording respiration rate was monitored using conventional contact methods (e.g. nostril thermistor, abdomen and chest movement sensor etc). There was a close correlation (correlation value 0.99) between respiration values obtained by thermal imaging and those obtained using conventional contact method.

The novel aspects of the study relate to the development of techniques that facilitated thermal imaging as an effective non-contact respiration rate monitoring in both normal and patient subject groups.

Acknowledgements

First of all, praise be to God for helping me to start and continue this research to its completion. Many thanks for my Government for providing me with financial support.

I would like to thank Dr. Reza Saatchi, my director of studies, for his support, encouragement, continuous guidance and friendship throughout the study.

I would like to thanks Dr. Derek Burke (Medical Director, Sheffield Children Hospital) and Dr Heather Elphick (Respiratory Consultant) for their immense support and continuous input to the work.

Particular thanks to Dr. Ruth Kingshott for organising the subject recordings. I am very grateful to the children who took part in the study and their parents for providing their consent

My deepest gratitude goes to my mother Muna Al- Naimee and my husband Tareq Abdullal AL-Khaykanee for their support during my study and specially for doing this project.
My deepest gratitude goes also to my sisters; brother and my children for care, support and encouragement through my education.

Finally, I would like to express my gratitude to the Iraqi staff in Sheffield Hallam University for their encouragement and their help.
Thanks to my close friends, Bashar, Selvan, and all who helped me throughout the years of my PhD studies.

Farah Qais Al-khalidi

Sheffield Hallam University-UK

Table of Contents

Abstract..... I

Acknowledgement II

Table of Contents..... III

List of Figures..... VIII

List of tables..... XIII

Author's Publications..... XIV

Chapter One

1. Introduction 1

1.1 Aim and Objectives..... 2

1.2 The Purpose of the Research..... 3

1.3 Problem Description..... 4

1.4 Contributions of this Study..... 4

1.5 Thesis outline 5

Chapter Two

2. Literature Review..... 6

2.1 Introduction 6

2.2 Analysis and Monitoring of Respiration Rate..... 7

2.2.1. Analysis Respiratory rate of Children..... 9

2.2.2 Contact Respiratory Monitoring Methods (Conventional Methods)..... 11

2.2.2.1. Acoustic Based Methods 13

2.2.2.2. Airflow Based Methods 14

2.2.2.3. Transcutaneous CO2 monitoring..... 15

2.2.2.4. Chest and Abdominal Movement Detection..... 15

2.2.2.5. Oximetry probe (SpO2) Based 16

2.2.2.6 Electrocardiogram (ECG) Derived Respiration Rate 17

2.2.2.7. Actimeter 18

2.2.2.8. Bio-shirts 18

2.2.3. Non-Contact Respiratory Monitoring Methods..... 19
2.3 Thermal imaging 29
2.4 Face Detection and Feature Extraction 33
2.5 Image processing techniques..... 37

Chapter Three

3. A Review of Image and Signal Processing Techniques Used in This Study..... 41
3.1 Introduction 41
3.2 Types of Imaging Systems..... 42
3.3 Image Data Types..... 44
3.3.1 Binary Images 44
3.3.2 Gray-scale Images..... 44
3.3.3 Colour Images..... 44
3.4 The Basic Concepts of the Image..... 44
3.5 Image Processing Techniques..... 45
3.5.1 Image Enhancement Techniques 45
3.5.1.1 The Smoothing Spatial Filters..... 46
3.5.1.1.1 The Average Filter..... 46
3.5.1.1.2 The Gaussian filter..... 47
3.5.1.1.3 Order-Statistic Filters..... 47
3.5.1.2 The Sharpening Spatial Filters..... 48
3.5.1.2.1 The Laplacian Filter..... 49
3.5.1.2.2 The Prewitt Filter..... 50
3.5.1.2.3 The Sobel Filter..... 51
3.5.2 Histogram 51
3.5.3 Segmentation Techniques..... 52
3.5.3.1 Manual Segmentation Technique 53
3.5.3.2 Automatic Segmentation Techniques..... 53
3.5.3.2.1 Edge Image Generation Techniques..... 53
- Prewitt Operators..... 54
- Sobel Operators..... 55
- Laplacian Operators..... 55

3.5.3.2.2 Thresholding Techniques..... 56
3.5.4 Subtraction Technique 57
3.5.5 Features Extraction Techniques..... 58
3.5.5.1 Visual Features..... 58
3.5.5.2 Statistical Features..... 58
3.5.5.3 Facial Physiological Features..... 59
3.5.6 Geometric Transformations Techniques..... 59
3.5.6.1 Affine transformations..... 60
3.5.6.2 Projective transformation..... 60
3.5.7. Registration (Alignment) Techniques 62
3.6 Biomedical Signal Analysis techniques..... 64
3.6.1 Signal Enhancement 64
3.6.2 Frequency-Time Analysis..... 66
3.6.2.1 Discrete Fourier Transform (DFT) 66
3.6.2.2 Fast Fourier Transform (FFT) 66
3.7 Conclusion 67

Chapter Four

4. Relevant Thermal Imaging Theory..... 68
4.1 Introduction 68
4.2 Basic Concepts 68
4.2.1 Sensitivity and Resolution 72
4.2.2 Thermo-graphic Measurement Techniques..... 73
4.2.2.1 Emissivity..... 73
4.2.2.2 Atmospheric Transmission..... 74
4.2.2.3 The Reflected Apparent Temperature..... 76
4.2.2.4 Distance 76
4.3 Thermal Images..... 76
4.4 Noise of Thermal Images 77
4.5 Thermal Applications 79

4.5.1 Medical Applications of Thermography 79
4.5.2 Temperature measurement Units 82
4.6 The advantage of Non-contact Thermal Measurements..... 82
4.7 Thermal cameras 83
4.7.1 Infrared (IR) Detectors 85
4.8 ThermaCAM™ Researcher Software..... 86
4.9 Conclusion 88

Chapter Five

5. Methodologies, Developments and Preliminary Results..... 89
5.1 Introduction 89
5.2 Thermal Image Recording System..... 89
5.2.1 Hardware Description 90
5.2.2 Software Description 91
5.2.2.1 Converting the recorded thermal videos into separate images..... 92
5.2.2.2 Filtering the thermal image..... 92
5.2.2.3 Segmenting the Region of Interest (ROI) from the rest of image. 99
5.2.2.4 Applying Feature Extraction to Extract the Respiration Signal..... 101
5.2.2.5 Processing the respiration signal to extract the respiration rate..... 111
5.3 Discussion of findings 120
5.4 Conclusion..... 122

Chapter Six

6. Techniques to Segment the Region of Interest (ROI)..... 123
6.1 Introduction 123
6.2 Segmenting the ROI..... 123
6.2.1 Manual Segmentation of the ROI 123
6.2.2 Automatic Segmentation of the ROI..... 126
6.2.2.1 First ROI Tracking Method 128

6.2.2.2 Second ROI Tracking Method 130
6.2.2.3 Third ROI Tracking Method..... 136
6.3 Results and Discussion..... 142
6.3.1 Analysis of the effect of the shape of the ROI 145
6.3.2 The Size of the ROI 147
6.4 Conclusion..... 149

Chapter Seven

7. Thermal Imaging Based Respiration Rate Monitoring in Children..... 150
7.1 Introduction..... 150
7.2 Description of Existing Contact Based Respiration Monitoring Systems..... 150
7.3 Patients' Details and Recording Procedure 152
7.3.1 Results and Discussion..... 154
7.3.1.1 Nasal Breathing 154
7.3.1.2 Respiration Monitoring in Subjects Breathing Through the Mouth..... 163
7.3.1.3 Detecting Respiration-Related Illnesses..... 166
7.3.2 Discussion of Respiration Rate Monitoring Issues..... 172
7.4 Conclusions..... 175

Chapter Eight

8. Conclusions and Future Work..... 176
8.1 Introduction..... 176
8.2 Conclusions..... 176
8.3 Scope of Future Work 179

References

References 181

List of Figures

Fig.2.1	Schematic representation of the respiratory system	7
Fig.2.2	The temperature distributions for the expiration, post-expiratory pause, and inspiration.....	8
Fig.2.3	Left: bio-shirt inner layer. Right: outer layer.....	19
Fig.2.4	Arrangement of the sensing system.....	22
Fig.2.5	The hardware design of the Ruiz approach.....	26
Fig.2.6	Ultrasound sensor output during manikin's breathing.....	27
Fig 2.7	Infrared sensor output during manikin's breathing.....	27
Fig.2.8	Schematic plot of respiration rate obtained using a webcam.....	28
Fig.2.9	Plot respiration signal using a webcam	29
Fig.2.10	Respiratory airflow profiles with the ROI.....	32
Fig.3.1	Medical spectra. (A) The electromagnetic spectrum includes the parts of Infrared spectrum. (B) Examples of medical images covering the electromagnetic spectrum.....	43
Fig.3.2	Image as a matrix of size $M \times N$ which is defined by function $f(x,y)$.....	45
Fig.3.3	Average filter with the mask 3×3	46
Fig.3.4	Gaussian filter with the mask 3×3	47
Fig.3.5	An example of the basic operation in median filtering.....	48
Fig.3.6	Two kinds of 3×3 Laplacian operator masks; it is valid to use the opposite sign convention.....	49
Fig.3.7	Two kinds of 3×3 Laplacian enhancement smoothing masks, it is valid to use the opposite sign convention.....	50
Fig.3.8	The masks of Prewitt operator in both horizontal and vertical directions.....	50
Fig.3.9	The masks of Sobel operator in both horizontal and vertical directions.....	51
Fig.3.10	(a) A thermal image, (b) Its histogram.....	52
Fig.3.11	A 3×3 area of an image.....	54
Fig.3.12	The affine transformation. The solid line represents the three input points in the image while the dashed line defines the three output points in the same image M and N are indicated in this figure as the row and column of the image.....	60
Fig.3.13	The projective transformations. The solid line represented the input quadrilateral while the dashed line defines the desired output quadrilateral.....	61
Fig.3.14	The Butterworth filter of order 5 and cutoff =1.5	65
Fig.4.1	Total radiation of incident radiation by a surface.....	70
Fig.4.2	Distribution of Radiated Energy from blackbody at various temperatures.....	71
Fig.4.3	The diagram of emitters of infrared energy for an object.....	74
Fig.4.4	Transmission spectrum of the atmosphere.....	75
Fig.4.5	The Reflected Apparent Temperature with Emission.....	76
Fig.4.6	Probability distribution histogram of Gaussian distributed noise.....	78
Fig.4.7	Diseases diagnosed by thermal imaging.....	80
Fig.4.8	FLIR camera A40 M with its accessories.....	84
Fig.4.9	A thermal image with ThermoVision in FLIR camera.....	87

Fig.5.1	System hardware description.....	91
Fig.5.2	The original noisy thermal image with its corresponding histogram.	92
Fig.5.3	Thermal image filtered using an Average filter and its corresponding histogram.....	93
Fig.5.4	Thermal image filtered using a Median filter and its corresponding histogram.....	93
Fig.5.5	Thermal image filtered using a Gaussian filter and its corresponding histogram.....	94
Fig.5.6	Thermal image processed using the Sobel filter and its corresponding histogram.....	94
Fig.5.7	Thermal image processed using the Prewitt filter and its corresponding histogram.....	95
Fig.5.8	Thermal image processed using the Laplacian filter and its corresponding histogram.....	95
Fig.5.9	The original thermal image and its corresponding histogram.....	96
Fig.5.10	The noisy thermal image and its corresponding histogram.....	96
Fig.5.11	Thermal image processed using the Average filter and its corresponding histogram.....	97
Fig.5.12	Thermal image processed using the Median filter and its corresponding histogram.....	97
Fig.5.13	Thermal image processed using the Gaussian filter and its corresponding histogram.....	98
Fig.5.14	Thermal image processed using the Sobel filter and its corresponding histogram.....	98
Fig.5.15	Thermal image processed using the Prewitt filter and its corresponding histogram.....	99
Fig.5.16	Thermal image processed using the Laplacian filter and its corresponding histogram	99
Fig.5.17	Snapshots of respiration. (a) Inspiration phases, (b) Expiration phases.....	100
Fig.5.18	(a) Respiratory signal for an adult without head movements obtained by averaging the temperature corresponding to the four highest frequencies for the ROI (b) Its filtered version.....	102
Fig.5.19	(a) Respiratory signal for an adult with large head movements obtained by averaging the temperature corresponding to the four highest frequencies for the ROI (b) Its filtered version.....	102
Fig.5.20	(a) Respiratory signal for an adult without head movements obtained by subtracting the upper and lower parts of the ROI. (b) Its filtered version.....	103
Fig.5.21	a(a) Respiratory signal for an adult with large head movements obtained by subtracting the upper and lower parts of the ROI. (b) Its filtered version.....	104
Fig.5.22	(a)Respiratory signal for an adult without head movements obtained by averaging the lower part of the ROI. (b) Its filtered version.....	104
Fig.5.23	(a)Respiratory signal for an adult with head movements obtained by averaging the lower part of the ROI. (b) Its filtered version.....	105
Fig.5.24	The ROI. (a) During the left head movements, (b) the face in front of the camera.....	106
Fig.5.25	(a)Respiratory signal for an adult with two types of head movements obtained by averaging the ROI. (b) Its filtered version.....	106

Fig.5.26	The ROI: partitioned into eight segments. (a) The position of ROI on the tip of the nose, (b) the eight segments of ROI.....	107
Fig.5.27	Respiration signals obtained using thermal imaging. The signals obtained from segments 1 to 8 are shown from top to bottom respectively.....	108
Fig.5.28	Respiration signal obtained by averaging pixel values from the complete ROI.....	108
Fig.5.29	The temperature histograms of the ROI segments 1 to 8.....	109
Fig.5.30	Respiration signals obtained using thermal imaging. The signals obtained from segments 1 to 8 are shown from top to bottom respectively.....	110
Fig.5.31	Respiration signal obtained by averaging pixel values from the complete ROI.....	110
Fig.5.32	The temperature histograms of the ROI segments 1 to 8.....	111
Fig.5.33	The different patterns of the expiration operation in the same recording	112
Fig.5.34	The different patterns of the inspiration operation in the same recording	113
Fig.5.35	The magnitude frequency spectrum of the respiratory for the clearest respiration signal in the ROI	114
Fig.5.36	The magnitude frequency spectrum of the respiratory for the clearest respiration signal in the ROI for the video with large head movements..	114
Fig.5.37	Windowing method of determining respiration rate.....	115
Fig.5.38	Respiration rate monitored over time in a case with no head movement.	116
Fig.5.39	Respiration rate monitored over time in a case with large head movements.....	116
Fig.5.40	Error produced as a result of rounding the fraction of cycle to full cycle	117
Fig.5.41	Respiration rate obtained by considering five complete respiration cycles.....	117
Fig.5.42	Average respiration rate plotted against time.....	118
Fig.5.43	Average respiration rate for a case with large head movements.....	118
Fig.5.44	The respiration signal. (a)The fluctuations immediately after the signal level changes are consistent in pattern in different respiration cycles. (b) Its filtered signal indicating the respiration (T).....	119
Fig.5.45	Respiration signal from segments 1 to 8 (from top to bottom respectively.....	121
Fig.5.46	Respiration signals. (a) Respiration signals in segments 2 and 7. (b) Respiration signals in segments 3 and 6 respectively.....	121
Fig.6.1	Alignment of two images (a) The reference image, (b) The image to be aligned with the reference image, (c) The aligned image (correlation value =0.61).....	124
Fig.6.2	Alignment of two images (a) The reference image, (b) The image to be aligned with the reference image (c) The aligned image (correlation =0.79).....	125
Fig.6.3	Alignment of two images (a) The reference image, (b) The image to be aligned with the reference image (c) The aligned image (correlation=0.72)	125
Fig.6.4	Alignment of two images (a) The reference image, (b) The image to be aligned with the reference image (c) The aligned image(correlation =0.82).....	126

Fig.6.5	Identifying the subject's boundary from the image background ; (a) Result produced when applying the Prewitt operator; (B) Result produced when applying the Sobel operator; (c) Result produced when applying the Laplacian operator.....	127
Fig.6.6	Determined the vertical and the horizontal pixel locations of the detected edges.....	128
Fig.6.7	Examples of Locating the ROI using the first method.....	129
Fig 6.8	Failure in locating the ROI using the first method.....	130
Fig.6.9	The warmest area in human face.....	131
Fig.6.10	The second warmest area in human face.....	131
Fig.6.11	The coldest region in human face.....	132
Fig.6.12	Examples of tracking the ROI using the second method.....	132
Fig.6.13	Highlighting the two warmest areas in the human face when the mouth is open, the first, warmest, region as a white colour and the second warm region as a blue colour.....	133
Fig.6.14	Determining the search area from the warmest regions. (a) When the mouth is open; (b) when the mouth is closed.....	134
Fig.6.15	Highlighting the coldest region in the human face when the mouth was open.....	134
Fig 6.16	Tracking the ROI using the second method when the mouth was open...	135
Fig 6.17	Failure of the tracking algorithm to locate the correct warmest areas due to a large head movement.....	135
Fig 6.18	Thermal image before thresholding.....	136
Fig.6.19	Thermal image after thresholding.....	137
Fig.6.20	Extraction of the subject from the image background: (a) results produced when only the Prewitt operator was applied; (b) Results produced when both thresholding and Prewittt operator were applied...	137
Fig.6.21	The position of the ellipse superimposed on the filtered thermal image..	139
Fig.6.22	The warmest facial area.....	140
Fig.6.23	ROI represented by a circle (mouth closed).....	140
Fig.6.24	ROI represented by a circle (mouth open).....	141
Fig.6.25	The flowchart of the third ROI tracking method.....	142
Fig.6.26	(a) and (b) Examples of third method in tracking the ROI during different head movements.....	144
Fig.6.27	Regular Movements.....	145
Fig.6.28	Random Movements.....	145
Fig.6.29	The rectangular representation of the ROI with large diagonal head movements.....	146
Fig.6.30	A head movement highlighting the nose very close to the edge of the image	146
Fig.6.31	The ROI highlighted by a circle.....	147
Fig.6.32	Average pixel value within ROI represented by different circle sizes.....	147
Fig.7.1	The standard contact respiration rate monitoring devices. (A) respiration belt transducer; (B) Nasal Pressure transducer; (C) Thermistor pod; (D) Transcutaneous Co2 transducer; (E) Respiratory sounds transducer (microphone); (F) Oximetry Probe (SpO2);(G) Eclectrocardiogram derived respiration probes.....	151
Fig.7.2	Placement positions of contact devices on a child's body.....	152

Fig.7.3	Respiration region of interest, its position centred on the tip of the nose.....	155
Fig.7.4	Respiration signals obtained using thermal imaging. The signals obtained from segments 1 to 8 are shown from top to bottom respectively.....	156
Fig.7.5	Respiration rates running average for the clearest respiration signals of the ROI for the sixteen children respectively.....	158
Fig.7.6	The magnitude frequency spectrum of the respiratory signal for the clearest segments of the ROI of the sixteen children.....	160
Fig.7.7	Respiration signals obtained using Nasal pressure, thoracic belt and CO_2 probe.....	161
Fig.7.8	Respiration rates running average for the clearest respiration signal of the ROI for the two children breathing through a nasal area covered by attached medical instruments.....	162
Fig.7.9	The magnitude frequency spectrum of the respiratory signals for the clearest segments of the ROI of the two children breathing through a nasal area covered by attached medical instruments.....	163
Fig.7.10	Segmenting the ROI into eight parts for a sleeping child. The ROI is centred on the mouth.....	164
Fig.7.11	An examples of respiration rate running average of clearest segments during mouth breathing for the children in Fig.7.10(a) and (b).....	165
Fig.7.12	The magnitude frequency spectrum of the respiratory signals (corresponding to the clearest segment of the ROI) for the children in Fig.7.10(a) and (b).....	166
Fig.7.13	Respiration signals obtained using thermal imaging. The signals obtained from segments 1 to 8 are shown from top to bottom respectively.....	167
Fig.7.14	An example of respiration rate running average of segment 1 shown in Fig.7.13 for a child who had apnea.....	168
Fig.7.15	Detect the apnea in the respiration signal obtained using transcutaneous CO2, thoracic belt, and nasal pressure.....	168
Fig.7.16	A plot of respiration rate values obtained using thermal imaging against values obtained using a convention method.....	172
Fig.7.17	The affect of the conventional measurement methods to the child's skin temperature.....	173
Fig.7.18	The child covers the nasal area and oral area with his /her hand.....	173
Fig.7.19	Illustrating the segmented parts of the ROI.....	174
Fig.7.20	Shows the inverse situation between signals. (a) Illustrates the inverse between S2 and S7. (b) Illustrates the inverse between S3 and S6. (c) Illustrates the inverse between S1 and S8. (d) Illustrates the inverse between S2 and S4.....	175

List of Tables

TABLE.2.1:	Typical respiration rates in healthy children.....	10
TABLE.2.2:	A summary contact based respiration rate monitoring studies.....	12
TABLE.2.3:	A summary of the non-contact respiration monitoring methods.....	20
TABEL.6.1	Tracking Analysis Results for Different Head Movements.....	148
TABLE.7.1:	Subjects' details included in the study.....	153
TABLE.7.2:	Summary of respiration rate analysis.....	169

Author's Publications

Journal papers

1. AL-Khalidi F., Saatchi R., Elphick H. ,Burke D. and Tan S. (2011), "Respiration Rate Monitoring Methods: A Review" in Journal Pediatric Pulmonology InterScience / Medical, Veterinary and Health Sciences, published by WILEY -Blackwell in United Kingdom 2011. Article first published online: 31 Jan 2011, DOI: 10.1002/ppuL21416. Web site http/onlinelibrary,wiley.com/doi/10.1002/ppul.21416 .

2. AL-Khalidi F., Saatchi R., Elphick H. and Burke D. (2011), "An Evaluation of Thermal Imaging Based Respiration Rate Measurement in Children", publication in the American Journal of Engineering and Applied Sciences.

Conference papers

1. Saatchi R., AL-Khalidi F., Elphick H. and Burke D. (2009) ,'Thermal image analysis of skin surface centred on the tip of the nose for respiration monitoring", IEEE sponsored International Conference on Electronic Design and Signal Processing-ICEDSP, 10-12th of December 2009, ManipaL India.

2. AL-Khalidi F., Saatchi R., Elphick H. and Burke D.(2010), "Tracking human face features in thermal images for respiration monitoring" in the 2010 ACS/IEEE International Conference on Computer Systems and Applications in Hammamet Tunisia on 16-19th of May, 2010. pp(s) 1 - 6, ISBN: 978-1-4244-7716-6.Available on Web site.http 7/ieeexplore.ieee.org/xpl/freeabs all.isp?arnumber=5586994 .

3. AL-Khalidi F., Saatchi R., Elphick H. and Burke D. (2010), "A Facial Tracking Method for Noncontact Respiration Rate Monitoring" in the 7th IEEE IET , International Symposium on Communication Systems , Networks and DSP-CSNDSP 2010,United Kingdom on 21-23rd of July, 2010; 827-830. ISBN-: 978-1-86135-370-2. pp(s): 751 - 754, INSPEC Accession Number: 11535400, Location: Newcastle upon Tyne. Available on Website httpy/ieeexplore.ieee.org/xpl/freeabs all.isp?arnumber=5580320 .

4. AL-Khalidi F., Saatchi R., Elphick H. and Burke D. Tan S. (2010)," Challenges in Thermal Imaging Based Respiration Rate Monitoring", Congress of the International Paediatric Sleep Association joint meeting with Paediatric Sleep Medicine Conference, Rome, 3-5th of December 2010. Web site: http7/www.pedsleep.org/.

Posters and Presentations

1. 'Thermal -camera to Monitor Respiratory Rate in Infants". Poster in Materials & Engineering Research Institute (MERI) research seminar, Sheffield Hallam University, UK. ERI seminar day on 20th of may 2008.

2. 'Thermo-graphic Image Processing and Analysis to Monitor Respiratory Rate in Infants". Presentation in MERI research seminar, Sheffield Hallam University, UK day on 18th of September 2008.

3. 'Thermo-graphic Image Processing and Analysis to Monitor Respiratory Rate in Infants". Poster and Presentation in Department of Health and Wellbeing research seminar, Sheffield Hallam University, UK. On 17th of December 2008.

4. **"Thermo-graphic Image Processing Enhancement to Monitor Respiratory Rate in children"** (presentation and poster) in Research conference organised by Leeds University on 22nd of April 2009.

5. **"Non-Contact Respiration Monitoring using Thermal Imaging Based"**, presentation in MERI seminar day, Sheffield Hallam University, UK on 15th of may 2009.

6. **"Respiration Monitoring Using Thermal imaging"** presentation in Research conference – Diagnostic Imaging UK on 9th of August 2009.

7. **"Non-Contact Respiration Monitoring using Thermal Imaging Based"**. Poster in MERI, Sheffield Hallam University, UK on 14th of October 2009.

8. Finally, **Chair- Section** in ACS/IEEE International Conference on Computer Systems and Applications in Hammamet Tunisia on 16th to 19th of May 2010.

Chapter One

1.Introduction

Respiration rate monitoring is an essential task in routine clinical diagnosis. It is used to monitor the progression of illnesses because an abnormal respiratory rate is an important marker of a serious illness (Fieselmann et al., 1993).

There is substantial evidence that alterations in respiratory rate can be used to predict potentially serious clinical events such as cardiac arrest or admission to an intensive care unit (Subbe et al., 2003; Cretikos et al., 2007). These studies have shown that respiratory rate information to be even more important than other vital measurements, such as heart beat rate and blood pressure, in discriminating between stable patients and patients at risk (Fieselmann et al., 1993). Using the changes in respiratory rate measurements, patients could be identified as high risk up to 24 hours before an illness with a specificity of 95% (Cretikos et al., 2007).

According to Murthy et al. (2004), there are deficiencies in the current respiration rate measurement methods, since the existing devices for monitoring respiratory rate only estimate the actual breathing rate. These devices can be classified in different ways, depending on the manner in which they operate and used.

Respiration rate monitoring devices are classified as either contact or non-contact. In the contact type, the instrument makes direct contact with the

subject's body, causing discomfort and in turn affecting the respiration rate value. In some cases the respiration rate is monitored visually by observing the patient's chest or by putting a hand in front of the patient's face to feel the exhaled air. The visual approach is subjective and can be significantly erroneous.

However, in non-contact methods, the respiration rate is measured without the sensing instrument making any contact with the subject's body. There are clear advantages to non-contact respiration monitoring methods. These include; improved patient's comfort (especially for long term monitoring) as the subject is not tied to an instrument, and improved accuracy as distress caused by a contact device may alter the respiration rate. A critical review of respiration monitoring approaches (both contact and non-contact) methods in medical care is provided in the next chapter.

This study presents the development of a novel respiration rate computation approach using thermal imaging. Concerns related to the patient's recording comfort, recording hygiene, and the accuracy of the respiration rate monitoring have resulted in a thermal imaging approach.

The devised method was tested in the Clinical Sleep Unit of Sheffield Children's Hospital and its performance was quantitively evaluated against the current conventional contact based approaches

This chapter provides an introduction to this research. It is organised as follows: Section 1.1 presents the studies' main aims and objectives; Section 1.2 provides the purpose of the research, Section 1.3 provides the problem description of research, Section 1.4 provides contributions of this study. Finally, Section 1.5 provides the outline and organisation of the thesis.

1.1 Aim and Objectives

The primary aim of this research was to apply and further develop thermal image processing techniques to monitor respiration rate in children. This

method is assessed against contact respiration methods that require an instrument to be attached to the patient.

The objectives of this study were:

i. Develop and evaluate a thermal imaging based method of monitoring respiration rate in children.
ii. Enhance the recorded thermal images to reduce unwanted noise
iii. Develop a tracking algorithm to automatically track the facial area associated with respiration (i.e. the region of interest, ROI).
iv. Devise a method to extract respiration features from the ROI.
v. Devise a method to automatically determine the respiration rate from the respiration signals using the selected ROI features.
vi. Critically evaluate the thermal imaging method by applying it to both suitable adults as well as an appropriate number of children.
vii. Compare the effectiveness of thermal imaging with conventional contact based methods.
viii. Critically identify the limitations of thermal imaging based respiration rate monitoring.

1.2 The Purpose of the Research

The principle behind a thermal imaging based respiration monitoring method is that exhaled air causes a rise in the temperature of the tip of the nose and to a lesser extent, the upper lip, whilst inhaled air reduces the temperature of those skin surfaces. These temperature changes can be recorded as a series of thermal images by a suitable thermal camera. The respiration rate can then be obtained by a careful processing and analysing of the images.

The study involved a careful evaluation of thermal imaging to monitor respiration rate in twenty infants and children. This was achieved in collaboration with the Sheffield Children's Hospital.

1.3 Problem Description

Although non-contact respiration monitoring techniques provide a more appropriate breathing monitoring in children, their implementation is not straightforward. The captured thermal images require processing in order to fulfil the requirements of the monitoring function. Among these requirements are image enhancement, segmentation, tracking the region of interest (ROI) as well as specifying the important features from the images. Another, essential requirement of the breathing monitoring system is the ability to produce the respiration signal from the ROI. Accuracy in extracting important features is very important in order to calculate respiration rate.

1.4 Contributions of this Study

Respiration rate monitoring is an essential task in clinical diagnosis. Traditionally, measuring respiration requires attaching the sensing device to the subjects, causing them discomfort and potentially affecting their breathing pattern.

Our research paves the way for novel respiration monitoring in a non-contact manner. Methods to enhance the thermal images were employed and then image processing techniques were utilised to extract the ROI. This region was partitioned into eight equal segments. A respiration signal was generated from each segment and respiration rate was determined from each signal. The developed methods were applied to 20 children enrolled for the study at Sheffield Children Hospital.

The study demonstrated the thermal imaging would allow respiration rate to be determined in a non-contact manner.

1.5 Thesis outline

The following chapters are:

Chapter Two: The Literature Review. This chapter outlines related research and work, highlighting and critiquing the current state of knowledge in this field related to this study.

Chapter Three: Review of Image and Signal Processing Techniques Used in This Study. This chapter explains the theoretical background for image processing and signal processing techniques that are used in this study to obtain the respiration rate values.

Chapter Four: Relevant Thermal Imaging Theory. This chapter reviews the features of the thermal camera used in the study (A40 FLIR) as well as the fundamental concepts in thermal imaging. It also provides an overview of the ThermaCAM™ Researcher 2.9 software which was used with FLIR A40 camera.

Chapter Five: Methodologies, Developments and Preliminary Results. This chapter discusses the System design (Hardware and Software) and the methodologies to obtain results.

Chapter Six: Techniques to Segment the Region of Interest (ROI). This chapter presents the analysis of thermal images to segment the region of interest (ROI) as well as the shapes and the sizes of this region.

Chapter Seven: Thermal Imaging Based Respiration Rate Monitoring in Children. This chapter describes the use of this system in the Sleep Unit of the Sheffield Children's Hospital and compares the results of developed thermal imaging method with those of conventional contact methods.

Chapter Eight: Conclusions and Future Work. This chapter presents the study's conclusions, main findings and suggests possible future work.

Chapter Two

2. Literature Review

2.1. Introduction

An introduction to this study is provided in this chapter. It gives background information about the research area and the relevant related research. A literature review of the publications related to this study is provided.

Respiratory rate is one of the main indicators of an individual's health and is the single most important physiological parameter, as it can be used to predict various life threatening disorders such as the child death syndrome and heart attacks. A number of traditional methods for monitoring respiratory rate already exist in hospitals. Additionally, many methods have been proposed due to rapid technological development. Yet, these respiration monitoring methods suffer from limitations. Most of the methods involve the sensing element being connected to the patient's body, causing them discomfort and also possibly affecting their breathing pattern.

Section 2.2 of this chapter provides an overview of respiration rate monitoring. An analysis of respiration patterns in children is provided in Section 2.2.1. The conventional methods for monitoring respiration rate are described in Sections 2.2.2 and 2.2.3. Section 2.3 provides a literature review of thermal cameras and thermal imaging. The following parts deal with detecting the face and the extraction of the features related to the human face. Finally image processing techniques, including image registration, feature extraction and image segmentation, are presented in Section 2.5.

2.2. Analysis and Monitoring of Respiration Rate

Vital physical signs that indicate a person is alive include respiration rate, heart rate, temperature and blood pressure. These signs can be measured and used to assess a person's level of physical functioning. Normal ranges of these vital signs vary according to the age, sex, weight, exercise tolerance, and body conditions (David, 2009).

The present study focuses on the measurement of respiration rate because it is an important indicator of an individual's health. Respiration is a human physiological task in living organisms. For human, this process results in air containing oxygen being inhaled into the kings, where the gas exchange occurs with the help of alveoli (Lausted and Jonston , 2006). Carbon Dioxide is excreted as a part of the process, in the air released through the nose or mouth. Fig.2.1 shows a schematic representation of human respiratory system The entire process from the inhalation to exhalation is known as a breathing (or respiration) cycle.

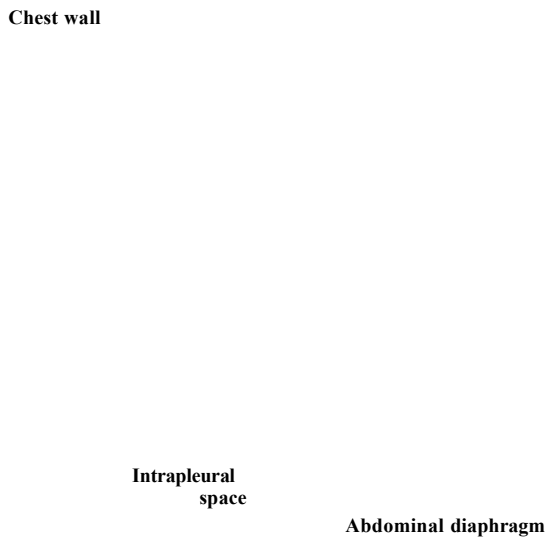

Fig.2.1: Schematic representation of the respiratory system (Lausted and Jonston, 2006).

Respiration plays a critical role in the diagnosis and control of respiratory diseases, especially in new bom children who have breathing problems (Fei et a1, 2005). Respiratory failure is difficult to predict and can become life threatening in a few minutes; however it can also build up gradually. Moreover, it can be used to predict disorders that may threaten life, such as cardiac arrest or admission to the intensive care unit or sudden death in infants (Fieseimann et a1, 1993; Subbe et aL, 2003; Cretikos et aL, 2007).

Respiration is a bodily function consisting of three stages. In the first stage, oxygen is taken or inhaled from air into the lungs (inspiration). In the second stage, carbon dioxide is taken out of the body (expiration). In the third stage, post-expiration occurs when there is equalization of pressures inside and outside the lungs, as shown in Fig.2.2 (Murthy et aL, 2004). The breathing cycle is defined as the time interval between the beginning of inspiration and the end of the post-expiratory pause. The present work lumps together inspiration and post-expiratory pause as it gives the same distribution as shown in Fig.2.2. Therefore, the respiration stages can be categorised as expiration and non- expiration.

Fig.2 ,2 The temperature distributions for the expiration, post-expiratory pause and inspiration (Murthy et al., 2004).

Monitoring of breathing function (or respiratory rate) has its applications in polygraphy, sport training, sleep tests, and patient monitoring. It depends on the physiological changes in humans that are relevant to the respiration operation such as the changes in the volume of the thorax and abdomen and may be dependent on the changes of the temperature between expired and inspired gases (Ye and Yuji, 1997). The main goal of this research is to develop an integrated non-contact respiration monitoring device that is accurate safe, reliable and is easy to use.

2.2.1. Analysis Respiratory rate of Children

A study on the respiratory rate of 1007 children which were less than six months old by doctors in Australia stated, that children when they are awake have an average mean rate of sixty one breaths per minute , with a range of forty three to sixty nine (Morley et al. 1990). Sleeping children have a significantly lower mean rate than those awake at forty two breaths per minute. Children when awake tend to move a lot and breathe irregularly. Children breathe much faster when awake, as compared to the periods they are sleeping. On the other hand, this study referred also to the sex of child, boys had a slightly higher respiration rate when awake than the girls. Boys had sixty one breaths per minute while girls had fifty eight breaths per minute. But there were no significant differences during sleep. Children who are crying or have tract infections had lower respiration rates when awake than healthy children (Morley et al., 1990).

Table (2.1) indicates the average respiration rate in healthy children related to their age. Older children have lower respiration rates (The Pennsylvania Child Welfare Training Program, 2009).

TABLE 2.1: Typical respiration rates in healthy children.

Age range	Average respiration rates (cycles per minute)
Infants	25 – 60
1 – 4 years	20 – 30
5 – 14 years	15 – 25
15 or more years	11 – 25

There has been much research conducted on the respiratory analysis of children. Most of these studies observed that there are many variables that influence a child's respiration such as age, sex and his or her physical state (Hoppenbrouwers et al. 1980; Adamson et al. 1981; Morley et al. 1990). In these studies they noted the effect of increasing age with decreasing respiration. Secondly, the affect of the gender differences in respiration rate. Males breathed significantly faster than females in the active awake or sleep. Thirdly, the respiration rate and regularity are reported to be lower during a child's quiet sleep than during active sleep (physical movements during sleep) and are greatest when the child is awake, except during the first week of life when the rates for active sleep and active awake were similar, being higher than the rates for quiet sleep (Hoppenbrouwers et al., 1980). For every type of respiratory equipment used, calculations of each breathing count is still obtained through counting the cycle of breathing. Every cycle of breathing consists of one inhalation followed by one exhalation, or vice versa.

Most of the mentioned respiration rate monitoring methods shares a common characteristic; they require the sending device to be connected to the child's body. A strain gauge is placed around child's chest and abdomen to measure the changes of strain of the thorax and abdomen during its expansion (inhaling operation) and contraction (exhaling operation). Alternatively a thermistor is placed in the child's nostril to measure temperature changes caused by inspiration and expression of air. Both methods are uncomfortable to children and may not be applicable because the body of the child is tiny and soft. These contact respiration applications were introduced as the first methods for

estimating respiratory rate. These methods have been proven to be effective and are often used to compare the performance of new respiratory monitoring devices (Cacioppo et al. 2007).

There have been several studies reporting the developments of various techniques for the detection and classification of respiration and other bio-physiological signals for the purpose of respiration monitoring. A review of both contact and non-contact based approaches is provided in the follow sections.

2.2.2. Contact Respiratory Monitoring Methods (Conventional Methods)

Also known as intrusive monitoring, these techniques require sensors that are attached to patient's body. They usually restrain natural motion. The several common contact methods of respiratory monitoring are based on measuring one of the following parameters: respiratory sounds, respiratory airflow, respiratory related chest and abdominal movements, respiratory CO_2 emission, oximetry probe (SpO_2) and actimeter.

These techniques are often used for long term (e.g. over night) respiration rate monitoring and only provide an estimate of respiration rate. These techniques require contact with the patient. This causes inconvenience to the patient under treatment and the critically ill patient may not tolerate any sensor in the nose, mouth, or band around the chest. Additionally, these techniques are desirable to measure the respiration rate in children but may sometimes affect the respiratory pattern activity and give inaccurate measurements (Folke et al., 2003; Tobin, 1988).

A summary of contact based respiration monitoring studies is provided in Table 2.2.

TABLE 2.2: A summary contact based respiration rate monitoring studies.

Authors	Year	Summary of the Method
Werthammer et al.	1983	The breathing sounds were detected through an electric microphone. The recorded acoustic signal reflected respiration rate.
Moody et al.	1986	Respiration rate was derived electrocardiogram (ECG)
Storck et al.	1996	Nasal temperature probe (thermistor) was used to measure the variation in the air temperature produced by inhaling and exhalation process.
Sadeh et al.	1995	using Actimeter , which is a wrist-watch like device that uses internal accelerometers to detect activity by sensing motion
Larsson and Staun	1999	Fibre-optic humidity sensors to measure respiration rate.
Nepal et al.	2002	Using the strain gauge is strapped around the patient's chest and measures the changes in thoracic or abdominal during the breathing.
Tarassenko et al.	2002	Breathing rate was estimated by measuring the changes in the electrical impedance pneumography (IP) signal across the chest, and the electrocardiogram (ECG) or the changes in light absorption which known as photoplethysmogram (PPG) across the finger.
Folke et al.	2002	A CO_2 sensor was used to detect respiration airflow
Folke et al.	2003	Using oral, nasal or oronasal thermistor sensors which detect changes in temperature between the inspired and expired air.
Mazzanti et al.	2003	Principal component analysis was used to identify which ECG lead was most effective to extract the respiration rate.
Nam et al.	2005	The patient wears the bio-shirt. This is a set of physiological parameters including skin temperature, ECG and respiration rate measured by using Bio –shirt.
Lee-Chiong	2006	Nasal pressure transducer was used to measure the respiration airflow.
James et al.	2006	Probes were placed on the forehead, big toe, fingertip or bridge of the nose to detect oxygen levels in the blood.
Butkov and Lee-Chiong	2007	Transcutaneous CO_2 was measured to estimate respiration rate. This was based on measuring the diffusion of gas to the skin.
Corbishley and Rordriguez-Villegas	2008	A miniaturised, wearable, and battery-operated respiration monitoring system was developed. A microphone was mounted on the neck to obtain the largest signal of breathing whilst eliminate the heartbeat signal.

2.2.2.1. Acoustic Based Methods

Respiratory sound can be measured using a microphone placed either close to the respiratory airways or over the throat to detect the variation of sound. Then a frequency analysis and estimation of the loudness of the sound can be carried out (Shneerson, 2005). A microphone can be used to convert the acoustic signal generated by respiration to an electrical signal.

Werthammer et al., (1983) reported a respiratory sounds measurement system to detect sleep apnea[1] in infants. The system depended on recording a signal derived from breathing sounds from the nose. This method was applied to eight premature infants. The acoustic monitor detects breathing sounds through an electric microphone. The signals from the microphone were amplifi ed and filtered to exclude environmental noise. Detection of the signal as a breath depends on the amplitude and duration of the signal. In order to measure the changes in breathing patterns they are compared to the integrated signal.
Although, this method could detect the absence of airflow during obstructed respiratory efforts or body movement, it had some limitations when the children were snorting loudly, or when the head was moved far from the microphone. Additionally, any environmental noises such as speaking, crying, coughing etc had a negative effect on the operating of the system. Therefore; the breathing signal was corrupted by noise. The sensor was useful only with obstructive or absent of breathing.

To avoid the limitations of the respiratory s ound measurement method, Corbishley and Rordriguez-Villegas (2008) proposed a miniaturised, wearable, and battery-operated respiration monitoring system, using a microphone. The acoustic sensor is mounted on the neck to obtain the largest signal of breathi ng, whilst eliminating the heartbeat signal. They mounted an omnidirectional microphone on an aluminium conical bell and attached it to the skin to measure the acoustic breathing signal. They suggested detecting the frequency of speech by recording the speech of the patient for ten minutes, while the acoustic sensor

[1] **Sleep apnea** is one of the most common respiratory diseases that causes stop in breathing or get it very shallow repetitively during sleep. The breath pause takes more than 10 seconds. These pauses can occur 20 to 30 times or more in an hour (Sleep apnea, 1995).

was attached to skin on the arm to attenuate other noise sources. The sensor had to be put in correct place to avoid any movements; otherwise the recording signal suffered interference from the heartbeat signal. Also, this approach was required to be implemented in electronic circuits as part of a miniature breathing detector. The complexity of the algorithm affected the complexity of the electronic circuits and hence added more constraints to the power consumption of the electronic circuits. Despite the success of this approach in a number of patients, there remained some limitations that made it inefficient in general measurement of respiration rate.

2.2.2.2. Airflow Based Methods

Airflow can be detected because exhaled air is warmer, has higher humidity and contains more CO_2 than inhaled air. These variations can be used for indicating the respiratory rate. Most airflow-sensing methods need a sensor, attached to the airways (Folke et al., 2003). The measurement of the airflow can be achieved by using nasal, oral or oronasal thermistor sensors which detects changes in temperature between the inhaled and exhaled air. This gives a semiquantitative estimate of airflow, but can become displaced.

Storck et al., (1996) used an airflow-sensing device to measure respiration rate. The device contained a nasal temperature probe with a thermoister which reacted to the variation in the air temperature. The thermoister was placed in the nostril to measure the change of temperature caused by inhaling and exhaling air. Although, the thermoister was small, easy to place and gave a good estimate of airflow in some patients, it is uncomfortable to use in children. They always suffered from difficulties in tolerating this method to measure respiration. Moreover, children tend to displace the thremistor thus producing errors in measurement. The probe also could be used only once for hygienic reasons, (so there are cost implications)

Larsson and Staun (1999) suggested using Hygrometer or fibre-optic humidity sensors to measure respiration rate. The sensor tends to overestimate the

respiratory rate by measuring the humidity of respiration, based on the fact that the expiration air has higher humidity than inspiration air. This sensor usually placed in front of nasal /oral region.

The nasal pressure transducer is another sensor which is already used to measure respiration rate. Nasal pressure is a more accurate measure of airflow than others as it based on the actual volume of the air exhaled (Shneerson, 2005; Lee-Chiong, 2006). It can be measured via dual nasal cannulae, mouthpiece or facemask. A problem with airflow measurement is that some patients may not feel comfortable with the sensor (Tobin, 1988).

Folke et al. (2002) have reported CO_2 sensor to measure respiration rate. Their study also indicated that subtle design changes in the collecting device could introduce large differences in sensor performance.

2.2.2.3. Transcutaneous CO2 monitoring

In this measurement technique the recording continuously and non-invasively uses a heated electrode (about 42° C) is applied to the skin usually the earlobe. This method relies on the diffusion of gas to the skin and provides an overall estimate of change in CO_2 level rather than minute by minute readings. The electrode is automatically calibrated prior to use. The electrode is surrounded by a solution to provide conductivity. Care needs to be taken to avoid skin burning on sensitive and neonatal skin (Butkov and lee-Chiong, 2007).

2.2.2.4. Chest and Abdominal Movement Detection

Chest and abdominal movements can best be measured by either mercury strain gauges or impedance methods. There are two bands; the thoracic band which is placed around the top of the thorax, passing under the arm pits and the abdominal band which is placed over the abdomen at the level of the umbilicus. Normally, the bands should be tight enough to detect the chest and abdominal movements. The bands are made from extendible/deformable conducting material, either a very fine wire or thin foil such that the conductivity can be maintained during the stretching process (Lee-Chiong, 2006; Blom, 2004).

Normally, the inspiratory thoracic and abdominal expansion is almost synchronous. However, if the upper airway is partially obstructed, there may be a change in the phase angle and timing of the movements of the thorax and abdomen. The movements become asynchronous, i.e. the thorax moves outwards, and the abdomen inwards. During expiration, this pattern is then reversed. These are detectable by movement monitors. The principle of the strain gauge sensor is based on increasing in the resistance of the conductor when the area of the conductor is increased during the respiration process. Equation (2.1) indicates how the change of resistance (ΔR) is converted into the measured strain (ε).

$$\varepsilon = \frac{\Delta R}{R_G} \tag{2.1}$$

Where R_G is the resistance of the strain gauge without any deformation (Konno et al., 1967).

The main reason that this method is not desirable for children is because the bands are put under the clothes to avoid being pulled off. Therefore it is difficult to use this method to measure respiration in children.

Nepal et al. (2002) studied the abdominal strain gauge transducer for measuring respiration rate. The strain gauge was strapped around the patient's chest and measured the changes in thoracic or abdominal circumference during the breathing. This method involved a classification algorithm to separate respiratory signals accurately as apnea, respiration, or respiration with motion, by using a zero cross algorithm.

2.2.2.5. Oximetry probe (SpO2) Based

Blood-Oxygen saturation (SpO_2) measurement is another technique for respiration rate monitoring. This method is based on the fact that saturation of oxygen in blood (SpO_2) changes regularly as a result of respiration.

When air enters the lungs, its oxygen binds to the haemoglobin in the red blood cells, the oxygen is then transported throughout the body as arterial blood. A pulse oximeter uses the red and infrared light frequencies to determine the

percentage of haemoglobin in the blood that is saturated with oxygen. This percentage is called blood saturation or SpO_2 (Konica, 2006). A SpO_2 meter simultaneously displays the SpO_2 levels as well as the electrocardiogram pulse rate.

A re-usable probe or sensor is placed on the forehead, big toe, fingertip or bridge of the nose to detect SpO_2 levels and pulse rate. It is secured in place with an adhesive tape and a bandage. This method is not perfect because it is insensitive in detecting changes in oxygen when it is nearly normal as well as inaccurate measurement, if the probe is not properly attached as it may detect a variety of noise. It can give an idea about the effectiveness of the person's breathing and how their body is handling oxygen reserves (James et al., 2006).

2.2.2.6. Electrocardiogram (ECG) Derived Respiration Rate

A method for monitoring respiration rate relies on electrocardiogram (ECG). This method is based on the fact that respiration is the most important modulator of heart rate and the source of short term heart rate variability.

Many studies have demonstrated that respiration signal and its rate can be extracted from the ECG. This method is generally referred to as ECG-Derived Respiration (EDR) monitoring.

In this approach, ECG electrodes are attached to the subject. The observations showed that the body-surface ECG is influenced by electrode motion relative to the heart position and changes of the lung volume. By measuring the fluctuation in ECG, respiration rate can be derived. This technique is based on a process known as sinus arrhythmia, i.e. the modulation of ECG by the breathing process (Moody et al. 1986).

Mazzanti et al. (2003) studied the modification of the EDR monitoring which is based also on small ECG morphology changes during the respiratory cycle caused by movement of the heart position relative to the electrodes and the change of lung volume by using principal component analysis to identify which ECG lead was most effective before extracting respiration rate (Mazzanti, et al. 2003).

Another study carried out for this method was suggested by Tarassenko et al. (2002). It is based on the changes in the electrical impedance pneumography (IP) signal across the chest, and the ECG or the changes in light absorption (photoplethysmogram, PPG) across a finger. They estimated breathing rate by adding the individual outputs for IP and PPG channels, after applying the Kalman filters for both waveforms. The limitation of this method was that movement artefact affected the both channels. This estimates of breathing rates inaccurate.

Additionally, there are several other studies using EDR based respiration monitoring such as Travaglini et al. (1998), Penzel et al. (2002), Park et al. (2008) and Zhao et al. (2008). However, these methods are relatively high cost, which means that they are impractical for long-term monitoring. Besides, they are considered as intrusive methods, and so many sensors are attached to the subject's body. Therefore, these methods are not appropriate for children.

2.2.2.7. Actimeter

Another widely used recording device is the actigraph, also known as an activity monitor. It is a wrist-watch like device that uses internal accelerometers to detect activity by sensing motion. This small lightweight activity-measuring instrument can be worn on the wrist or ankle to record physical activity near to the SpO2 probe (Sadeh et al., 1995).

2.2.2.8. Bio-shirts

Another contact method which has recently been used to measure respiration rate is the bio-shirt. A set of physiological parameters including skin temperature, ECG and respiration rate are measured by using Bio–shirts. Sensors are embedded into the bio-shirt. Once the patient wears the bio-shirt, the measurement process starts to transmit the measured values to a computer for further analysis (Nam et al., 2005). Fig.2.3 shows the using of the bio-shirt.

Fig.2.3: Left: bio-shirt inner layer. Right: outer layer (Nam et al., 2005).

In all contact methods, the sensing devices attached to the patient is inconvenient for the patient, causing them discomfort and may affect their respiration pattern Finally, the most commonly used method of respiratory rate monitoring in clinical practice is by visually observing the patient. The observation of the abdominal or rib cage movements gives a subjective clinical estimation of tidal volume, but there is a tendency to overestimate. This could be dangerous at low tidal volume and could give inaccurate estimation of the respiration rate (Semmes et al 1985). On other hand, there are several studies which introduced non contact measurements for respiration rate. These methods will be explained in the following section

2.2.3. Non-Contact Respiratory Monitoring Methods

A critical review of non-invasive respiratory monitoring in medical care was provided by Folke et at (2003). Non-contact methods of respiratory monitoring are also known as nonintrusive, touch-less or contact free methods monitoring, are techniques where no device is used inside the body nor attached to the skin surface. There are clear advantages to non-contact respiration monitoring methods. These include inproved patient comfort (especially for long term monitoring) as the subject is not tied to an instrument and inproved accuracy as distress caused by the contact device may alter the respiration rate.

The basic principle of these methods is the ability of the tools to detect the radiated energy either by ultrasound, laser, infrared or thermal sensors. A summary of a number of non-contact respiration monitoring studies is provided in Table 2.3.

TABLE 2.3: A summary of the non-contact respiration monitoring methods.

Authors	Year	Summary of the Method
Greneker	1997	In this study a Radar Vital Signs Monitor (RVSM) system was used to detect chest's movements.
Nakai et al.	2000	A thermal camera was used to detect the patient's chest movement during respiration.
Nakajima et al.	2001	A static camera was used to detect thorax movements and then the respiration rate.
Aoki et al.	2001	Respiration patterns were detected using a Fibre Grating (FG) vision sensor and Charge-Coupled Device CCD camera.
Folke et al.	2003	An ultrasound sensor was used which emitted a continuous waveform toward the chest. The chest movements during respiration were measured by using the Doppler radar.
Hsu and Chow	2005	They used a thermo-sensor which was placed on the mask to detect the breathing.
Sato and Nakajima	2005	Respiration patterns were detected by using a Fibre Grating (FG) vision sensor and two CCD cameras.
Zhu et al.	2005	A thermal camera was used to detect the respiration rate from the skin surface regions under the nose. These regions were selected manually and were tracked using the Mean Shift Localization-Based (MSL-based) particle filtering.
Murthy and Pavlidis	2006	A thermal camera was used to detect the respiration rate from a region of interest (ROI). This region was selected to be under the tip of the nose. The method was based on the fact that the temperature of exhaled air is higher than the typical background temperature of indoor environments (such as walls).
Wang et al.	2006	Using infrared video information to recognize the abnormal breathing activity when compared with body movement. It based on the shape of movements and degree of motion .
Chekmenev et al.	2006	A thermal camera consisting of a focal plane array for a long-wave infra-red (6-15 μm) sensor was used to measure the temperature changes around the neck region, carotid vessel complex, and the nasal region.
Wel	2008	Two web cameras were used to monitor the respiration operation. This method depended on the principle of triangulation to monitor the chest movements. The region of interest in this system was either the chest or abdomen images.

TABLE 2.3: A summary of the non-contact respiration monitoring methods (continue).

Authors	Year	Summary of the Method
Alobaisi	2008	A thermal camera to measure breathing by applied neural network.
Ruiz	2008	An ultrasound sensor was used to detect the chest movements during the respiration operation. This was based on the distance and the time of transmitted and reflected wave from the sensor.
Chan	2008	Two ultrasound sensors were used to detect the chest movements during the respiration.
Feing	2008	An infrared light sensor was used to detect chest movements during the respiration operation.
Pai et al.	2009	A sensors embedded in a chair was used to detect the pressure on a cushions which are placed on the back rest of the chair at the level of the thorax and the abdomen. The respiratory sensing circuit acquires the pressure signal from the cushions and converts it into an electrical signal.
Tan et al.	2010	Video image processing techniques were employed to extract respiration rate from the videos recorded using a webcam. The webcam monitored chest movements caused by respiration.

Greneker (1997) reported one of the first non-contact respiration rate monitoring systems, which was developed by researchers at Georgia Tech Research Institute (GTRI). They applied a system to detect human heartbeat and respiration rate without any physical connection to the patient. The system is called Radar Vital Signs Monitor (RVSM). This system was developed to monitor the performance of Olympic athletes at distances exceeding 10 meters. The RVSM detects breathing–induced movements of the chest based on the Doppler phenomenon. A band-pass filter is used to separate the heartbeat from the respiration signals. The limitation of this method was the motion artefacts which could corrupt the respiration signals.

While another non-contact measurements technique of respiration rate was modified by Aoki et al. (2001). They reported a non-restrictive visual sensing method to detect the respiration pattern by using a Fibre Grating (FG) vision sensor and processor unit. The system consisted of two parts. The first was the Fibre Grating projecting sensor. This provided an array of invisible infra-red light spots (wavelength 810nm). The second part was a Charge-Coupled Device (CCD) camera with an optical band- pass filter, as illustrated in Fig.2.4.

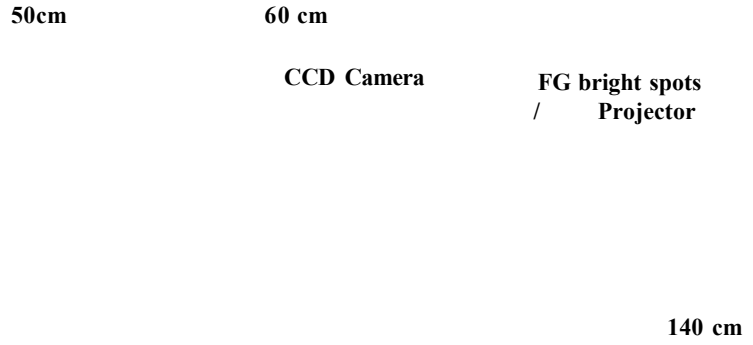

Fig.2.4: Arrangement of the sensing system (Aoki et al., 2001).

Infrared light was used to project a set of bright spots on the subject, while the CCD camera was used only to capture the scene of bright spots; image processing techniques were used to detect the barycentre of each of the bright spots. The detection of the thoracic movements caused shifting the location of bright spots. These were detected in each inter image frame using inter image subtraction techniques. The moving distances of bright spots in each image were extracted and were classified as a respiration (periodic displacement), or rolling over (large amount of displacement) of the subject.
The dangerous states were specified if the calculation of respiration rate was dramatically different from the typical respiration frequency of a quietly sleeping person.

Up to this point, the Fibre Grating vision sensor seemed to be the preferred choice. Sato and Nakajima (2005) tried to improve the method by designing a system consisting of three units: a fibre grating vision sensor and two CCD cameras. The second camera was placed far from the first camera such that the sensitivity of the height change detection, or the resolution was increased. The same process as the previous method was repeated for both of the CCD cameras, where both of them were used to capture the scene of bright spots; the amount of movements of the spots between successive frames were obtained. The performance of the system was justified by comparison of spirometer's

results. In addition, the correlation coefficient between the results proved the accuracy of this method. Although this system was simple and introduced an efficient algorithm to estimate the respiration motion by looking at its volume change in real time, it still suffered from difficulties in distinguishing significant patient's movements from the respiration operation.

To overcome the limitations of these methods Wang et al., (2006) suggested a system to recognize the abnormal breathing activity when compared with body movements using infrared video information. This technique was developed as a non-intrusive video monitoring for detecting when there were abnormal breathing activities, not simply general body movements, without geometric constraints and position limitations. This approach was based on the shape of movements and degree of motion through analysing human breathing behavior and comparing these with general body movements; because there were important in going accurate breathing monitoring by camera. Wang et al. (2006) analysis depended on observing differences in the features of each activity, for example breathing activity was considered to be a relatively slow motion as compared to general body movements. During breathing, the elements of the entire surface move forward and backward, in contrast with body movements where the elements move to different positions.

Another non-contact method was modified by Nakajima et al. (2001). They used a static camera to detect thorax movements to determine respiration rate. The projection of the surface of the thorax was represented as a region with a range of brightness intensities. Respiration was monitored by quantifying the variations of the locations of the image intensities over time.

Chest movements caused by respirations can be measured in a non-contact manner using Doppler radar. This approach was based on the variation in thorax volume occurring during breathing. An ultrasound sensor emits a continuous waveform toward the chest. The phase of the reflected signal is computed and then the location of the chest is determined using Equation (2.2).

$$x(t) = \frac{\lambda\theta(t)}{4\pi} \tag{2.2}$$

Where $x\ (t)$ is the chest location, λ is the wavelength of the transmitted signal and $\theta(t)$ is the measured phase shift of the reflected signal at time (t).

Another non-contact method was reported by Hsu and Chow (2005). They reported a thermal sensor based respiration rate monitoring system. Their device could monitor the temperature change of the breathing airflow and detect respiratory frequency. In this approach there was no contact with the children's skin, thus avoiding the possibilities of any skin irritations. The sensor could detect temperature changes induced by respiration and then the data were analysed simultaneously by a personal computer that can link to the central nurse's room. To avoid missing the detection of breathing signals, an ellipsoid-shaped mask was made and the thermo sensors were placed on the mask so that breathing could be detected when the child's head turned. The problem with this method was that by putting the mask closed to the child's face the children could detach the sensors causing the system to malfunction.

Another non-contact method was suggested by Pai et al. (2009). He described a respiratory monitoring system which acquired the respiratory signal of a subject through sensors embedded in a chair, and then calculated the respiratory rate and monitors the respiratory activity. In this approach the mechanical setup consisted of a set of inflatable air cushions and a bulb for inflating them to an optimum pressure. The cushions were placed on the back rest of a chair at the level of the thorax and the abdomen. The inflated cushions were compressed due to the respiratory movements and these pressure changes were picked up by the respiratory sensing circuit. The respiratory sensing circuit acquired the pressure signal from the cushions and converted it into an electrical signal. Moreover a mechanical filter could be used before the respiratory sensing circuit to further reduce the effects of jerky movements on the respiratory signal. This method was unable to deal with significant pressure changes due to sudden and jerky movements by the subjects, which resulted in false readings.

Also the cushions placed at the thoracic level were sensitive to both respiratory and jerky movements. In addition this method was not suitable for children because of the difficulty of making the children sit properly and regularly on the chair.

A number of non-contact methods proposed at Sheffield Hallam University in collaboration with the Sheffield Children's Hospital, most of them are either in the study phase or in the implementation phase. The major aim of this work was to design, evaluate and commercialise a non-contact method of respiration monitoring principally for children.

Ruiz (2008), Chan (2008) and Feing (2008) developed non-contact methods to monitor respiration rate. These methods focus on investigating how ultrasounds waves or infrared light beam are transmitted to the child's chest as shown in Fig.2.5. Both approaches were carried out by sensors which calibrated the maximum and minimum ranges of a baby manikin's inhaling and exhaling position.

Child breathing causes the chest to move therefore the distance of the sensor to the chest was calculated. The time of the transmitted and reflected wave from the ultrasound or infra-red sensors to the chest was measured. Since the speed of sound differs from the speed of light in air, the measurement of distance can be computed after the delay measured as the Equation (2.3)

$$\text{Distance} = \frac{\textit{signal speed} \times \textit{time delay}}{2} \qquad (2.3)$$

Light velocity is $3*10^8$ m/s. while the velocity of sound in air is about 331.3 m/s.

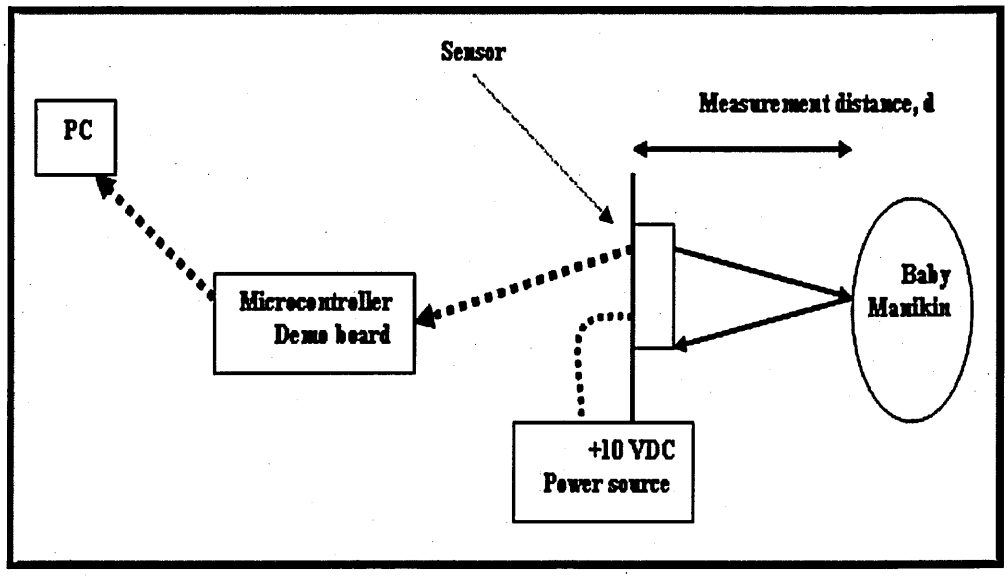

Fig. 2.5: The hardware design of the Ruiz approach (2008).

Figs.2.6; 2.7 show the ultrasound and infrared sensors output during manikin's breathing respectively.

These approaches were carried out using manikins, which means that there was no test on real infants or children. It did not have to deal with the noise that occur in real life implementation by using an ultrasound or infrared sensor such as child movements or environment noise. Also the resolution of these sensors was not good enough to accurately detect the movements of child's chest during the inhaling and exhaling process. The results indicated that although the infrared sensor was cheaper than the ultrasound sensor, it was less effective and least accurate in monitoring respiration rate. It has high sensitivity to optical noise; the output voltage did not responed linearly with distance like the ultrasound sensor. All the test results indicated that the infrared sensor in its current form has not sufficient resolution to monitor respiration rate.

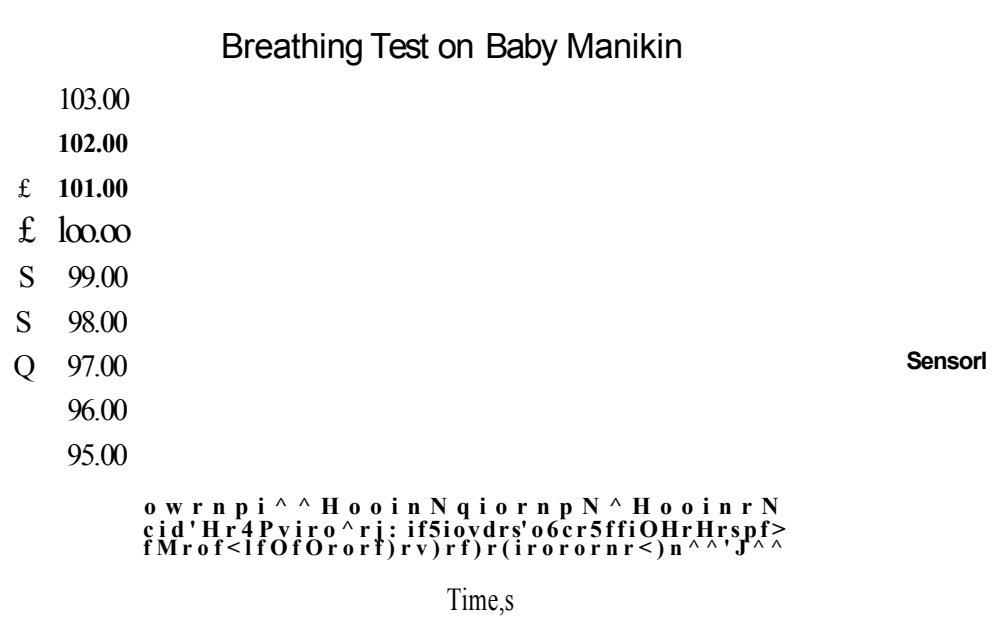

Fig.2.6: Ultrasound sensor output during manikin's chest movements (Chan, 2008).

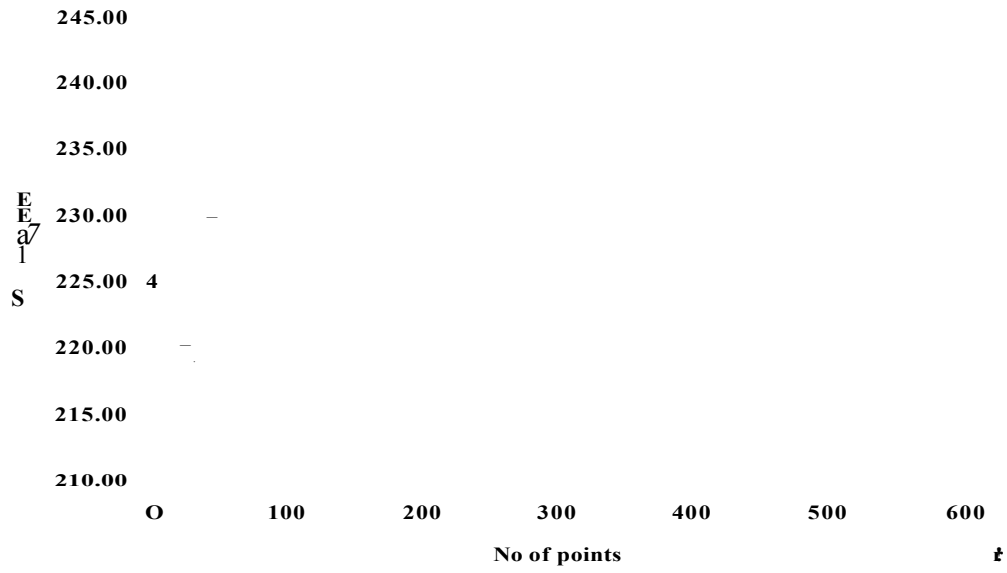

Fig. 2.7: Infrared sensor output during manikin's chest movements (Feing, 2008).

So far, it has been observed that using an ultrasonic sensor seemed to be more suitable than an infrared sensor to measure respiration rate; therefore future work is required to improve results.

Another respiration method that detected chest and abdominal movements was based on video image processing. The manikin's chest can be manually

pumped, making its chest move forward and backward similar to the process of respiration. The method was applied only on manikins as a first stage for study. This method was improved by Wei (2008) who suggested using two web cameras to measure respiration rate. The modification eliminated the need to use chest marker and depended also on using the principle of triangulation to monitor the chest movements. The region of interest in this system was either the chest or abdomen images. The system was able to track and estimate in 3-D location of a single salient feature of the cloth worn by the manikin and then determine the respiration rate.

A related approach was suggested by Tan et al (2010). Chest movement detection was performed by subtracting successive images of the chest recorded using a webcam. A typical respiration signal obtained using this approach is shown in Fig. 2.8.

Fig.2.8: Schematic plot of respiration rate obtained using a webcam (Tan et al., 2010).

Two lobes were observed representing the inhalation and exhalation phases. The lobe associated with the inhalation is larger. The reason for the shape of the respiration signal is that the vertical axis of the plot represents chest and abdominal movements. During the exhalation, the chest's wall initially moves slowly inward, its movement increases with time, reaching a peak and then, the

amount of movement decreases. A similar process occurs during inhalation, but this time the chest's wall moves outward. Fig. 2.9 shows the plot of $jc_{(t)}$ during two respiration cycles. An algorithm was developed to extract the respiration rate from the recorded signal in real-time (Tan et al, 2010).

Fig.2.9: Plot respiration signal using a webcam (Tan et al., 2010).

There were also several studies for measuring respiration rate by using thermal imaging; these are explained in the following section. Non-contact methods which have been described above use expensive sensors, or combinations of multi-modal sensors, to detect respiration. Additionally, most of them lack accuracy in measurement. In some cases they are capable of detecting respiration only for a person without movement or are uncomfortable to use it with children

2.3. Thermal Imaging

Thermography2 is the process of using a camera designed to detect heat emission by way of Infrared (IR) energy waves. Unlike light waves, IR is invisible to the naked eye. Medical infr ared, popularly known as IR - thermography has been utilized since the 1960s to measure and map skin

2 Thermography, Digital Infrared Thermal Imaging (DITI), Thermology, Thermal Imaging, Thermograms (the images) all these names refer to the same medical imaging (Buddharaju et al., 2006).

temperatures. Interpretation and evaluation of thermographic measurements has improved during the past forty years (Buddharaju et al., 2006).

Thermal imaging was considered a diagnostic tool for several reasons (Ng and Sudharsan, 2000). Firstly, the physiological test equipments are completely non-invasive, passive, and harmless. Secondly, they are ideal for detecting hot and cold spots, or areas of different emissivities on the skin surface since humans skin radiate infrared energy very efficiently. The emissivity of human skin is approximately in the range from 0.92 to 0.99. Thirdly, the data can be collected, recorded and sent to a computer for processing. Finally, the equipment is highly portable, fully self-contained and does not need any sources for illumination, thus making day and night imaging possible (Buddharaju et al., 2006). For these reasons thermal imaging is effective in the field of polygraph and for remotely monitoring breathing rate (Murthy and Pavlidis, 2006).
IR thermal imaging is a useful, objective tool for medical and physiological-based investigations such as detecting breast cancer, anxiety and illegal immigrants, monitoring breathing, face recognition and also lie-detection. The details of thermal imaging techniques will be explained in Chapter 4.

Head et al. (2000) suggested using infrared imaging to diagnose breast cancer. They demonstrated that the use of IR imaging for detection and diagnosis of breast cancer was limited by an inability of IR to localize the tumour position. Although IR imaging is a completely non-invasive technique and does have an important role in screening for breast cancer, there is also a need for mammography and physical examination in order to have an early diagnoses of breast cancer. Thermal imaging is importance since it is used for research and development in the phenomenology of breast cancer detection early, and for screening and multimodal diagnosis (Diakides et al., 2006).

Pavlidis et al. (2000) suggested the use of a thermal camera to detect anxiety in people. The detection depends on the fact that the fear or anxieties increase the blood flow in the Periorbital Region (PR), which causes a sudden change in skin temperature; this is readily visible in human faces. The thermal camera can sense the variations in face temperature. The infrared imaging has proved its

potential in deception detection when thermal image analysis was used by Pavlidis et al. (2000) to detect facial patterns at a distance. Although the results of this experiment so far are not sufficient, it does seem promising.

Instead of specifying one region for monitoring, Tsiamyrtzis et al. (2005) suggested temperature recordings at two specific parts of the human face. This approach was achieved by using tandem tracking techniques, for two regions of interest in the human face, to develop a thermal imaging for lie detection and noise suppression. This method depended on the changes of the subject's physiological parameters during investigation, such as blood volume, pulse change, respiratory rates, and electrodermal activity. Therefore the skin temperature was heavily modulated by superficial blood perfusion as mentioned before.

Nakai et al. (2000) proposed using the thermal camera of a focal plane array of mid-wave infra-red sensors to monitor respiration rate. The measurement techniques used for patients were in real time. The region of interest (ROI) was detected around the patient's chest. The largest change occurring between frames was determined by subtraction technique. Respiration rate was derived from the observed images (image analysis and interpretation). The optimal position of ROI in this method depended on the largest change occurring. Therefore the problems can be seen when the patient either left his bed or when the patient moved into his bed.

Instead of using the patient's chest as a ROI, Murthy and Pavlidis (2006) suggested detecting the ROI in the background, exactly under the tip of the nose as shown Fig.2.10. This was based on the fact that the air is breathed out has higher temperature than the typical background temperature of indoor environments such as walls. Therefore the particles of the expired air emit at a higher power than the background. The classification of the frame as expiratory or non-expiratory was achieved based on the statistical modelling for the thermal data. A thresholding technique of the colour values were applied to segment the skin region from the background and to specify the ROI.

Fig.2.10: Respiratory airflow profiles with the ROI (Murthy and Pavlidis, 2006).

This approach had several limitations; the ROI was selected manually in the background, therefore the respiration rate may be affected by the background noise. Also the ROI was affected due to head movements when the subject rotated his/her head towards or away from the camera. Also the method was specific to measuring respiration rate for the patient when he/she turned his face to the side and without any head movements.

To overcome the limitations of the pervious method Zhu et aL (2005) developed a non-contact method to monitor respiration rate. They designed a tracking algorithm that could follow facial features related to respiration by infrared imaging. These features were selected manually from a reference image (ie. the first image in the video) by specifying three windows. Two of these windows covered the areas between the bridge of nose and the inner comer of the eyes (ie. the periorbital regions) and another window was placed on the apex of nose. Their algorithm tracked these three windows in the following recorded images. The respiration signal was obtained from a rectangular region under the nose. This method still suffered from some limitations. For example, the tracking method was based on specifying human face features manually in the form of three windows in the reference image and following them in all the sequent images. This process had a high probability of failure or loss in one or more of these areas during significant head movements.

Additionally the ROI was specified as a rectangle. The limitations of this technique is discussed in Chapter 6.

Instead of using a focal plane array of mid-wave infra-red sensors, Chekmenev, et al. (2006) suggested using a thermal camera consisting of a focal plane array for a long-wave infra-red (6-15 μm) sensor to measure the temperature change around the neck region, carotid vessel complex, and the nasal region. The selection of these regions was done manually. A wavelet-based method, kernel with second derivative of the Gaussian function, was used to decompose the image to a different scale. Three-scale decomposition was used to decompose the image. The mean value for each region for all frames was plotted with respect to time. A wavelet analysis was developed to extract the heart pulse and the respiration rate. Although this method gave good results there were obstacles to identifying the region of interest which represented carotid arteries, because these were mostly under the muscles of the neck. So this area had to be detected manually.

Alobaisi (2008) modified the thermal imaging method to monitor respiration rate by using neural network. This technique classified the images either breathing in or breathing out to compute the respiration rate. The ROI was selected manually as a rectangle in the centre of the first image (i.e. the reference image).

As mentioned above, there are several studies that described monitoring respiration rate by using thermal camera, yet they were limited in their scope of investigation. Also they were not applied and evaluated on infants and children.

2.4. Face Detection and Feature Extraction

Face detection is one of the most common biometric authentication technologies which is based on physiological characteristics and can be used in a wide range of applications such as identity authentication, access control, measuring breathing and surveillance (Guo et al., 2000). Feature extraction techniques are the most important and critical step within pattern recognition

and image processing. The concepts of features extraction is to look for significant information in an image (Nixon and Aguado, 2002). These techniques will be explained later in Chapter 3.

This section provides a literature review of the face detection and feature extraction. The problem of detecting the face and facial features in images has become a popular area of research due to their important applications. There are several variables that affect the performance of face detection such as wearing glasses, different skin colouring, facial hair and facial expressions. Additionally light conditions and the orientation of faces in an image are the most frequent and difficult problems (Wong et al. 2001).

Human face has changeable structures that cannot easily be detected or recognised. This fact makes a computer aided recognition or detection system very complex (Hjelmas and Low, 2001). One simple solution to this problem would be based on matching the test image with a template. This approach was modified by Brunelli and Poggio (1993). They suggested detecting the human face based on a template-based approach; by selecting four templates for each person, to contain the eyes, nose, mouth and whole face. The recognition technique was achieved by comparing the test image with the database images. Correlation was computed for each feature template; a vector of matching scores for each feature was calculated. The test subject was then classified as the subject with the highest score. This approach introduced a significant method to store the face area by discrimination ability (eyes, nose and mouth in order). This method succeeded in recognising a number of people, it had some limitations because it deals only with the static and frontal images, so it was unable to deal with head movements. Additionally the illumination must be controlled; the same powerful light was used for the test and data base images.

Another suggestion for face detection was proposed by Rowley et al. (1998). They modified a method to detect a face region by using a neural network. This method was suggested to deal with the light problem in the face detection process. The image was segmented into several regions. The neural network was also used to classify the regions into two groups, either face or no face. Pre-processing steps were applied for each region by using a light correction

algorithm and histogram equalization techniques. The light correction needed a statistical analysis for the background colour to be approximately estimated across the image. While the histogram equalization techniques were used to adjust the histogram of the image in a variety of ways either by averaging the histogram for an image or enhancing the contrast of image. The light condition and skin colour problems remained problems with the face detection technique.

To solve the problems of the lighting effect and also the orientation of the face, another modification was proposed by Wong et al., (2001) for detecting human face and feature extraction. The approach was based on locating the face region and facial features based on the characteristics of eye regions.

Genetic algorithm and the eigenface techniques were also applied. The genetic algorithm is applied to search for possible face regions in images, while the eigenface is used to determine the fitness of the regions. To reduce the searching space, the human eye regions were selected by testing all the valley regions in an image using a genetic algorithm. The face regions were segmented based on a pair of possible eye candidates. The size of human face (h_{face}) is proportional to the distance between two eyes (d_{eye}) as in Equation (2.4)

$$h_{face=}1.8\ d_{eye} \tag{2.4}$$

A possible face region which contains the eyebrows, eyes, nose, and mouth was determined, based on this relationship. The facial features are then extracted from the detected face regions. The fitness value for each face candidate was calculated by eigenfaces. After a number of iterations a good candidate region was selected, and then features were extracted from this region. The selected face was then further verified by measuring the symmetries and determining the existence of the different facial features. This method can achieve a high performance in detecting human faces, and feature extractions in complex and simple backgrounds.

Another technique is based on the skin colour. Skin colour can be considered as a significant feature that can be used to detect human face. It has proved effective because it gives a fast detection and provides robust results enough to perform real-time tracking (Bovik, 2000). This process depends on the colour of the human face which can be tracked and distinguished from the colour of other objects in the scene and the colour of the background. However significant limitations of this method appeared when there is a wide variety of skin colours, light conditions and there are problems with grey level images. Sometimes it can be used as a first step in face detection, but is not suitable for high level feature extraction and analysis. A modified method to detect the human face in visible domain using the skin colour was proposed by Turkan et al., (2006). They also used a skin colour to detect the human face region. They suggested another technique to reduce the effect of significant limitations of the skin colour by filtering the selected region using a high-pass filter of a wavelet transform to highlight the edges of the regions.

Horizontal, vertical and filter-like projections of the region were used as feature vectors. The feature vectors were then classified as face or non face by using either Dynamic Programming or support vector machine techniques. Dynamic Programming is a classification technique which is used for computing the best possible match path between the original feature vector and template feature vector. The similarity between these two vectors is determined by measuring the Euclidean distance. And then the decision face or no face is based on thresholding the resulting distance. This approach confirmed that the use of the support vector machine technique is more accurate, faster and cheaper than Dynamic Programming to face detection process.

Instead of the above methods, Tian and Bolle (2008) developed a method to detect facial expressions for the human face. Facial expression analysis automatically combines a number of tasks which includes face detection, facial features extraction and facial features represented. Based on this analysis the face was classified as Neutral face[3] or Non-Neutral. After the face region was extracted by using skin -colour technique. Detec tion and extraction were

[3] **Neutral face** is a relaxed face without the six universal expressions (happiness, sadness, disgust, anger, surprise, fear) (Tian et al. 2008).

focused on the six facial point features from the image which were less affected by noise than other parts of the images. The features includes: -two pupil centers, two eyebrow inner end-points and the two corners of the mouth. The distance between these points was calculated. Further, the features of the eyes and the mouth were extracted by an ellipse fitting algorithm and the histogram technique respectively. All the features were inputted to Neural-Network to detect the decision of being Neutral or non- Neutral. This approach was an important technique to reduce the error rates for face recognition, because universal expressions are one of the important reasons for inaccuracy in the recognition process. This approach could detect the face and extract the facial expression and recognition.

Different techniques have been proposed to detect human face and facial features extraction including, principal component analysis (Turk and Pentland, 1991) neural networks (Rowley et al., 1998), colour analysis (Bhuiyan et al., 2001) and Support Vector Machines (Guo et al., 2000). The problem of face detection still receives considerable attention among researchers because the human face is a dynamic object and has a high degree of variability in its appearance, which makes face detection a difficult problem in computer vision.

2.5. Image Processing Techniques

Image processing techniques refer to the manipulation and analysis of image information. It represents any operation that acts to improve, correct, analyse, or in some way change, an images called image processing (Baxes, 1994).

Image registration (alignment) is one of the digital processing advance techniques which is based on extracting the features of the images. These techniques can be used to correct the geometric difference between two or more images, one of them is the reference image and the other is the input image of the same scene. This task has become very important in medical imaging. Moreover it is useful for comparing images taken of the same structure at different times, from different viewpoints, and/ or by different sensors

(Semmlow, 2004). Image registration techniques can be classified into two classes, namely the interactive registration (manual image registration) and the unassisted image registration (automatically image registration), the details of these techniques are provided in Chapter 3.

Secondly, segmentation is also an image processing technique which is based on the features that are extracted from the image. It is a very complex process because it uses partitioning of an image into regions representing the different objects in the image.
This section contains a review of the literature related to image processing techniques, segmentation, registration and other image processing techniques.

A modified approach was suggested by Linh et al., (2003). They suggested registering a medical image in different modalities for the same object. This approach was based on acquiring information from two images and low-pass filtering and high-pass filtering to improve the quality of images. Histogram equalisation processing was used to enhance the images and the contrast was adjusted. They segmented the same features in a pair of image manually. These features were used to register the second image to the reference one.

Richard and Cohen (2003) reported a registration method for medical images. They tried to design an automatic tumour detection system for a computer aided diagnosis (CAD) by segmenting a pair of images (mammograms of left and right breasts of a women). The registration technique was based on segmenting the region of interest (i.e., breasts) through a thresholding procedure and matching the intensity-based approach for the ROI. This is not applicable/ reliable for complicated medical images. Additionally this system is very sensitive to the noise of image.

Other significant technique in image processing is segmentation (Banik et al., 2009). It also had a role in extracting features and detecting the face from the background as well as registration, which was mentioned earlier in Section 2.4. Here we will try to refer to the most popular segmentation methods used in the

medical field such as the thresholding; edge segmentation and region growing. These methods are used either separately or collectively.

Mehtre (1993) modified a segmentation method for fingerprint imaging based on a thresholding technique. The thresholding technique was used because the background regions of the fingerprint image generally exhibit a very low grey-scale variance value than the foreground regions. Therefore, segmentation can be achieved by thresholding technique. This technique was applied by dividing the image into several blocks and calculating the grey-scale variance for each block in the image by using intensity a histogram technique. If the variance was less than the global threshold, then the block was assigned to be a background region; otherwise it was assigned to be part of the foreground.

Instead of using the histogram to specify the threshold value in segmentation, Sonka et al. in (1993) suggested basing the thresholding technique on the concept of minimizing the variance between foreground and background elements. Although the method assumes two different grey levels, it works well even when the distribution is not bimodal. The approach uses an iterative process to find a threshold that minimizes the variance between the intensity values on either side of the threshold level. This method was modified by Semmlow (2004). He suggested improving the determination of the thresholding during the histogram. This method was based on calculating the histogram techniques after eliminating the edge boundaries of the image. Eliminating the edge boundaries can be achieved by using edge detection filters, either Prewitt or Sobel. The result produces a binary image which converts to a boundary mask by inverting the image. And then the multiplication operation between the original image and the boundary mask. The results of this method showed an improvement in the histogram and threshold value.

Various other segmentation approaches have been reported. Clarke et al, (1995) suggested the use of the region growing technique for segmenting the image. This approach was based for finding the regions that share some common characteristic features. Another approach to segment an image was suggested by Grau et al., (2004). They used the watershed segmentation algorithm. This

algorithm was achieved by dividing the image into several regions and then determining the local minima for each region.

To conclude, respiration is one of crucial human processes and it needs easy and accurate monitoring applications. The use of thermal imaging for monitoring respiration is promising and could be more convenient for both patients and health practitioners. However the use of the captured thermal images to monitor breathing is not straightforward and requires further processing before applying the measurement techniques. In the next chapter the image processing techniques used in this study will be discussed.

Chapter Three

3. A Review of Image and Signal Processing Techniques Used in This Study

3.1. Introduction

Digital imaging can be defined as the acquisition and processing of visual information by computer; it can be categorized into two fields:

- Image Processing
- Computer Vision

These two categories are not totally separate and distinct, since some operations which use image processing are also needed as an intermediate processing step in computer vision and vice versa.

Image processing can be considered as manipulation of an image in order to extract information from the image or to produce an alternative representation of the image. Most image processing operations can be categorized into two classes, either eliminating unwanted information that is corrupting the image such as removing noise, enhancement and threshold etc., or changing the form of images to extract more information, such as Fourier Transform, Wavelet Transform and Image Compressions. On the other hand Computer vision

operations aim to use computer techniques to extract, characterize and interpret the information of the images (Gonzalez et al., 2004).

Computer imaging can be integrated by the presence of a mathematical system which helps to process images using packages such as Matlab software, thus offering ease, consistency, support, and visualisation of the results (McAndrew, 2004).

Digital Signal Processing (DSP) techniques are also used in this study. These techniques are defined as the application of analogue or digital techniques to improve the utility of a data stream. Signal processing plays an important role in biomedical engineering applications because it improves the quality of diagnostic information (Jahne and Haubecker, 2000).

In this chapter there is information about various image processing techniques and mathematical operations which can be used to extract a respiration signal from thermal images, as well as giving a brief review of the concept of the signal processing techniques to enhance and calculate respiration rates. Section 3.2 provides an overview of the types of imaging systems. Image Data Types are explained in Section 3.3. Section 3.4 provides the basic concepts for an image. Image processing techniques which are used in this thesis are explained in Section 3.5. Section 3.6 focuses on Biomedical Signal Analysis techniques which are used to analyse the respiration signal.

3.2. Types of Imaging Systems

Imaging systems vary and can be defined and categorised according to their energy sources. The principle energy source for images is the Electromagnetic (EM) spectrum. Other important sources of energy include ultrasound, acoustic and electronic. Fig.3.1 (a) illustrates the images formed by using different types of energy emission in the electromagnetic spectrum. Fig.3.1 (b) illustrates examples of medical images which cover the electromagnetic spectrum (Gonzalez and Wood, 2002). The present work will focus on infrared imaging; the details of this type of image will be explained later in Chapter 4.

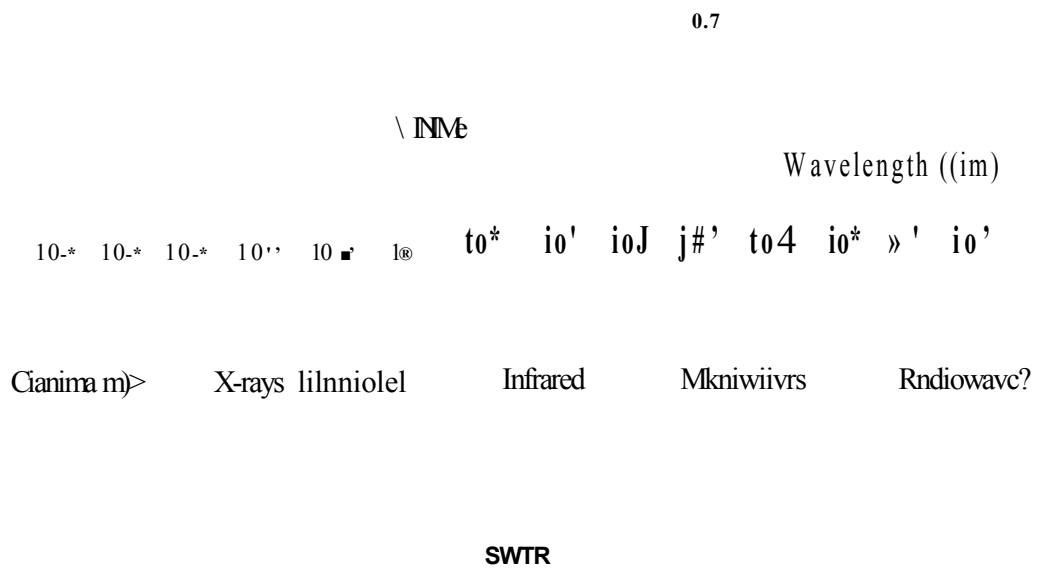

(a)

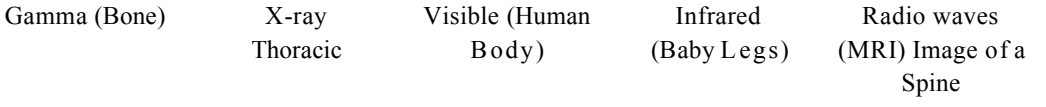

(b)

Fig.3.1: Medical spectra, (a) The electromagnetic spectrum includes the parts of Infrared spectrum, (b) Examples of medical images covering the electromagnetic spectrum (Gonzalez and Wood, 2002; NASA, 2007).

3.3. Image Data Types

There are different types of image data representation.

3.3.1. Binary Images

Binary images are the simplest type of image and can take two values, (0) and (1). 0 refers to black and 1 refers to white. A binary image is referred to as a 1 bit/pixel image because it takes only 1 binary digit to represent each pixel. Binary images are often created from gray-scale images via a threshold operation, whereby every pixel above the threshold value is turned white (1) and those below it are turned black (0) (Pratt,2007).

3.3.2. Gray-scale Images

Gray-scale images are referred to as monochrome or one–colour images. The number of bits used for each pixel determines the number of different brightness levels available. An image that contains 8 bits per pixel provides 256 (0-255) different (gray) levels (Pratt, 2007).

3.3.3. Colour Images

Colour images can be modelled as three–band monochrome image data, whereby each band of data corresponds to a different colour. Colour images are represented as red, green and blue, and a colour image has 24 bits per pixel, i.e. 8 bits for each of the three colour bands (R, G, B) (Pratt, 2007).

3.4. The Basic Concepts of the Image

A computer image is basically a matrix of pixels (2-dimensional array), where each pixel value is relative to the brightness of the corresponding point in the scene. The image matrix size is usually M by N pixels, where M is the number of rows and N is the number of columns. Therefore, an image can be defined as a function $f(x,y)$ where x and y denote spatial coordinates and f is the pixel value at that point. Therefore, the image can be regarded as a matrix, as shown in Fig.3.2 (Bankman, 2009).

$$f(x,y)=\begin{bmatrix} f(0,0) & f(0,1) & .... & f(0,N-1) \\ f(1,0) & f(1,1) & .... & f(1,N-1) \\ . & . & .... & . \\ f(M-1,0) & f(M-1,1) & .... & f(M-1,N-1) \end{bmatrix}$$

Fig.3.2: Image as a matrix of size $M \times N$ which is defined by function $f(x,y)$.

3.5. Image Processing Techniques

Image processing can be considered as a tool to change the nature of an image by using a computer in order to either improve its pictorial information for human interpretation, or to render it more suitable for autonomous machine perception (Bovik, 2000). Additionally, these techniques are very important in the medical field to improve the diagnostic process. In this section there is an explanation of most of the image processing techniques which are related to our study such as image enhancement, segmentation, histogram, feature extraction, subtraction, as well as image registration.

3.5.1. Image Enhancement Techniques

Image enhancement techniques are used to emphasize and sharpen image features for display and analysis. The principal objective of enhancement techniques is to process an image so that the resulting image is more informative than the original one. Enhancement techniques are carried out either as a preprocessing step to other imaging tasks or as post-processing to create a more visually desirable image. However, these techniques cannot be expected to insert any additional information that was not originally available.

Image enhancement includes highlighting, sharpening, or smoothing some features for display and/or further analysis. Therefore, it can be categorized into two general types. The first category is smoothing spatial filters and the second category is sharpening spatial filters. Spatial filters can be implemented by using a mask of size for example 3×3, 5×5 or 7×7 (Bankman, 2000).

3.5.1.1. Smoothing Spatial Filters are used for blurring and noise reduction. They select low frequency components and reduce high frequencies. An increase in the filter (or kernel) size leads to an increase in blurring of the image. Noise reduction can be accomplished by linear or non-linear filters. Smoothing filters are also known as low-pass filters (LPFs). Examples of smoothing filters are average filters, order statistical filters, and Gaussian filters. Examples of statistical filters include Maximum, Minimum and Median filters The filters commonly used for enhancing biomedical images are Median, Average and Gaussian filters (Bankman, 2009; Hashim et al., 2002).

3.5.1.1.1. The Average Filter is a linear filter used to reduce the intensity variation between neighbouring pixels. It operates on local groups of pixels called neighbours and replaces the centre pixels in these neighbours. This replacement is done with a convolution mask such as the following 3×3 mask below in Fig.3.3.

$$1/9\times\begin{bmatrix}1 & 1 & 1\\ 1 & 1 & 1\\ 1 & 1 & 1\end{bmatrix}$$

Fig.3.3: Average filter with the mask 3×3.

This has the effect of eliminating pixel values which are unrepresentative of their surroundings. The final value for the pixel at the kennel centre (the one being filtered) is obtained by multiplying each of the nine values including the pixel itself by 1/9 and summing the result, as indicated by Equation 3.1.

$$g(x,y)=1/N\sum_{(x,y)\in S} f(x,y) \qquad (3.1)$$

Where $g(x, y)$ is the filtered image, $f(x, y)$ is the original image before being filtered, S is the set of coordinating pixels in the neighbourhood of pixel(x, y) including the pixel(x, y) itself, and N is the total number of pixels in the

neighbourhood. All pixels included in the filter size are added up and the result is divided by the number of pixels (Gonzalez and Wood, 2002).

3.5.1.1.2. The Gaussian filter is a linear filter with a 2-D convolution operator that is used to blur images and remove noise by the Gaussian function that is expressed as:

$$G(x,y)= \frac{1}{2\pi\sigma^2} e^{-\frac{x^2+y^2}{2\sigma^2}} \qquad (3.2)$$

Where σ is the standard deviation and $G(x,y)$ is the filtered image with the Gaussian filter. Gaussian operation is similar to the average filter, but it uses a different kernel that represents the shape of a Gaussian. The degree of smoothing is determined by the standard deviation of the Gaussian σ . The Gaussian filter can be selected from 3 × 3 up to 7 × 7 kernel size. Fig.3.4 illustrates the Gaussian filter with the mask 3×3 (Gonzalez and Wood, 2002).

$$1/16\times \begin{bmatrix} 1 & 2 & 1 \\ 2 & 4 & 2 \\ 1 & 2 & 1 \end{bmatrix}$$

Fig.3.4: Gaussian filter with the mask3×3.

3.5.1.1.3. Order-Statistic Filters are non-linear filters; these filters are based on ordering the pixels contained in the image area encompassed by the filter, and then replacing the value of the centre pixel with the value determined by the ordering result. A Median filter is one of the most popularly used in biomedical imaging because it provides excellent noise reduction capabilities for random noise (Gonzalez and Wood, 2002). Therefore, it is used to reduce the noise rather than blurring edges. The idea of the median filter is to replace each pixel in the image by the median value of its neighbouring pixels. The median is based on the size of the kernel. The pixel values are sorted into their numerical order and then the considered pixel is replaced with the middle pixel value(s). With a kernel size of 3×3, the resulting value is the median, number 5 out of

the sorted list of 9 (Pratt, 2007). Fig 3.5 illustrates an example of applying the median filter to an image.

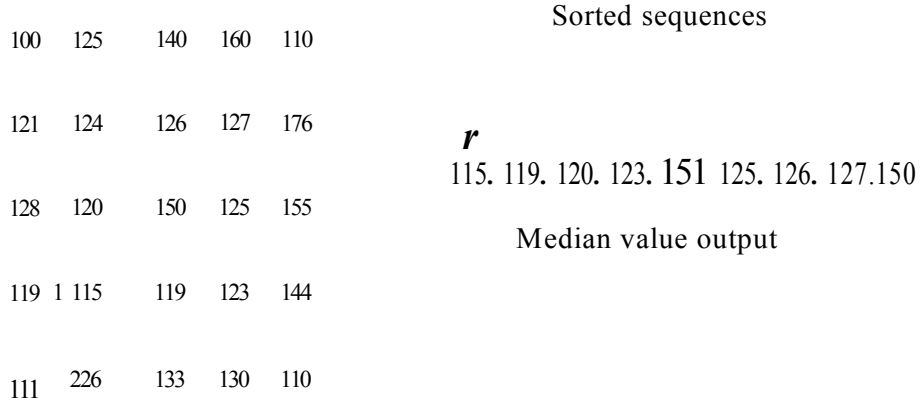

Fig.3.5: An example of the basic operation in median filtering.

Shown in Fig.3.5 is as an example of the 3x3 window neighbourhood values which includes: 124, 126, 127, 120, 150, 125, 115, 119, and 123. These nine values are then sorted. The value in location (9+l)/2 in the sorted list is the median. Hence the central pixel value of 150 is replaced with the median value of 124.

3.5.1.2. Sharpening Spatial Filters refers to the second type of image enhancement techniques that are used to highlight specific features in an image, such as edges or boundaries of objects, or for enhancing details which have been blurred through errors or an imperfect capturing device (Bovik, 2009). They are also used to pass the high frequency components and to reduce or eliminate the low frequencies. Image blurring can be implemented by smoothing filters; hence sharpening can be implemented by operators that invert smoothing operations. Sharpening filters are also known as a high-pass filters (HPFs). Examples of sharpening filters are Sobel, Prewitt, Gradient and Laplacian filters. The filters commonly used for sharpening biomedical images are Sobel, Prewitt and Laplacian (Hashim et aL, 2002; Baxes, 1994).

3.5.1.2.1. The Laplacian Filter is a linear spatial filter which can be selected from 3×3 up to 7×7 kernel sizes and uses a second derivative. The Laplacian of an image $f(x, y)$, denoted $\nabla^2 f(x, y)$ is defined as

$$\nabla^2 f(x, y) = \frac{\partial^2 f}{\partial x^2} + \frac{\partial^2 f}{\partial y^2} \tag{3.3}$$

Where $f(x, y)$ is the input image and $\frac{\partial^2 f}{\partial x^2}$ and $\frac{\partial^2 f}{\partial y^2}$ are second partial derivatives with respect to x and y, respectively.

The second derivative in the x-direction:

$$\frac{\partial^2 f}{\partial x^2} = f(x+1, y) + f(x-1, y) - 2f(x, y) \tag{3.4}$$

While the second derivative in the y-direction:

$$\frac{\partial^2 f}{\partial y^2} = f(x, y+1) + f(x, y-1) - 2f(x, y) \tag{3.5}$$

After the implantation of the second order derivative in Equation 3.3, is calculated as:

$$\nabla^2 f(x, y) = [f(x+1, y) + f(x-1, y) + f(x, y+1) + f(x, y-1)] - 4f(x, y) \tag{3.6}$$

This expression can be implemented for all points of the image by either of the two masks, as in Fig.3.6.

$$\begin{bmatrix} 0 & 1 & 0 \\ 1 & -4 & 1 \\ 0 & 1 & 0 \end{bmatrix} \qquad \begin{bmatrix} 1 & 1 & 1 \\ 1 & -8 & 1 \\ 1 & 1 & 1 \end{bmatrix}$$

Fig.3.6: Two kinds of 3×3 Laplacian operator masks; it is valid to use the opposite sign convention (Gonzalez et al., 2004).

Enhancement of images using the Laplacian filter is based on Equation 3.7

$$g(x, y) = f(x, y) + c[\nabla^2 f(x, y)] \tag{3.7}$$

Where $f(x, y)$ is the input image, $g(x, y)$ is the result of enhancement image and $\nabla^2 f(x, y)$ is the implementation of the Laplacian operator to the image; the value of c is 1 if the centre coefficient of the Laplacian mask is positive, otherwise it is -1.

All points (x, y) in an image are convolved with one of the following masks (Gonzalez and Wood, 2002).

$$\begin{bmatrix} 0 & -1 & 0 \\ -1 & 5 & -1 \\ 0 & -1 & 0 \end{bmatrix} \qquad \begin{bmatrix} -1 & -1 & -1 \\ -1 & 9 & -1 \\ -1 & -1 & -1 \end{bmatrix}$$

Fig.3.7: Two kinds of 3×3 Laplacian enhancement smoothing masks; it is valid to use the opposite sign convention (Gonzalez et al., 2004).

3.5.1.2.2.The Prewitt Filter is a linear spatial filter, which is used to enhance edges in all directions. It is implemented through using one independent convolution mask with the image. This filter can be used to emphasise the horizontal or the vertical edges by using a 3-by-3 filter. Fig.3.8 shows the two Prewitt masks in both horizontal and vertical directions. The details of the Prewitt operator will be explained later in Section 3.5.3.2.1.

Row Mask *Column Mask*

$$\begin{bmatrix} -1 & -1 & -1 \\ 0 & 0 & 0 \\ 1 & 1 & 1 \end{bmatrix} \qquad \begin{bmatrix} -1 & 0 & 1 \\ -1 & 0 & 1 \\ -1 & 0 & 1 \end{bmatrix}$$

Fig.3.8: The masks of Prewitt operator in both horizontal and vertical directions.

3.5.1.2.3.The Sobel Filter is a linear spatial filter that performs a similar operation to the Prewitt filter, though it uses different mask coefficients. This filter can be used to emphasise the horizontal or vertical edges by using a 3×3 filter (Gonzalez and Wintz, 1987). Fig.3.9 shows two Sobel masks, in both horizontal and vertical directions. The details of the Sobel operator will be explained later in Section 3.5.3.2.1.

Row Mask *Column Mask*

$$\begin{bmatrix} -1 & -2 & -1 \\ 0 & 0 & 0 \\ 1 & 2 & 1 \end{bmatrix} \qquad \begin{bmatrix} -1 & 0 & 1 \\ -2 & 0 & 2 \\ -1 & 0 & 1 \end{bmatrix}$$

Fig.3.9: The masks of Sobel operator in both horizontal and vertical directions.

3.5.2. Histogram

An image histogram is a plot of the distribution of intensities, or gray level values, in an image versus the number of pixels at that value (Gonzalez and Wood, 1992). The horizontal axis of this plot in the gray level images is in the range [0, L- 1], while the vertical bar represents the number of occurrences of each value in the image.

The shape of a histogram provides information about the nature of the image, or sub-image, if we are considering an object within the image (Bovik, 2009). In other words, a histogram describes the frequency of existence of pixels of the same intensity in a whole image, or in a sub-region of the image. The intensity of the histograms can be very helpful in selecting threshold values, not only for the original image, but for images produced by various segmentation algorithms. A thermal image histogram has the same concept, but is slightly different. The histogram represents a process which describes the variation of temperature in the image instead of the colour values. The intensity of the histogram shows the distribution of the temperature in all the entire images (Diakides and Bronzino, 2008). Fig.3.10 shows the histogram of a facial thermal image.

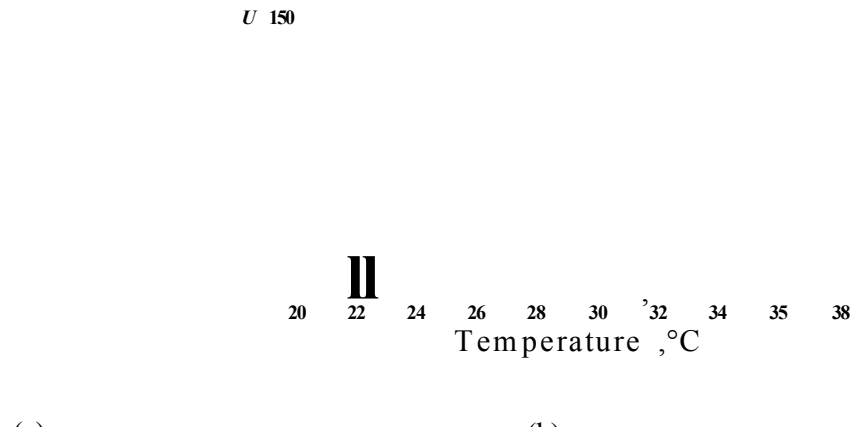

Fig.3.10: (a) A thermal image, (b) Its histogram.

3.5.3. Segmentation Techniques

Segmentation can be defined as a process of partitioning an image into regions representing the different objects in the image. These techniques are based generally on one of two basic properties: discontinuity and similarity.

Discontinuity represents sudden changes between the objects and the background in an image, while similarity refers to the homogeneity within an object or region in an image (Banik etaL, 2009).

Segmentation is an important tool in medical diagnosis as mentioned in Chapter 2. It is a necessary process to extract feature measurements and it provides richer information than that which exists only in the original image (Bovik, 2000).

The present study will focus on the segmentation techniques which separate the object from the background and also segment regions which are more affected than others by the respiration operation in order to calculate the respiration rate.

There are several methods that can be used in order to perform segmentation techniques. The most common techniques used in the present thesis are *Manual*

Segmentation and *Automatic Segmentation* which includes edge-based techniques, thresholding techniques and region-based techniques.

3.5.3.1. Manual Segmentation Technique

This technique is commonly used in the medical field for its simplicity and ease of implementation. This type of segmentation forces the user to select the interesting part of an image manually. This method is based on visual observation for the required area and the complexity of the shapes for the segmentation process (Banik et al., 2009). In this study, the region of interest (ROI) was initially selected manually to compute the respiration rate, as will be explained later in Chapter 6.

3.5.3.2. Automatic Segmentation Techniques

Automatic Segmentation can be classified into several methods which include threshold-based techniques, edge-based techniques, and region-based techniques (Banik et al., 2009). In this study, we focused on using edge-detection as well as thresholding techniques to identify the boundaries of the subjects from the image background.

3.5.3.2.1. Edge Image Generation Techniques

Edge detection is an automatic segmentation technique that can be defined as a process of transforming an input image into an edge maps which can be viewed as a line drawing image. The goal of edge detection is to find the boundaries of an object. It is based on the idea that the edge information in an image is found by looking at the relationship of a pixel with its neighbours (Banik et al., 2009). If a pixel's value is similar to those around it, there is probably not an edge at that point. However, if a pixel has neighbours with widely varying values, it may represent an edge point. In other words an edge separates two distinct objects. Ideally, these techniques are applied to images that have apparent edges caused by changes in colour or texture, or by specific lighting conditions being

present during the image acquisition process. There are many methods for conducting edge detection. The most common method for edge detection is to calculate the differentiation of an image. The first-order derivatives in an image are computed using Prewitt and Sobel; the second-order derivatives are obtained using the Laplacian.

• **Prewitt Operator** is a first-order derivative edge detection mask that looks for the edges in both the horizontal and vertical directions. It combines this information into a single metric. Its mask is shown by the image neighbourhood. Let the 3×3 area shown in Fig. 3.11 represent the values in a neighbourhood of an image. One of the simplest ways to implement a first-order partial derivative at point Z_5 is to use the following Prewitt cross-gradient operators in Equations 3.8 and 3.9

$$\begin{bmatrix} Z_1 & Z_2 & Z_3 \\ Z_4 & Z_5 & Z_6 \\ Z_7 & Z_8 & Z_9 \end{bmatrix}$$

Fig.3.11: A 3×3 area of an image.

$$\text{Row mask} \quad G_x = (Z_7 + Z_8 + Z_9) - (Z_1 + Z_2 + Z_3) \tag{3.8}$$

$$\text{Column mask} \quad G_y = (Z_3 + Z_6 + Z_9) - (Z_1 + Z_4 + Z_7) \tag{3.9}$$

Fig.3.8 illustrated the two masks for the Equations 3.8 and 3.9 as each one is convolved with the image to produce the first order derivatives G_x and G_y. At each pixel location, there are two numbers: G_x corresponding to the results from the row mask and G_y corresponding to the results from the column mask.

The gradient of an image *f(x,y)* at location *(x,y)* is defined as the vector

$$\Delta f = \begin{bmatrix} G_x \\ G_y \end{bmatrix} = \begin{bmatrix} \frac{\partial f}{\partial x} \\ \frac{\partial f}{\partial y} \end{bmatrix} \quad (3.10)$$

An important quantity in edge detection is the magnitude of this vector, denoted Δf; it is computed by Equation 3.11

$$\text{Edge Magnitude} \quad \Delta f = \sqrt{G_x^2 + G_y^2} \quad (3.11)$$

Another important quantity is the direction of the gradient vector; it is computed by Equation 3.12 (Gonzalez and Wood, 1992)

$$\text{Edge Direction} \quad \alpha(x, y) = \tan^{-1}\left[\frac{G_y}{G_x}\right] \quad (3.12)$$

• **Sobel Operator** is another first-order derivative edge detection mask that is commonly used due to its simplicity and speed. This edge detection mask is similar to the Prewitt, but with different mask coefficients: it looks for the edges in both horizontal and vertical directions as in the row and column masks represented in Equation 3.13 and 3.14

$$\text{Row mask} \quad G_x = (Z_7 + 2Z_8 + Z_9) - (Z_1 + 2Z_2 + Z_3) \quad (3.13)$$

$$\text{Column mask} \quad G_y = (Z_3 + 2Z_6 + Z_9) - (Z_1 + 2Z_4 + Z_7) \quad (3.14)$$

These Equations are represented by two masks as shown in Fig.3.9.The edge magnitude and the edge direction are then found in a similar way to the Prewitt operator by using Equations 3.11 and 3.12 (Gonzalez and Wood, 1992).

• **Laplacian Operators** The Laplacian of a 2-D function *f (x, y)* is a second-order derivative as defined in Equation 3.3. They are applied by selecting one

mask and convoluting it with the image. There are two digital approximations to the Laplacian for a 3×3 region:

$$\Delta^2 f = 4z_5 - (z_2 + z_4 + z_6 + z_8) \tag{3.15}$$

Or

$$\Delta^2 f = 8z_5 - (z_1 + z_2 + z_3 + z_4 + z_6 + z_7 + z_8 + z_9) \tag{3. 16}$$

Where the Zs are defined in Fig.3.11, masks for implementing these two equations are shown in Fig. 3.6.

3.5.3.2.2. Thresholding Techniques

Thresholding is a common region segmentation method which is based on selected threshold values T_s that can segment the image into two or more regions. Several thresholding techniques have been developed. Most of them depend on an image histogram; others depend on local properties such as the standard deviation or the local gradient. The most popular approach is global usually called the normal thresholding technique. This approach can be applied when only one threshold value T is selected for the entire image, based on the image histogram. This technique is used to convert the image into a binary, i.e. the pixel value is either one or zero depending on the threshold value selected (Russ, 2007; Weszka, 1978).

In this study, thresholding was applied to extract the facial thermal image from the background, i.e., pixels with a value lower than the threshold (T) represented the image background and were set to zero, while the other pixels, with a value equal or greater than the threshold, represented the facial regions. This is shown in Equation 3.17.

$$g(x,y) = \begin{cases} Zero & if \quad f(x,y) < T \\ f(x,y) & if \quad f(x,y) >= T \end{cases} \tag{3.17}$$

Where $g(x,y)$ is the thresholded image and $f(x,y)$ is the original image, T is the threshold value. Any pixel with temperature $f(x, y)>= T$ is assigned as foreground; otherwise the pixel is assigned as background.

Another type of thresholding segmentation is the local threshold. This type of threshold is applied when both the object and the background vary throughout the image. In some cases the global threshold is not very helpful as it will not extract the complete image from the background. In such cases local or adaptive thresholding is used by selecting more than one threshold for the entire image. This is achieved by breaking the image into more than one piece and then into individual thresholds (Haralick and Shapiro, 1985).

3.5.4. Subtraction Technique

This is another image processing technique which is based on the mathematical subtraction method. This technique is applied to images that have similarities between them. It is used either to enhance the difference between two images or to remove common background information from images of identical scenes. Furthermore it can be used to determine the object motion between two images for the same scene. The resulting image contains only the differences between images and removes the constant information. Equation 3.18 shows the implantation of the subtraction technique to the images.

$$g(x,y) = I_1(x,y) - I_2(x,y) \tag{3.18}$$

Where $g(x,y)$ represents the resulting image of the subtract method between the first image $I_1(x,y)$ and the second image $I_2(x,y)$. Images that have different scenes, or are captured in very different conditions or have a significant motion, may need to be registered (Baxes, 1994).

3.5.5. Features Extraction Technique

This technique is applied by selecting the common features from the images by finding the relationship between them. The concept of features for image processing is represented as an interesting part of an image, or can be defined as the important information which represents, for example, an edge or corner (Nixon and Aguado, 2008). In this technique it is useful to segment the image by determining some of its specific properties or features of its pixels (Dhawan et al., 2008). The most difficult and critical steps within the images are extracting the features. In this study we used these techniques to find common facial features in order to calculate the respiration rate.

Features can be categorised automatically into three types as follows:

3.5.5.1. ***Visual Features:*** which include the known features found by human or logical design. This type of feature can be classified into two types:

- *Low-level features*: this level represents the basic features that can be extracted automatically from an image without any shape information, such as corner detection, pixel, line and curvature.
- *High-level features:* in this level, the feature extraction concerns either finding shapes in computer images, such as major facial shapes including the eyes, ears, nose and mouth, or can be represented as a basic geometric shape in the image such as circle, triangle, rectangle or square (Nixon and Aguado, 2002; 2008).

3.5.5.2. ***Statistical Features:*** once the regions are segmented in the image, the values of pixels within the region can be used for statistical computation

- *Averaging*: also called the mean. The image mean is the average pixel value of an image. This feature can be applied either to the whole image or to certain parts of it by using the Equation 3.19

$$\mu = \frac{1}{n}\sum_{i=1}^{n} x_i \qquad (3.19)$$

Where μ is the mean value, n represents the number of pixels in the region or image and x_i is the value for each pixel (Nixon and Aguado, 2002; 2008).

- *Distribution:* this type of feature can be extracted from either the whole image or one or more parts. It can be represented by using histogram techniques, as mentioned previously in Section 3.5.2.

3.5.5.3. *Facial Physiological Features*: A thermal facial image is characterized by a particular type of property which makes it different from other images. The blood flow in the vessels creates a large, substantial convective heat effect that appears in the thermal imagery (Bronzino, 2006). The variance of blood flow in these vessels creates spatial physical features for the facial thermal image which are represented by several hot and cold regions in the face. The higher temperature areas of the face are represented by the periobital region (the two areas between the bridge of nose and the inner corners of the eyes), forehead and the corners of the mouth, while the lower temperature areas are represented by the nose, earlobes and cheeks. The reasons for these cooler areas are the lower blood supply and also higher exposure to the ambient environment allowing a convection effect (Diakides and Bronzino, 2008; Pavlidis et al., 2005; Sheskin, 2004). In this study, once the face region is extracted from the rest of the image, features extraction can be applied to extract the ROI, the region representing the area between the tip of the nose and the upper lip of the mouth.

3.5.6. Geometric Transformations Techniques

Another image processing technique is Geometric Transformations. This gives the facility to change the location of pixels within an image by using a mathematical transformation. The pixels are relocated from *(x, y)* coordinates in the input image to the (x',y') coordinates in the output image (Baxes, 1994). These transformations are used for correcting geometric distortion in an image as well as being used in image registration techniques. There are two types of

geometric transformations in the spatial domain, such as Affine Transformation and Projective Transformation (Hajnal et al., 2001).

3.5.6.1. Affine transformations: this type of geometric transformation is more commonly used than others. In these transformations the straight lines remain straight and parallel lines remain parallel, but the rectangles might become parallelograms. These transformations include translation, rotation and scaling. This type of transformation needs three points, as shown in Fig.3.12 (Semmlow, 2004).

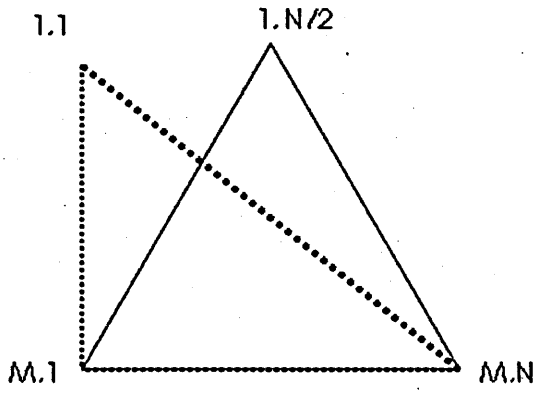

Fig.3.12: The affine transformation. The solid line represents the three input points in the image while the dashed line defines the three output points in the same image M and N are indicated in this figure as the row and column of the image.

3.5.6.2. Projective transformation: this type of geometric transformation also includes translation, rotation, and scaling. In these transformations the straight lines remain straight but parallel lines converge towards the vanishing points (Semmlow, 2004). This type of transformation needs four points, as shown in Fig.3.13.

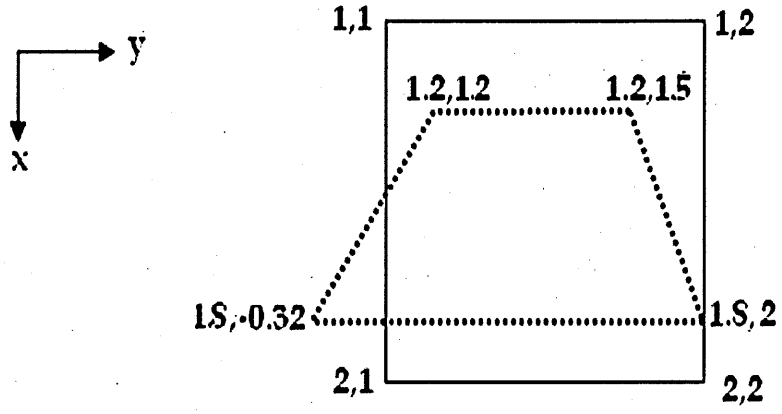

Fig. 3.13: The projective transformations. The solid line represented the input quadrilateral while the dashed line defines the desired output quadrilateral.

Geometric Transformations can rotate an image, enlarge and shrink it, and move it in different directions. The operations that can be introduced are explained in the next sections.

• ***Translation image***: translates the image in different directions. An x value defines the amount of up or down direction while a y value defines the amount of left or right directions. Equations 3.20 and 3.21 illustrate the translation equations for an image

$$x' = x + T_x \tag{3.20}$$

$$y' = y + T_y \tag{3.21}$$

Where x and y represents the coordinates of the input image, and T_x specifies the displacement along the x axis, T_y specifies the displacement along the y axis, while x' and y' represented the coordinates of the output image.

• ***Scaling image:*** This enlarges and shrinks an image. An x value defines the amount of x direction scaling, while a y value defines the amount of y- direction scaling. Equations 3.22 and 3.23 illustrated the scaling equations for an image.

$$x' = x \times S_x \tag{3.22}$$

$$y' = y \times S_y \tag{3.23}$$

Where S_x scale factor along x, S_y scale factor along y.

• ***Rotation image***: spins images about the centre point. The coordinate transformation equations for image rotation are

$$x' = x\cos\theta + y\sin\theta \tag{3.24}$$

$$y' = -x\sin\theta + y\cos\theta \tag{3.25}$$

θ Specifies the angle of rotation maximized (Goshtasby, 2005; Zaitova and Flusser, 2003).

3.5.7. Registration (Alignment) Techniques

Image registration is one of the image processing advance techniques that can be used to correct the geometric difference between two or more images. This task has become very important in medical imaging; it is useful for comparing images taken of the same structure at different times, from different viewpoints, and/or by different sensors. The registration geometrically aligns two images (the reference and input images). Image registration can be classified into two general types (Semmlow, 2004).

The first type is *interactive registration* (manual image registration) where humans help the registration process by selecting Control Points (CP) between the image pairs using visually clear features such as line intersections or corners. This method has some limitations: it is very time consuming to select the CP, and this type of registration needs an operator knowledgeable in the application domain to choose the CP in both images. Furthermore it is a repetitive task if there are number of images to register.

The second type is *unassisted image registration* (automatic image registration) where an algorithm generates the alignment which can be applied without human intervention. This method is more affected to registration number of images. Moreover it gives less time to register the images. This method also has

some limitation due to the difficulties in detecting the best way to select the CP automatically (Zaitova and Flusser, 2003; Hajnal et al., 2001).

Image registration procedure usually consists of five steps.

- **Pre-processing images** to prepare the two images for features extraction. This step can be applied by using image enhancement techniques, as mentioned in Section 3.5.1.

- **Choosing the control points in the images** can be applied either manually or automatically. This step can represent salient and distinctive features as mentioned in Section 3.5.5.

- **Feature matching** using the correspondence between the features detected in the reference and input images. Techniques used for this purpose include cross correlations or other statistical measures.

- **Determination of the Transformation Function** the appropriate transformation functions are applied to obtain the transformation coefficients such as affine transformation or projective transformation.

- **Re-sampling,** the last step of image registration, is achieved by using the transformation coefficients to transform the input image to the reference image in order to obtain the register image.

In general, image registration can be considered as a pair of images, for example M_1 *and* M_2, and then finding the similarity measures $S(M_1, M_2)$ to determine the optimal transformation T such that $S(T(M_1, M_2))$ is maximized. This helps to increase the correlation between M_1 and M_2 (Goshtasby, 2005; Fonseca and Manjunath, 1996). The correlation coefficient (ρ), obtained using Equation 3.26, for the two images.

$$\rho = \frac{\sum\left(x-\bar{x}\right)\left(y-\bar{y}\right)}{\sqrt{\sum\left(x-\bar{x}\right)^2 \sum\left(y-\bar{y}\right)^2}} \qquad (3.26)$$

The variables x and y represent the images and $\bar{x}$ and $\bar{y}$ are their respective means.

In this study we tried to align the images with the reference (the first image in the video) to deal with the problem of head movements, and to specify the ROI to compute the respiration rate.

3.6. Biomedical Signal Analysis techniques

Biomedical signals emanate from living bodies. These vital signals give much information to probe the state of the body. The measurement techniques for these signals provide clinicians and researchers with an interpretation for significant diagnoses.

The signals detected are commonly affected by noise; therefore it is difficult to extract information from a raw signal before it is processed. Signal processing techniques are used to remove noise and enhance the signal (Bronzino, 2006). Signals can be processed in either the time domain or the frequency domain. Some types of information are most evident from the time domain representation of a signal, for example, to detect if the signal is periodic or random, and also easily to calculate additional values for the signal, such as mean, standard deviation or variance. On the other hand, there is other information that can be extracted from the frequency domain, such as the frequency content of the signal (Stranneby and Walker, 2004).
The data used in the current study analysis is in the time and frequency domain. Therefore, the following section gives a brief description of signal processing techniques. Signal enhancement in the time domain is provided in Section 3.6.1. Section 3.6.2 gives an overview regarding the frequency domain.

3.6.1. Signal Enhancement

An important step in signal processing techniques is cleaning the signal from noise without losing important features or distorting the signal. The main types

of filters which are used to enhance the signal are Low-Pass Filters, High-Pass filters and Band-Pass Filters (Madisetti et aL, 1999).

The respiration thermal signal is very weak (Murthy et aL, 2004) and also suffers from a high frequency noise component. To process the signal, we used Low-Pass Filters (LPF) to reduce these high frequency components. Specifically, we used the Butterworth digital filter (Smith, 2003).

The Butterworth filter, also known as a maximally flat magnitude filter, meaning that there is no ripple in the passband, is one of the most common filters in digital signal processing. Its main advantage is that it has a flat pass band and provides a good roll-off (Stranneby and Walker, 2004). Butterworth can be implemented by using Equation 3.27

$$M(w) \quad 1 \qquad (3.27)$$

Where, $H(w)$ is the transfer function, n is the filter order, w is angular frequency and c is the cutoff frequency (Bianchi and Sorrentino, 2007).

The filter used in this study had a cutoff frequency of 1.5 Hz; its order was 5. Fig.3.14 illustrates the magnitude response of this filter.

Frequency , Hz

Fig.3.14: The Butterworth filter of order 5 and cutoff =1.5.

3.6.2. Frequency-Time Analysis

Time-frequency analysis is the study of how the frequency of a signal changes over time. It is used to detect and extract information related to the frequency of a signal and the time; that means it refers to the frequencies present in the signal at any given time. A thermal respiration signal is quasi-periodic in nature. Therefore this signal can be processed and analysed by this technique.

3.6.2.1. Discrete Fourier Transform (DFT) This operation can be used to convert the signal from the time domain into a set of points in the frequency domain. The input to the DFT is a set of N values. This algorithm requires a considerable time, and computation, if N is very large. The DFT algorithm is applied to the input signal by using Equation 3.28.

$$X(k) = \sum_{n=0}^{N-1} x(n) e^{-\frac{2j\pi}{N}kn} \quad , \qquad k = 0,1,2,.....,N-1 \qquad (3.28)$$

Where $x(n)$ denotes the input signal at time (sample) n, $X(k)$ denotes the kth spectral sample (output signal), N is the number of sample value and $j=\sqrt{-1}$ is the basis for the complex (Smith, 2008). To shorten the duration of the computation of the respiration rate in the discrete domain, Fast Fourier Transform is used.

3.6.2.2. Fast Fourier Transform (FFT): This is an efficient implementation of a discrete (DFT) algorithm to convert a signal from the time domain into a set of points in the frequency domain. This algorithm can be applied if N is even and can be represented as a power of 2, such as ($N=2^M$).

This algorithm is used to reduce the computation time that is needed to convert the signal from the time domain into the frequency domain. An FFT algorithm gives the same results as the DFT but more quickly. Computing the arithmetical operations for the DFT takes (N^2) while an FFT can compute the same result in only ($N \log N$) operations. Therefore, the differences in speed will be evident when dealing with long data, where N (the total number of points) is very large

(Smith, 2008). The periodicity of the FFT signal is caused by its symmetry. Eliminating repetition in data can be achieved by taking the first half of the magnitude values, which means taking the information from 0 to $N/2$.

3.7. Conclusion

Image processing techniques play a significant role in medical analysis. At the same time, signal processing techniques are useful to integrate the analysis of data and medical diagnosis. In this chapter we tried to clarify the details of image processing techniques which included enhancement, segmentation, registration and features extraction, as well as a brief description of the signal processing techniques which are used in the present thesis.

Chapter Four

4. Relevant Thermal Imaging Theory

4.1. Introduction

Thermal imaging is a technique used to convert thermal radiation patterns that are invisible to the human eye into visible images. Thermal imaging can be considered as passive technique that requires no external sources of illumination. This allows day and night operations. The technique is ideally used to detect hot and cold surface, or to detect areas of different emissivities. Thermal radiation can penetrate smoke or mist more than visible radiation, and allows the visual detection of obscured objects. It can be performed in real time and is valuable for remote sensing technique (Burnary et al., 1988).

Thermography is an emerging and exciting branch of image processing. This branch has advanced considerably in the industrial, medical, scientific fields amongst others. In this chapter the most relevant thermal imaging techniques are described. An overview of the main principles of infrared radiation and the type of noise affecting is provided. The chapter finally provides an overview of thermal cameras and the ThermaCAM™ Researcher Software which is used to analyse thermal videos.

4.2. Basic Concepts

Objects are continually emitting infrared radiation at a specific rate and specific wavelength. This depends on the object's temperature (T) and object's spectral emissivity (ε). Thermal imaging is a conversion of this radiation into visible images (Burnary et al., 1988). The infrared radiation spectrum refers to

wavelengths from 0.7-14 μm of the electromagnetic spectrum, as described in the Chapter 3. It is one portion of the electromagnetic waves that lies between the visible and microwave portions. It is usually divided into four spectral regions

- Near infrared light (NIR) is close in wavelength to visible light. This corresponds to the wavelengths ranging from the wavelengths ranging from 0.76 to 1.1 μm.
- Short wave infrared light (SWIR) has wavelengths ranging from 1.1 to 2.5 μm.
- Middle wave infrared (MWIR). This corresponds to the wavelengths ranging from 2.5 to 6.0 μm.
- Long wave infrared (LWIR) is closer to the microwave region of the electromagnetic spectrum, the wavelengths is 6 to 14 μm (NASA, 2007; Levi, 2007).

Both NIR and SWIR wavelengths regions rely on reflected solar radiation and can only be used in daylight or illuminated conditions (Burnary et al., 1988). On the other hand the two longer wave regions (MWIR) and (LWIR) are where thermal imagers detect the thermal emission from observed objects in total darkness or daylight. Every object whose temperature is more than absolute zero, i.e. more than 0 K or more than -237.15 ° C emits radiation that falls in the infrared region of the electromagnetic spectrum (Thermal imaging, 2009).

When the thermal radiation reaches another surface (W) it is called the radiosity. Part of the radiation energy is absorbed and represents the emissivity of the surface (W_E); another portion is reflected from the surface (W_R), while another portion is transmitted from the surface (W_T) if the body is not opaque.

The total radiation as shown in Fig.4.1 consists of the summation of three components which add up to the initial value of radiation that left the source and is described by Equation 4.1 (Merchant and Manager, 2009).

Total radiosity = $W E$ -h $W R$ -+- $W r$ (4.1)

Incident Radiation

Transmission

Reflection

Surface

Fig.4.1 : Total radiation of incident radiation by a surface.

A surface can be categorised into either blackbody or non blackbody (Burney et aL, 1988). A blackbody does not mean black in colour but is a term which describes an object which can absorb all incident radiation which falls on it. Therefore it is a perfect emitter of maximum infrared energy for a given temperature. A non blackbody would absorb less energy than a blackbody under similar conditions and hence would radiate less infrared energy even though it was at the same temperature (Williams, 2009).

The radiative (the number of photons emitted) and the wavelength distribution are given by laws of thermal radiation. There are two physical laws (Planck's Blackbody and the Wien's displacement law) which are used to define and measure the emission of infrared energy from a surface (Al-Azzawi, 2007).

The Planck's Blackbody Radiation Law (Burney et aL, 1988) gives the level of radiation within a body which can be expressed in the mathematical formula derived by Plank. It described by Planck's blackbody radiation law as shown in Equation 4.2

(4.2)

A *e ^ - 1*

Where $M(A,T)$ is the black body radiation emitted at temperature T (Kelvin), X is the wavelength in $/m$, $cx = 3.7411 \times 108[watt \times jam^* / m2]$ and $c2 = 1.4388 \times 104$ [/zra x , 7' is the temperature of the blackbody cavity [in Kelvin, K]. The distribution of energy across a portion of the infrared spectrum is shown in Fig.4.2. The curves in the graph have been constructed using Planks Law.

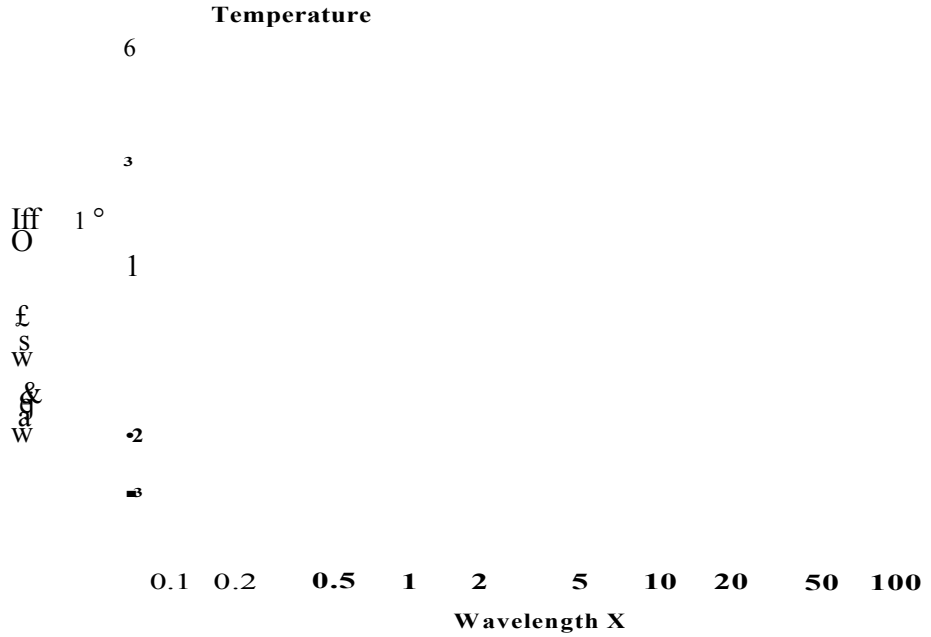

Fig. 4.2: Distribution of Radiated Energy from blackbody at various temperatures (Pandya, 2009).

Fig.4.2 shows that higher temperature of blackbody increases the amount of energy emitted at any wavelength. The peak emission values shifts towards the shorter wavelengths. The mathematical manipulation of Wien's law can describe the relationship between the wavelength at which peak energy occurs for a given object temperature (Al-Azzawi, 2007).

The Wien's Displacement Law gives the wavelength where the peak radiation occurs at a given temperature. Wien's Law is stated as:

$$\lambda_{max} = \frac{B}{T} \tag{4.3}$$

Where λ_{max} is the wavelength in μm at which the maximum energy is emitted by a black body at temperature T (Kelvin). B is the Wien's displacement constant has a value of 2897 μm K, and T represents the surface temperature in °K. Wien's displacement law can be used to calculate the wavelength from any object at different temperature (Pandya, 2009).

4.2.1. Sensitivity and Resolution

The two influential parameters in thermal image quality are thermal sensitivity and pixel resolution. Each one has a significant impact on thermal image quality. Good sensitivity sensors can detect temperature differences and increase the contrast of the image in the camera. Thermal sensitivity changes with object temperature. When the object temperature increases the effect will be to increase the signal output of the detector. This is the reason why viewing hotter images is easier.

The sensitivity parameter is very important in medical diagnosis because good sensitivity gives a better quality image to detect variations in temperature caused by tumors or other types of diseases (Dorf, 2006).

The second major parameter that impacts on image quality is the temperature resolution. IR is identical to the number of colours in a computer display or colour photograph. The resolution of the camera is determined by the size of the image or pixels count. There are three resolution standards; Low Resolution 160×120 (19,600 pixels), Medium Resolution 320×240 (76,800 pixels) or High Resolution 640×480 (307,200 pixels). Just like a digital camera, the greater the number of pixels, the better the resolution and the sharper the infrared image (Understanding Infrared Camera Thermal Image Quality, 2008). An ideal resolution gives the camera the facility to detect difference in temperature. Moreover, it gives a significant improvement in image quality and the ability to zoom in on a scene while maintaining good image quality. The most popular camera in medical diagnosis takes 320×240 pixels; the performance of this type

of resolution is equal to the performance of a 640×480 resolution and is less expensive. The priority in medical field is a camera with good sensitivity as well as resolution (Dorf, 2006).

4.2.2. Thermo-graphic Measurement Techniques

The radiation emitted from the object can be considered as a tool to make the camera able to detect and display the temperature. However, the radiation measured by the camera does not represent the temperature of the object only, but the emissivity of the object as well. There are several parameters that affect the accuracy of measuring temperature. These include emissivity, atmospheric transmission, reflected apparent temperature and distance.

4.2.2.1. Emissivity

An important object parameter for accurate thermal measurement is emissivity. It can be defined as a measure of radiation that is emitted from an object, as compared to the blackbody at the same temperature. Equation 4.4 defines the emissivity.

$$\varepsilon = \frac{\text{Radiation Emitted by Target object at Temperature (T)}}{\text{Radiation Emitted by Black Body at Temperature (T)}} \qquad (4.4)$$

The ideal sources of infrared energy are the black body, thus infrared thermometers are calibrated in terms of black body radiation. Practically there are no ideal emitters of infrared. Although an object has the same temperature as the black body, it tends to radiate less energy than a black body. Fig.4.3 shows the reflected energy when moved toward the surface. Emissivity's value is between [0, 1]. The variance in this value relates to several factors, such as the degree of surface roughness, surface shape (cavities and concavities increase the value), viewing angle and the temperature itself.

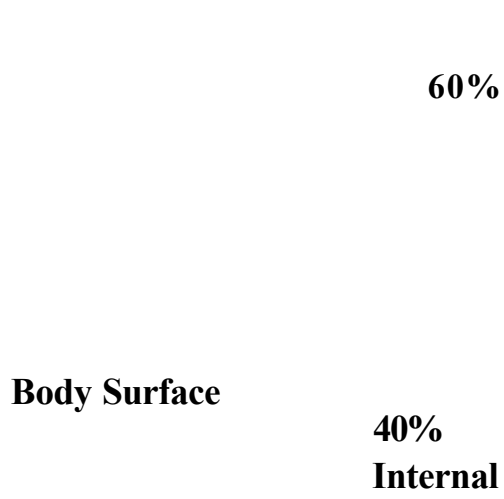

Fig.4.3: The diagram of emitters of infrared energy for an object (Burnay et aL, 1988).

When an opaque object Emissivity + Reflectivity =1.0. The object that is non reflective such as asphalt, would have a high emissivity while in contrast a highly reflective material, such as rolled aluminum, would have a low value of emissivity. Therefore, there is an inverse relationship between the emissivity and reflectivity (Diakides and Bronzino, 2008).

The human skin behaves like a blackbody. The high emissivity value of human skin makes it to have the same properties as the blackbody. Observations in different studies (Otsuka et aL, 2002; Diakides and Bronzino, 2008) confirmed that the emissivity of human skin is approximately in the range from 0.92 to 0.99.

4.2.2.2. Atmospheric Transmission

Infrared radiation from a target surface needs to pass through a transmission medium to reach the infrared lenses. When a perfect vacuum is available no energy is lost, otherwise the atmosphere attenuates the radiation in two processes, scattering and absorption. Scattering is a phenomenon that causes a change in the direction of a beam of radiation and is also caused by the absorption and subsequent re-radiation of energy by suspended particles.

Light mist and smoke have a small effect on infrared wavelengths. Infrared radiation can penetrate mists and smoke better than visible radiation. However, rain, fog and aerosols have larger particles and consequently scatter infrared and visible radiation to a similar degree (Burney eta1, 1988).

Some parts of the infrared region of the spectrum are not usable for imaging systems due to atmospheric attenuation, such as the absorption properties of $C\ 0\ 2$ (carbon dioxide), $H\ 20$ (water), and $0\ 3$ (ozone), which caused poor transition of infrared radiation as shown in Fig.4.4.

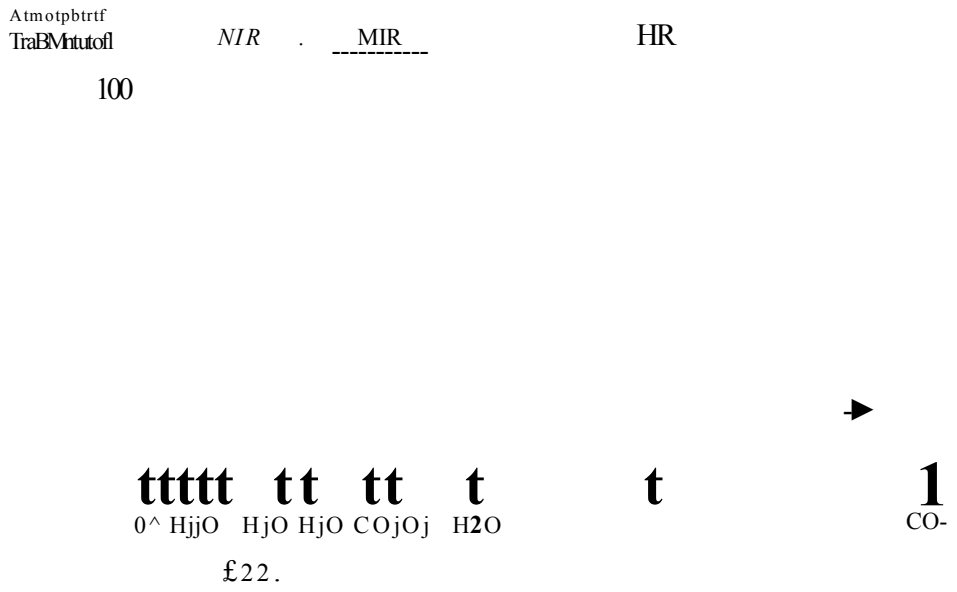

Fig.4.4: Transmission spectrum of the atmosphere (Thermal imaging, 2009).

Wavelength bands with good atmospheric transmission are in the range 8 to 14 fim (LWIR) which offer very good visibility for most terrestrial objects as does in the range of 3 to 6 $/im$ (MWIR) with the added benefit of lower ambient background noise. While 0.35 to 3 jum (visible, NIR and SWIR) rely on illumination to provide good imagery of objects at room temperature. Therefore the best transmission is between typically 3 to 6 jum and 6 to 14 jum respectively. Ranges of wavelengths are known as a window. Infrared imaging devices are designed to operate in one of these two windows (Thermal imaging, 2009; Gabbott, 2008).

4.2.2.3. The Reflected Apparent Temperature

The other important object parameter for accurate measurement is the reflected apparent temperature. It expresses all heat sources impinging on the scene we aim at, which are reflecting in the direction of camera. In other words it is all the reflected temperature from the surrounding objects received by the camera and is called Reflected Apparent Temperature as shown in Fig.4.5.

Fig.4.5 : The Reflected Apparent Temperature with Emission.

4.2.2.4. Distance

Distance is an important parameter between the object and the front lens of the camera. When the radiation from the target is absorbed by the atmosphere, because of the effects of atmospheric gases, the greater distance between the object and camera, the greater the loss of the energy and error in temperature reading (Bumay et aL, 1988).

4.3. Thermal Images

Thermography is the conversion of radiated or reflected heat into real-time pictures or images. Thermal imaging is the technique of using a special camera designed to detect heat emission by way of Infra Red (IR) energy waves. Unlike light waves, IR is invisible to the naked eye. The scale in thermal images shows

the hotter parts of an object in whiter shades while the darker shades are given to the cooler parts. These images can be mapped into pseudo colour where red typically refers to the hot regions while the blue refers to the cool regions of the objects. This representation can easily be reversed in many devices by reversing the setting of the device (Diakides and Bronzino ,2008). If there is no temperature difference the infrared image does not show any contrast and there is no possible analysis. The temperature value of the pixels gradually increases or decreases in the same frame of the thermal image means there is no sudden change in temperature values of the neighboring pixels. Therefore, the boundary lines, or the edges of objects, are not greatly visible (Scribner et al., 2000).

4.4. Noise of Thermal Images

Images generated by a thermal camera are generally low in contrast and are sensitive to different kinds of noise, some of which can be corrected while others are incorrect able.

The noise in the raw thermal images can be considered as undesired information which contaminates the image. The infrared images are corrupted with two types of noise sources. These are temporal noise and spatial noise.

The spatial noise is more or less static between frames. It can be seen as a fixed pattern in each frame and is usually referred to as fixed pattern noise (FPN). FPN is the dominant noise source in most infrared systems. The main cause of FPN is imperfections in the detectors. Each detector can show significant differences in temperature and noise. The differences are caused by the fact that individual detector elements respond differently to incoming irradiance which is perceived in images as a superimposed pattern, approximately constant from frame to frame. A non-uniformity correction (NUC) process can efficiently cancel out FPN. This process is one of the tools which improve the image quality (Understanding Infrared Camera Thermal Image Quality, 2008).

Thermal imaging suffers mainly from temporal noise, which may change from frame to frame, and can be caused by electronic noise. This type of noise includes

temperature fluctuation noise, background noise or thermal noise, commonly known as Johnson noise or Gaussian noise.

Background noise is caused by statistical fluctuations of the radiation inside the camera. This noise is independent of the performance of the detector and is not correctable.

The fundamental limit is set by temperature fluctuation noise which results from the random exchange of energy between the detector and its environment (Williams, 2009; Kruse and Skatrude, 1997).

Noise is often modeled by an additive Gaussian (thermal) distributed noise. This means that each pixel in the noisy image is the sum of the true pixel value and a random Gaussian distributed noise value. As the name indicates, this type of noise has a bell shaped probability distribution function, given by

$$(f > - m y$$

Where g represents the gray level, m is the mean or average of the function and o is the standard deviation of the noise. Graphically, its probability distribution histogram is represented as shown in Fig.4.6 (Bovik, 2000).

Noise Intensity

Fig.4.6: Probability distribution histogram of Gaussian distributed noise (Bovik, 2000).

Some detectors are designed to reduce Johnson noise and the temperature fluctuation noise. In the final analysis it is unimportant which noise mechanism dominates, provided the total noise is the minimum for a given responsively.

The camera used in our study was the ThermoVision A40 that uses an amorphous silicon detector 320 ×240 pixels focal plane array. The detector has two types of NUC tables, gain and offset. The gain of NUC is factory set and the offset of NUC is recreated continuously with the help of a mechanic shutter which goes in front of the detector to recalculate and adjust the offset for each pixel (Mollmann et al., 2006).

4.5. Thermal Applications

Thermal imaging is one of the traditional sensing technologies that have been widely used in various fields. It is mainly used in military and policing applications such as target detection, officer safety to prevent ambush or to locate hidden suspects and use in law enforcement. It is also used in industrial and civil applications such as manufacturing, fire fighting, building integrity and moisture detection in wall and roofs and in electrical and mechanical pipeline surveys. Environmental applications use thermal imaging, such as oil pollution control, and energy conservation (Burnary et al., 1988). Night vision in the automobile industry, security, surveillance and many other applications are based on temperature measurements or evaluating temperature differences (Jones, 2006).

Finally, thermal imaging plays an important role in medical applications; this will be discussed in the following section in order to demonstrate how a thermal system assists in medical diagnosis and treatment.

4.5.1. Medical Applications of Thermography

Thermal imaging for medical applications dates back to the 1960s when Dr Browling Barnes developed a thermographic camera aimed at the detection of early symptoms of stroke and breast cancer. Later, after 1982 the clinical applications of thermography were reported and thermal imaging was accepted

in breast test to try to differentiate between normal and malignant breast tissues (Diakides and Bronzino, 2008).

In general, medical thermography is non-invasive diagnostic techniques that can be used to visualise and quantify changes in skin surface temperature. It focuses on the measurement of the skin's temperature, because it can give an insight into many physiological problems as the skin represents the interface between deeper tissues and the environments and also maintains the deep body temperate within fine limit (Bumary et aL, 1988). Thermal imaging uses a device to convert infrared radiation, emitted from the skin surface, into electrical inpulses that were visualised in colour on a monitor. Today, infrared cameras have become one of the most efficient techniques for the study of skin temperature. They provide high performance and sensitive diagnostic for many types of diseases such as the early detection of breast, skin and lung cancer, and vascular disorders such as diabetes. They monitor the changes in overall health and detect the causes of back pain, leg pain, and arthritis, rheumatism and in surgery (open heart, transplant), and many other applications (Diakides and Bronzino, 2008; Houdas and Ring, 1982).
Fig.4.7 illustrates the diagnosis of thermal imaging for different diseases. Recently the thermal cameras helped the search for swine flu and other viral diseases in airports, hospitals, stations, terminals, etc (FLIR Systems, 2009).

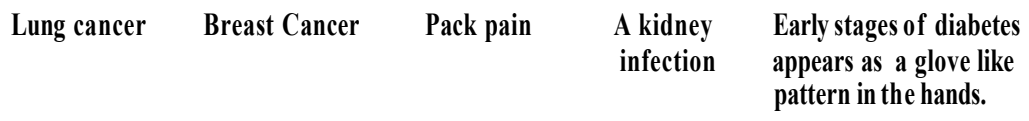

Fig.4.7: Diseases diagnosed by thermal imaging (Dorf, 2006; Medical Thermal Imaging, 2009).

As mentioned before, the changes in skin surface temperature can be detected and measured by thermal cameras. The deep tissues conduct the heat energy directly to the skin. The quantity of heat which passed through the surface will be determined by the thermal conductivity of the intervening structures. For example, the bony structures and fat will impede some of the heat transfer and will cause cooler skin compared with other areas with higher thermal conductivity (Burnary et al., 1988).

There are differences in the temperature found on the skin surface based on the fat thickness and the blood perfusion status which in turn are based on several factors that may affect the temperature of the skin such as:

- **Age** is an important factor in determining skin surface temperature; younger children have a higher temperature than older people.
- **Obesity,** the temperature of the skin for the fatty areas appears colder than other areas (Burnary et al., 1988).
- **Environment** changes in the environmental conditions will affect skin temperature. The sun's heat may increase or decrease the skin temperature through sweating and vaporization. Wind may decrease the skin temperature and also rain. For these reasons, thermal measurement should be made in a temperature-controlled environment (Williams, 2009).
- **The psychological state** (emotion), this factor refers to the human nervous system which responds by increasing the blood flow and thus raising the skin temperature (Bronzino, 2006).
- **Exercise,** the effects of exercise also increase the blood flow in the body and raise the temperature of the skin surface.
- **Human health** sick people have a higher skin temperature than healthy people. Furthermore, abnormal parts of the human body appear warmer than the rest of the body, making them easily detectable with thermal cameras as in the case of breast cancer (Otsuka et al., 2002).

The change in the skin temperature, for all these reasons, will be affected by the measurement performed by thermal camera. Although there are very large

differences in temperature distributions among individuals, there is usually a basic thermal distribution which is less affected by these factors such as facial physiological features in humans as mentioned before in Chapter 3. The measurement system for the skin temperature will be explained in the following section.

4.5.2. Temperature measurement Units

The temperature of an object is a measure of the heat level of that object and is expressed in either absolute or relative terms. There are two absolute scales called Rankine (English system) and Kelvin (metric system). While the two relative scales are called Fahrenheit (English system) and Celsius or centigrade (metric system) (Temperature, 2009). Absolute zero in Kelvin is equal to –273.1°C and to –459.7°F. The relationships between these are provided by Equations 4.6-4.9.

$$T_{\text{Celsius}} = 5/9\,(T_{\text{Fahrenheit}} - 32) \tag{4.6}$$

$$T_{\text{Fahrenheit}} = 9/5\,(T_{\text{Celsius}} + 32) \tag{4.7}$$

$$T_{\text{Rankine}} = T_{\text{Fahrenheit}} + 459.7 \tag{4.8}$$

$$T_{\text{Kelvin}} = T_{\text{Celsius}} + 273.16 \tag{4.9}$$

In FLIR (Forward Looking Infrared) camera, Celsius (T_{Celsius}), Kelvin (T_{Kelvin}) and Fahrenheit ($T_{\text{Fahrenheit}}$) are supported (Kaplan, 2007; ThermoVision^{TM} ,2004).

4.6. The advantage of Non-contact Thermal Measurements

Although thermal imaging is an expensive technique, it has several advantages which make it very useful as a measurement tool, these include:-

- It is non-contact, fast, non-destructive and reliable equipment for measuring;
- It can be used remotely, and is the only method when the object (target) is distance, or inaccessible to, contacting sensors;
- It is an effective method if multiple measurements are required. It will measure many points from the same target quickly (Kaplan, 2007).

- Applicable as part of a surveillance system.
- Appropriate with fragile objects, when thin webs, tissues or any delicate materials are measured.
- It can detect the objects in the dark regardless of colour, clothing or shadow.
- It can be used to measure through obscuring phenomena such as smoke and haze.
- It has low power consumption.
- It operates in real time, enabling very fast scanning of stationary and moving targets.
- Completely harmless; using no harmful radiation or chemicals. Therefore it is safety for human.
- High range performance.
- It is very sensitive to detecting changes in temperature (Richmond and DeWitt, 1985).

All these factors along with the high accuracy make the infrared imaging an appropriate method for monitoring skin temperature.

Although IR systems have many advantages for temperature screening, other than its cost, there are many variables that can affect its accuracy (Ng and Sudharsan, 2001). Ideally, the thermal imager should be operated in a stable indoor environment with stable operating ambient conditions. Environmental infrared sources such as sunlight and nearby electrical sources can affect the accuracy of IR systems and should be minimized. The target should be located in an area free from draft and direct airflow. The accuracy of the thermal imager is also highly dependent on the skill and knowledge of the operator (Ng and Sudharsan, 2001).

4.7. Thermal cameras

An infrared camera, sometimes called a FLIR is a device to measure the emitted infrared radiation from an object and convert it as an image.

The radiation can be considered as a tool to enable the camera to calculate and display the temperature. However, the radiation measured by the camera, does

not represent the temperature of the object only, but the emissivity of the object (ThermoVision™, 2007). The thermal camera converts infrared radiation into a visible image. Moreover it allows the user to visualise a scene more completely, even if it is obscured by smoke and other visual disturbances. Several factors influence camera selection, including its cost, temperature and wavelength range, resolution, sensitivity and accuracy.

The wavelength range for measurements required for our study was 7.5 to 14 *jum*. In our study, respiration rate was determined the FLIR A-40 model camera. Fig.4.8 shows the FLIR A40 thermal camera and some of its accessories.

Fig.4.8 : FLIR camera A40 M (ThermoVision™, 2007) with its accessories.

The FLIR A40 camera was one of the most appropriate devices for our study. It has been used in many applications, including medical, industrial development and research and for preventive maintenance (FLIR Systems, 2009). The camera captures an image array of 320 x 240 pixels using an uncooled device (temperature sensitive electrical resistor called the mierobolometer) for measuring the incident radiation. It uses a Focal Plane Array (FPA) detector that employs several uncooled microbolometer FPA detectors for thermal imaging. The detector has a high thermal sensitivity in the light spectrum wavelength range of 7.50-14.00 *jum*. This type of camera has a thermal sensitivity of 0.08 K at 30 °C with an accuracy of ± 2 °C under normal temperature and pressure (ThermoVision™, 2007). The highest speed for capturing images is between

50-55 frames per second. It provides for image capture control on the camera itself, when used with the ThermaCAM™ Researcher pro 2.9 Software, which is explained later in this chapter. The camera connects to a Laptop or PC via firewire in order to provide data output.

4.7.1. Infrared (IR) Detectors

The most important part of a thermal camera is the detector or detector array. It plays an important role in determining the spatial resolution for a given field of view (FOV). IR detectors are electro-optical detectors that absorb electromagnetic radiation and output an electrical signal proportional to the intensity of the incident electromagnetic radiation (irradiance). IR detectors can be categorized into two main types, namely thermal and photonic detectors (Physics of Electro-optic Detector, 1998).

▪ *Thermal detectors* operate by converting the incoming photon flux to heat. The incident radiation causes the thermal detector's temperature to increase or decrease until it comes into quasi-equilibrium with the radiation being absorbed, this change in temperature is sensed by a bolometer. The bolometer measures the temperature change due to the absorption of radiation by measuring a change in resistance in the material. A microbolometer is a specific type of bolometer used as a detector in a thermal camera. It is also known as uncooled or thermal detector. The microbolometer grid is commonly found in three sizes, a 640×480 array, a 320×240 array or less expensive 160×120 array. This type of detector is different from others; it does not require exotic and expensive cooling methods, such as stirling cycle coolers and liquid nitrogen coolers. These methods of cooling made early thermal imagers expensive to operate and unwieldy to move. Also, older thermal imagers required a cool down time in excess of 10 minutes before being reusable. In general the thermal detectors are slow compared to quantum detectors but have the great advantage that they do not require the cooling methods. However, some type of thermal detectors need their temperature to be controlled to ensure that they operate under optimal conditions (DeCusatis ,1997; Williams, 2009).

• In *Photon (or quantum) detectors,* the incident photons interact with the material of the detector to produce charge carriers (electronic) that generate a voltage across the detector element, or change its electrical resistance (Williams, 2009). Generally the mechanism involves converting absorbed photon energy into released electrons, as a result moving it from one band energy level to another. The change in charge carrier state changes the electrical properties of the material. These electrical property variations are measured to determine the amount of incident optical power. There are two types of photon detectors Photoconductive and Photovoltaic. In general these types of detectors provide a higher sensitivity and faster speed than thermal detectors. Hoverer, the drawbacks of photonic detectors are that they need to be cooled for accurate measurement, which makes them large, expensive and complicated to fabricate (Technical information SD-12 Characteristics and use of infrared detectors, 2004).

4.8. ThermaCAM™ Researcher Software

ThermaCAM™ Researcher 2.9 that is part of the FLIR camera runs under Windows XP, 2000, and Vista, The main purpose of this Software is to process and visualise live IR images obtained through the camera interface. This software allows for high, medium and slow speed thermal event to be captured depending on the hardware. This software introduced several features and benefits such as:

• **Analysis of the Temperature**

The software supplies fast and extensive temperature analysis during the measurement such us isotherms, spot measurements, line and area measurements. Object parameters can be modified, as shown in Fig.4.9, including emissivity, distance, and reflected temperature by using the software package. Moreover, the speed of the video (number of image per second) can also be specified using this software.

• Static Image Analysis

It can analyse static or sequences images stored in the infrared camera, PC or Laptop.

• Multiple Camera Connection Using the FireWire Interface

More than one Firewire camera can be connected to the same PC, and each camera can be viewed and controlled in its own researcher window.

• Easy Data Export -Automatic Conversion of IR Images to Matlab Formats.

This software provides a facility to convert a video into a sequence images and then into Matlab format. This software also has the facility to export the image or area into a CSV (Comma Separated Values) file, which can be opened to Excel or other programmers.

• Full Control of the IR Camera from a PC

When the camera is connected to the PC, its lull control is possible. Focus, span adjustment, temperature range adjustment, colour palette, etc. can all be controlled from the PC without touching the camera.

• Finally, Compatible with Windows 95, 98, ME, NT, 2000, vista and XP (ThermoVision™ , 2004).

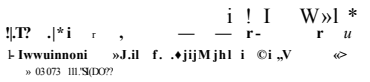

Fig.4.9: A thermal image with ThermoVision in **FLIR** camera.

4.9. Conclusion

Infrared or thermal imaging is the ability to measure the irradiance variations between objects in a scene and to convert them to visible images. This infrared (IR) radiation is found between visible light and microwaves in the electromagnetic spectrum. All objects with a temperature above 0°K emit IR radiation. The intensity and wavelengths of the radiation depends on the temperature. The higher the temperature the more radiation is emitted ,and the shorter the peak wavelength of the emissions. An object that does not reflect any incoming radiation is called a blackbody. Thermal imaging is used in many applications, with a particullay significant role in medical diagnosis. In this chapter the details of thermal imaging, the parameters used to capture the video, the details and advantages of the thermal camera were explained. Finally, we gave a brief overview of the ThermaCAM™ Researcher 2.9 with the FLIR A40 camera which is used to capture the videos.

Chapter Five

5. Methodologies, Developments and Preliminary Results

5.1. Introduction

Respiration rate plays an important role in the diagnosis of respiratory related diseases such as sleep apnea and asthma. In this study, respiration monitoring approaches were implemented based on thermal imaging. These were based on detecting temperature changes of skin surface centred on the tip of the nose and the upper lip. This part of the face is more affected by respiration and is referred to here as the region of interest (ROI). Temperature changes in the ROI are caused by the difference in the temperatures of inhaled and exhaled air.

The proposed methodologies for monitoring respiration rate are discussed in this chapter. The chapter provides an overview of the system setup along with a description of the hardware set up. The software designed during the study is described. A number of preliminary results are included in this chapter to ease understanding of the methodologies.

5.2. Thermal Image Recording System

Both hardware and software aspects of the thermal image recording system are explained in this section.

5.2.1. Hardware Description

A thermal camera FLIR-A40 was used to record temperature changes in the ROI. The camera settings were: emissivity=0.92, reflected temperature=15C° and relative humidity=50%. The thermal sensitivity of this camera is 0.08 degrees Kelvin at 30°C which was considered adequate for the task. The image capture rate used was 50 frames per second, thus providing 3000 images per minute. The recording time was two minutes. This provided sufficient sampling for respiration signals as the maximum respiration rate is about 60 cycles per minute.

The thermal camera was connected to a personal computer via one of its USB ports. The computer used in the study was a laptop Sony VGN-FW48E/H that had 3GB of RAM, a 2.1 GHz processor and a 320 GB hard disk. The computer was installed with Windows XP, Matlab software and the FLIR software (ThermaCAM™ Researcher Pro 2.9). The FLIR software was described in Chapter Four. Recording began when the camera was connected and the FLIR software (ThermaCAM™ Researcher Pro-2.9) was running. Fig.5.1 shows the hardware equipment used and the system setup.

In this setup the patient either sat on a comfortable chair in front of wall or slept in a bed. The FLIR A40 camera was fixed on a tripod in front of the subject's face at a distance of about one metre. After the recording was finished, the software determined the respiration rate by using the developed image and signal processing techniques.

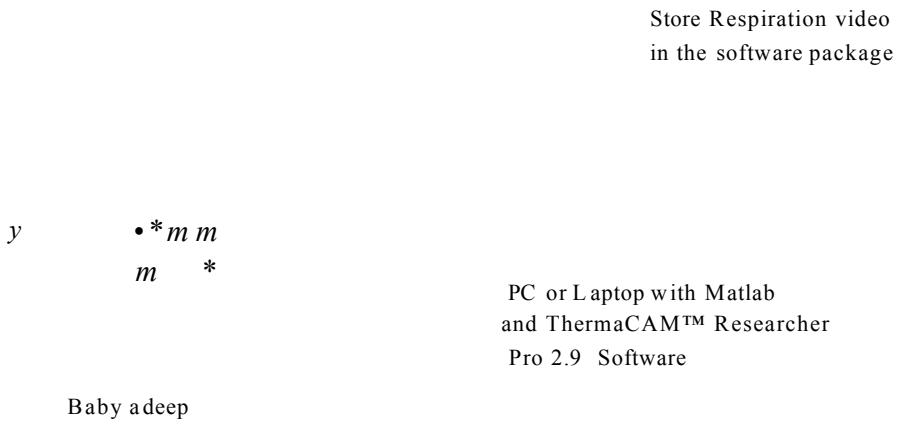

Fig.5.1: System hardware description.

5.2.2. Software Description

The first step was to capture and record thermal videos using "ThermaCAM™ Researcher pro 2.9". The videos were processed. Different software tools in Matlab were designed to track facial motion, localise the region of interest (ROI) and to analyse the extracted signal to compute the respiration rate. Each of these issues is explained in this section and the following chapter.

The operations involved in respiration rate monitoring were:

1. Converting the recorded thermal videos into separate images.
2. Filtering the thermal images to reduce obscuring noise.
3. Segmenting the region of interest (ROI) from the rest of image.
4. Applying feature extraction to extract the respiration signal.
5. Processing the respiration signal to determine respiration rate.

5.2.2.1. Converting the recorded thermal videos into separate images

ThermaCAM™ researcher software was used to convert the recorded video into individual images, and then each image was ready for processing using the Matlab software.

5.2.2.2. Filtering the thermal image

Thermal images, like other types of images, suffer from noise. One of the important causes of the appearance of noise is environmental temperature variation, as described in Chapter 4.

To improve the quality of thermal images and to reduce the noise, for the sequence of images, image enhancement techniques were applied through the use of low-pass filters (LPFs) and high-pass filters (HPFs), as mentioned previously in Chapter 3.

Fig.5.2 (a) shows a facial thermal image. The video was recorded in a room at a temperature of about 30°C. The image in this recording was obscured by infrared radiations from the recording environment. This noise caused the values for some pixels to be much higher than the person's expected body temperature. The distribution of the thermal image pixel values is provided in Fig.5.2 (b).

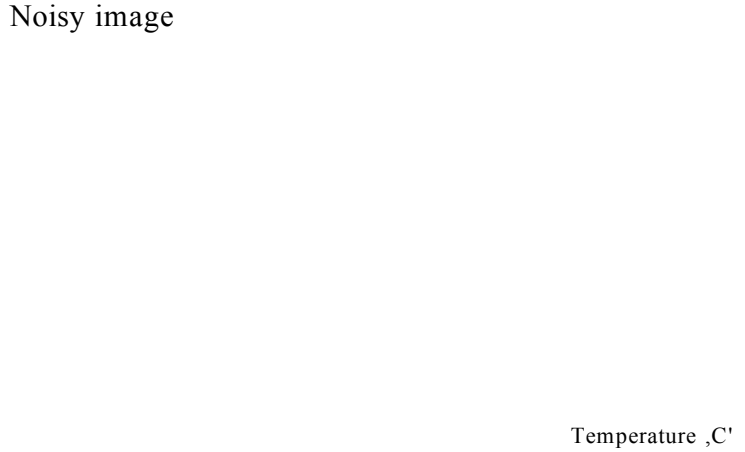

(a) (b)

Fig.5.2: **The original noisy thermal image with its corresponding histogram.**

Suitable filtering techniques were necessary to reduce the effect of noise in the thermal images. The effectiveness of a number of lowpass filters (LPFs) to enhance the images was investigated. These filters are described in detail in Section 3.5.1.1 of Chapter 3. They were:

- Average filter using a 3x3 mask;
- Median filter (size =5);
- Gaussian filter using a 3x3 mask.

Figs.5.3, 5.4 and 5.5 illustrate the effect of LPFs in enhancing the thermal images.

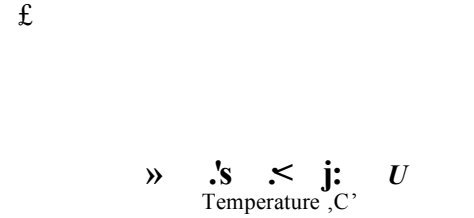

Fig.5.3 : Thermal image filtered using an Average filter and its corresponding histogram.

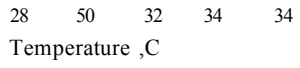

Fig.5.4 : Thermal image filtered using a Median filter and its corresponding histogram.

Fig.5.5 : Thermal image filtered using a Gaussian filter and its corresponding histogram.

Lowpass filtering process managed successfully to reduce the environmental noise from the images. The Median filter was more effective in reducing unwanted noise and smoothing the images than the other filters.

The effectiveness of several highpass filters (HPFs) in highlighting distinct features of the images was also investigated. These filters are described in Section 3.5.1.2 of Chapter 3. They were the Sobel filter, Prewitt filter and the Laplacian filter. The results produced by applying these filters are provided in Figs. 5.6, 5.7 and 5.8 respectively. The results show that the HPFs do not enhance the thermal images, as the images are further obscured.

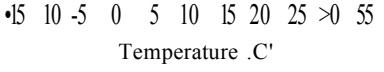

Fig.5.6 : Thermal image processed using the Sobel filter and its corresponding histogram.

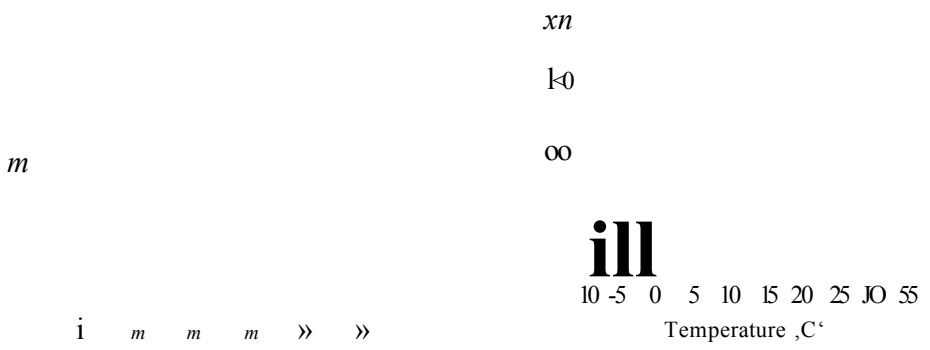

Fig.5.7 : Thermal image processed using the Prewitt filter and its corresponding histogram.

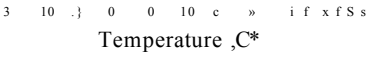

Fig.5.8 : Thermal image processed using the Laplacian filter and its corresponding histogram.

The results indicated that the LPFs were more suitable than HPFs in enhancing the thermal images. Of these, the Median LPF was more effective than the others in enhancing the image and removing noise.

In order to further demonstrate the suitability of the Median LPF, thermal noise was added to test thermal images. Thermal noise can expressed by Equation 4.5, as outlined in Chapter 4. Histograms were also used to provide information about the distribution of temperature before and after adding noise as well as after filtering. In the present study, thermal noise was produced and added to the thermal images by using Equation 5.1

$$g(x,y) = f(x,y) + n(x,y) \quad (5.1)$$

Where f(jt, y) represents the original image, $n(x, y)$ the thermal (Gaussian) noise, $g(x, y)$ represents the noisy image.

Fig.5.9 shows the facial thermal image for a sleeping child aged nine months.

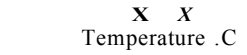

Fig.5.9 : The original thermal image and its corresponding histogram.

Fig.5.10 illustrates the image after inserting the thermal noise and the corresponding histogram.

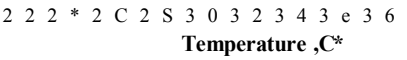

Fig.5.10: **The noisy thermal image and its corresponding histogram.**

Fig.5.11 shows the effect of the average LPF in reducing the noise from the noisy thermal image. Though this filter managed to reduce the noise, it could

not be considered as the most suitable because significant residual noise remained, as shown in the figure.

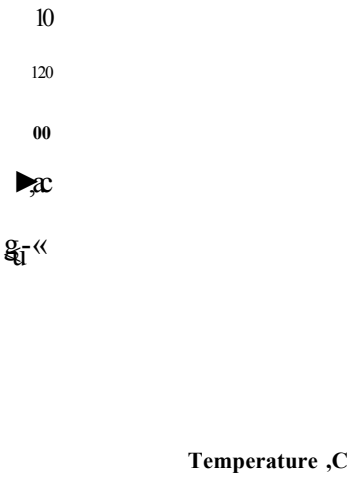

Fig.5.11: Thermal image processed using the Average filter and its corresponding histogram.

Fig.5.12 illustrates the effect of the Median LPF. This filter removed a larger amount of the thermal noise than the Average filter. This is illustrated visually in the image and its corresponding histogram.

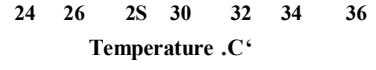

Fig.5.12: Thermal image processed using the Median filter and its corresponding histogram.

Fig.5.13 illustrates the effect of the Gaussian LPF in reducing the noisy thermal image. Its performance in reducing the noise was not as good as the Median filter.

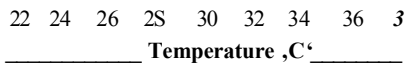

Fig.5.13: Thermal image processed using the Gaussian filter and its corresponding histogram.

Figs. 5.14, 5.15 and 5.16 show the application of the HPFs, Le. Sobel, Prewitt, and Laplacian respectively, to the noisy thermal images. As shown in these figures the HPFs caused significant distortion.

133

Fig.5.14: Thermal image processed using the Sobel filter and its corresponding histogram.

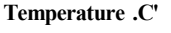

Fig.5.15: Thermal image processed using the Prewitt filter and its corresponding histogram.

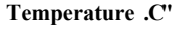

Fig.5.16: Thermal image processed using the Laplacian filter and its corresponding histogram.

5.2.2.3. Segmenting the Region of Interest (ROI) from the rest of image.

Segmentation was carried out after the images had been enhanced by the Median LPF. Segmentation extracted the identified ROI from the rest of the image. The ROI represents the facial area most affected by respiration. This area was the tip of the nose and the upper lip.

Fig.5.17 (a) shows thermal snapshots of the children during inspiration. Lower temperatures can be observed around the nasal area. The colour of the nasal area

tends to be darker, due to the absence of hot expired air during the inspiration operation.

Fig.5.17 (b) shows the thermal snapshots of the children during expiration. It is observed that the higher intensity of temperature values appear around the nasal area. The colour of the nasal area tends to be brighter and indicates higher relative temperature. The contrast in the intensity of the temperature values around the nasal area during inspiration and expiration was used to measure the breathing signal and its rate.

Several approaches were investigated in order to determine the respiration region of interest (ROI), including its most appropriate shape and the size with different type of head movements. The discussions associated with these are included in Chapter 6.

(a) **(b)**

Inspiration Expiration

Fig.5.17: Snapshots of respiration, (a) Inspiration phases, (b) Expiration phases.

5.2.2.4. Applying Feature Extraction to Extract the Respiration Signal.

After selecting the ROI in the previous step, the respiration signal from the ROI was obtained. Different processes were applied to extract a suitable signal from the ROI. Initially six images per second were captured. The analyses of several video recordings showed that the low sample rate at six images per second (*fps*) produced under sampling as the thermal images were obscured. Therefore the sample rate was increased to fifty images per second. This provided a sufficient sample rate for the maximum respiration of 60 cycles per minute.

The respiration feature was then extracted from the images as follows:

Method 1: averaging the temperatures which corresponded to the four highest values for the frequencies in the histogram of the ROI. The four highest peaks were more affected than others by the changes of temperature during the respiration process. Equation 5.2 was used to apply this feature to the ROI.

$$A_v = \frac{T_1F_1 + T_2F_2 + T_3F_3 + T_4F_4}{F_1 + F_2 + F_3 + F_4} \tag{5.2}$$

Where T_1, T_2, T_3, T_4 are the temperatures which correspond to the highest frequencies, F_1, F_2, F_3, F_4 respectively. A_v for each region was plotted against time. Fig.5.18 (a) shows the plot of the A_v values for 6000 images against time, namely 120 seconds. This signal was obtained from an adult without head movements. Fig.5.18 (b) shows this signal following its filtering by a 5^{th} order Butterworth filter (cutoff frequency 1.5 Hz).

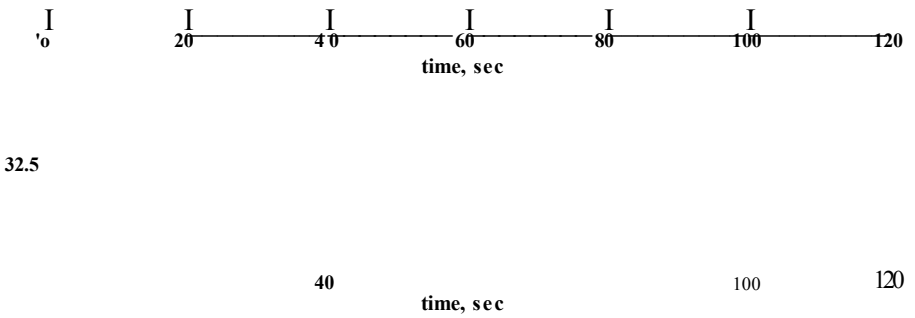

Fig.5.18: (a) Respiratory signal for an adult without head movements obtained by averaging the temperature corresponding to the four highest frequencies for the ROI (b) Its filtered version.

Fig.5.19 shows the plot of the values for the same subject but with large head movements.

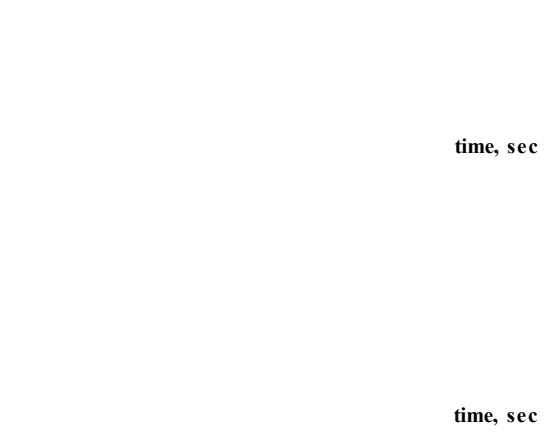

Fig.5.19: (a) Respiratory signal for an adult with large head movements obtained by averaging the temperature corresponding to the four highest frequencies for the ROI (b) Its filtered version.

Method 2: The ROI was divided into upper and lower parts. The pixel values within each part were averaged to obtain a single value representing each part.

The justification for this was to compare the temperature in the upper part that is less affected by respiration with the lower part, Le.

$$D_{suh} = Average^{\wedge} - AverageB \tag{5.3}$$

Where, $Averagev$ and $AverageB$ are the average pixel values in the upper and lower parts of the ROI respectively. The process was repeated for the 6000 images (Le. 50 images per second x120 seconds recording duration) and then the value of D_{suh} for each image was plotted against time to represent the respiration signal.

Fig.5.20(a) shows the plot of the D_{suh} values for 6000 images against time, namely 120 seconds. This signal was obtained from an adult without head movements. Fig.5.20(b) shows this signal following filtering by a 5th order Butterworth filter (cutoff frequency 1.5 Hz).

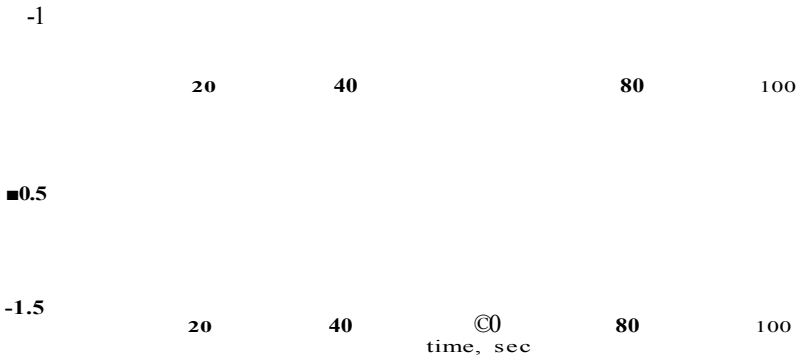

Fig.5.20: (a) Respiratory signal for an adult without head movements obtained by subtracting the upper and lower parts of the ROI. (b) Its filtered version.

Fig.5.21 shows the plot of the D_{sub} values for the same subject but with large head movements.

Fig.5.21: (a) Respiratory signal for an adult with large head movements obtained by subtracting the upper and lower parts of the ROI. (b) Its filtered version.

Method 3: To improve the respiration signal for the videos with significant head movements, the pixel values within the bottom part of the ROI were averaged to obtain a single value. The process was repeated for the 6000 images and plotted against time.

Fig.5.22(a) shows the plot of averaged values of the bottom part of the ROI for 6000 images against time, namely 120 seconds. This signal was obtained from an adult without head movements. Fig.5.22(b) shows this signal following filtering by a 5th order Butterworth filter (cutoff frequency 1.5 Hz).

Fig.5.22: (a) Respiratory signal for an adult without head movements obtained by averaging the lower part of the ROI. (b) Its filtered version.

Fig.5.23 shows the plot of averaged values the bottom part of the ROI for an adult with large head movements.

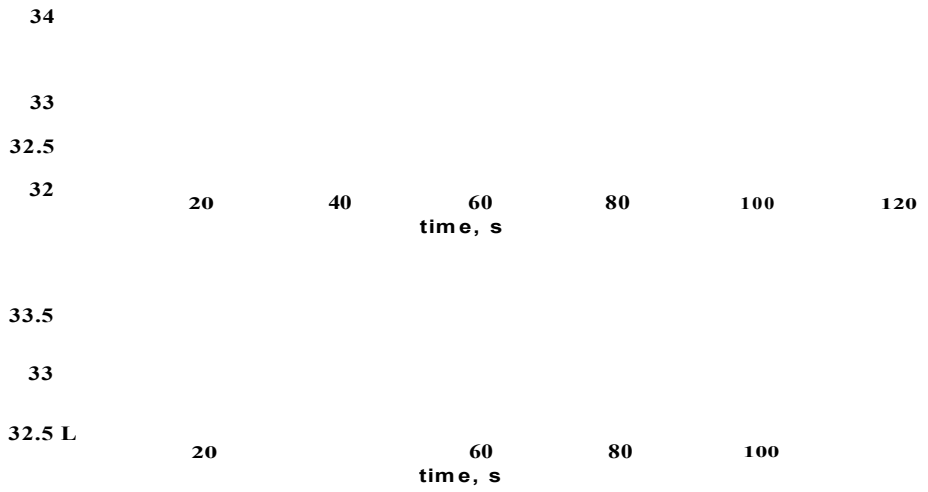

Fig.5.23: (a) Respiratory signal for an adult with head movements obtained by averaging the lower part of the ROI. (b) Its filtered version.

Several technique features were extractedfrom the ROI to obtain a clear respiration signal. Most of these were successful in detecting a clear respiration signal for the recording without head movements or with small head movements. However, there were problems during large head movements. From this point onwards, analysis of the effect of this type ofmovement on measuring breathing was investigated.

A recording video was captured which contained only two types of head movements. The first part of the recording was 2357 frames when the face was turned approximately 45° to the left side from the camera, as shown in Fig.5.24(a). The second part of the recording included 3643 frames when the face was forward, as shown in Fig.5.24(b). The pixels in the ROI were averaged and then plotted against time.

M.rc

Fig.5.24: The ROI, (a) During the left head movements, (b) the face in front of the camera.

Fig.5.25(a) illustrates the respiration signal for the recording of 6000 images during 120 seconds with two types of head movement. Fig.5.25(b) shows the same signal filtered using the Butterworth filter.

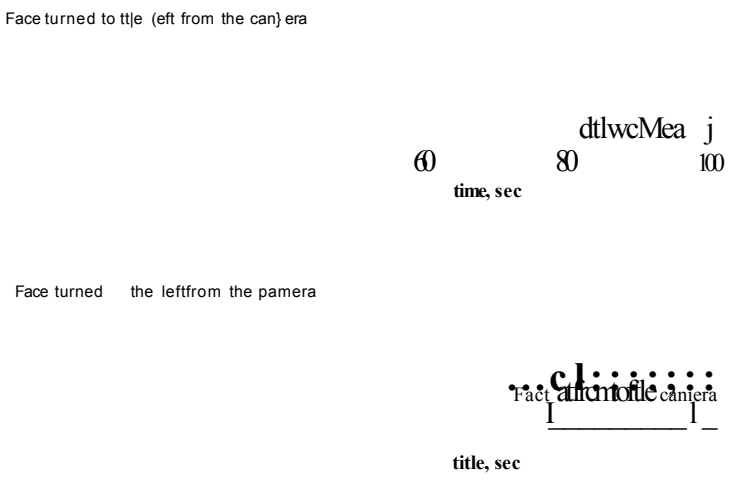

Fig. 5.25: (a) Respiratory signal for an adult with two types of head movements obtained by averaging the ROI. (b) Its filtered version.

As shown in Figs 5.25(a) and 5.25(b) the signal contains two parts. The first part of recording is 2357 frames where the face is turned to the left side from the camera to approximately 45°. The signal is unclear for two reasons. Firstly, the ROI does not represent the desired region although it is placed in the correct position, and thus one of the main parts of the nose is lost. Secondly, the camera picks up unrelated sections of the face and is unaffected by the respiration

operation, as shown in Fig.5.24(a). The analysis of this recording showed that the temperature decreased more than two degrees when the head turned away from the camera. Therefore we suggested segmenting the ROI into 8 parts and selecting the clearest part for calculation of the respiration rate.

Method 4: The ROI was partitioned into 8 equal segments, as shown in Fig.5.26. The justification for this was to analyse the temperature variation in each small section of the ROI and to select the segment that best provided a respiration signal.

(a) (b)

Fig.5.26: The ROI partitioned into eight segments, (a) The position of ROI on the tip of the nose, (b) The eight segments of ROI.

The pixel values for each segment were averaged. This was repeated for all 6000 images and the resulting values were plotted against time. Fig.5.27 shows the resulting respiration signals for an adult. The recording was carried out with the subject sitting in a chair about a metre from the thermal camera. The subject was asked to refrain from head movements. The visibility of individual respiration cycles in the eight segments differed. Segments 3 and 7 provided the clearest signal, segment 1 providing the least clear signal. The specific segments that provided clearest respiration cycles varied from subject to subject. This was because the respiration pattern and the specific manner it affects the area around the nose varies in different subjects. This result indicates that for respiration monitoring it is appropriate to partition the ROI and consider each resulting segment separately.

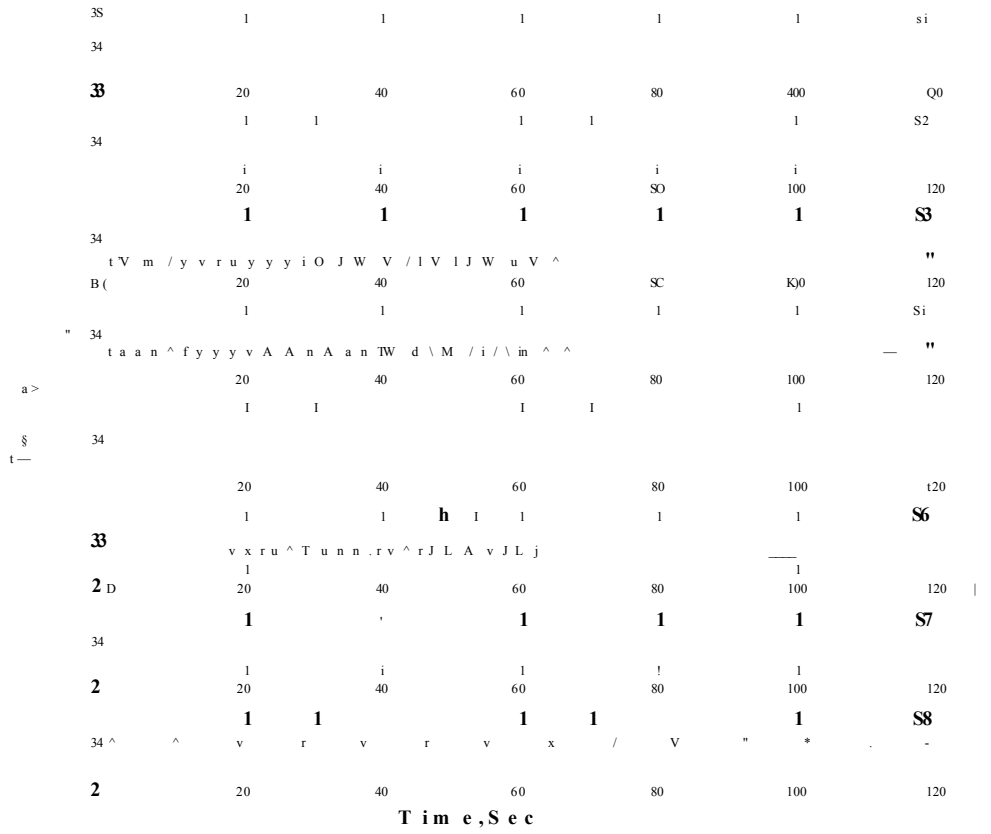

Fig.5.27: Respiration signals obtained using thermal imaging. The signals obtained from segments 1 to 8 are shown from top to bottom respectively.

Fig.5.28 shows the signal produced by averaging the pixels from the complete ROI. The respiration cycles appear distorted, confirming the need to partition and process the different parts of the ROI separately.

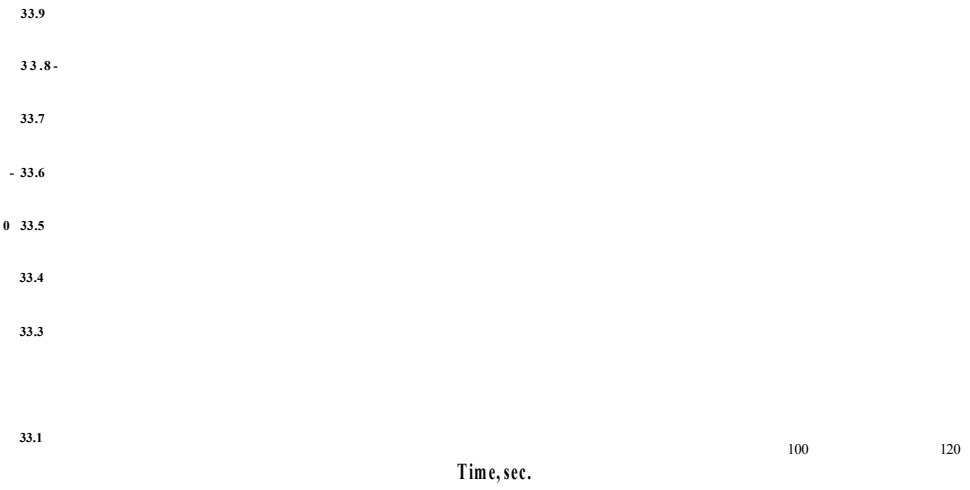

Fig.5.28: Respiration signal obtained by averaging pixel values from the complete ROI.

Fig 5.29 shows the histograms of pixel values for the eight segments of the ROI of a subject. The two main peaks that are visible in the histograms of segments 2, 3, 4 5, 7 and 8 indicate the lower temperature (during inhalation) and higher temperature (during exhalation) of air. The temperature distributions for the segments vary significantly. The segments that have the highest separation of these two peaks are the most suitable for extracting the respiration signal and respiration rate.

Fig.5.29: The temperature histograms of the ROI segments 1 to 8.

The same process was applied to another person with large head movements. Fig.5.30 shows the respiration signals for the eight segments of the ROI. The respiration signals from segments 1, 2 and 5 are clearer than those from the remaining segments.

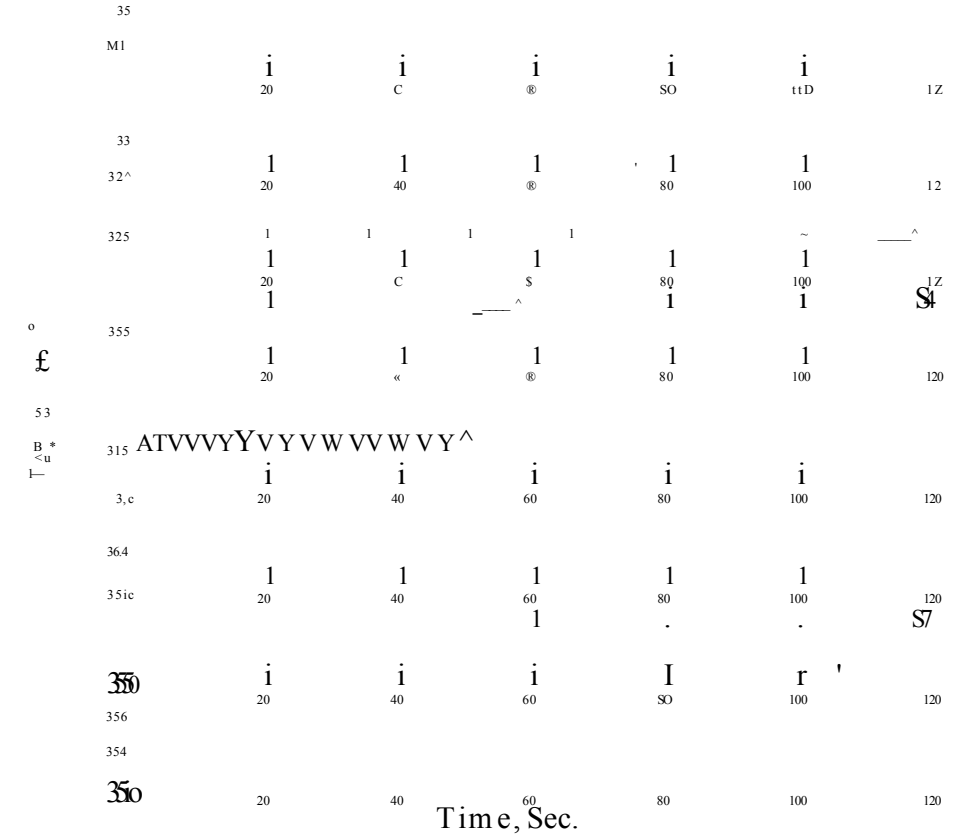

Fig.5.30: Respiration signals obtained using thermal imaging. The signals obtained from segments 1 to 8 are shown from top to bottom respectively.

Fig.5.31 shows the plot of average pixel values obtained from full ROI (Le. segments 1 to 8 combined). This signal appears distorted as compared with those from individual segments of the ROI.

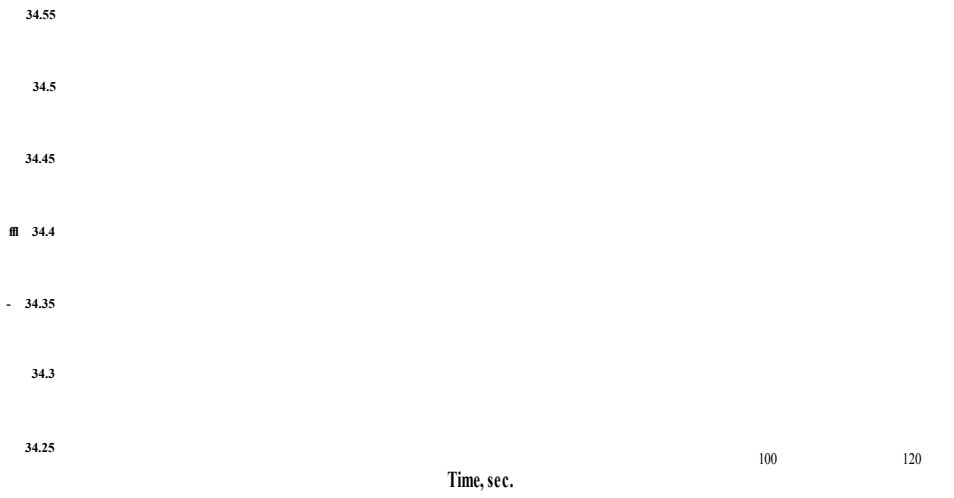

Fig.5.31: Respiration signal obtained by averaging pixel values from the complete ROI.

Fig 5.32 shows the histograms of pixel values for the eight segments of the ROI of a subject. The two main peaks that are visible in the histograms of segments 1, 2, 3 and 5 indicate the lower temperature (during inhalation) and higher temperature (during exhalation) of air. The temperature distributions for the segments vary significantly. The segments that have the highest separation of these two peaks are the most suitable for extracting the respiration signal and respiration rate.

Fig.5.32: The temperature histograms of the ROI segments 1 to 8.

5.2.2.5. Processing the respiration signal to extract the respiration rate

Respiration is a rhythmic phenomenon characterised by the repetition of inspiration and expiration. Figs. 5.33 and 5.34 show examples of clearest respiration signals for expiration and inspiration patterns respectively, for the same person in a sequence over time. As shown in these figures, there are occasional irregularities in the amplitude and general shape of these patterns. These characteristics need to be considered when extracting the value of respiration rate from respiration signals.

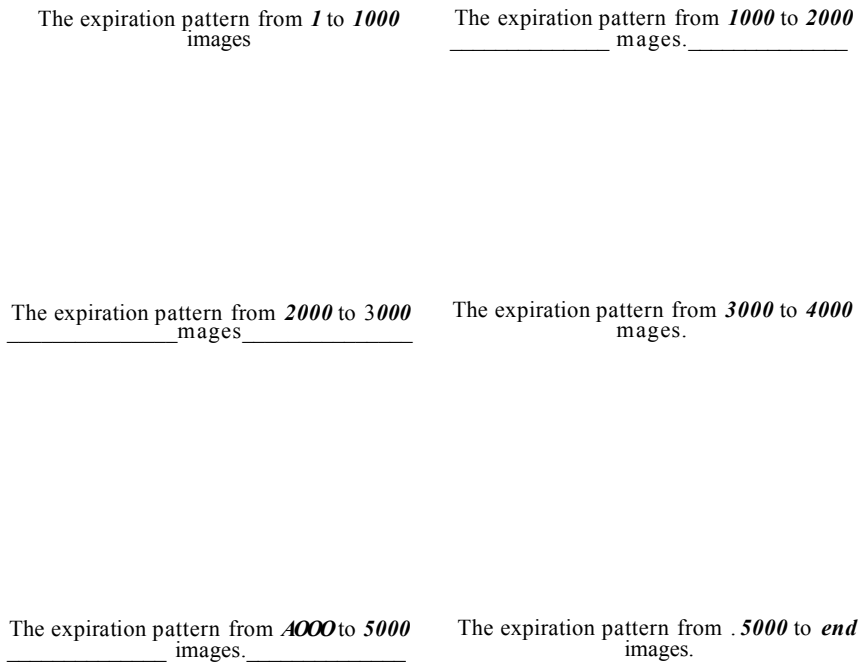

Fig.5.33: The different patterns of the expiration operation in the same recording.

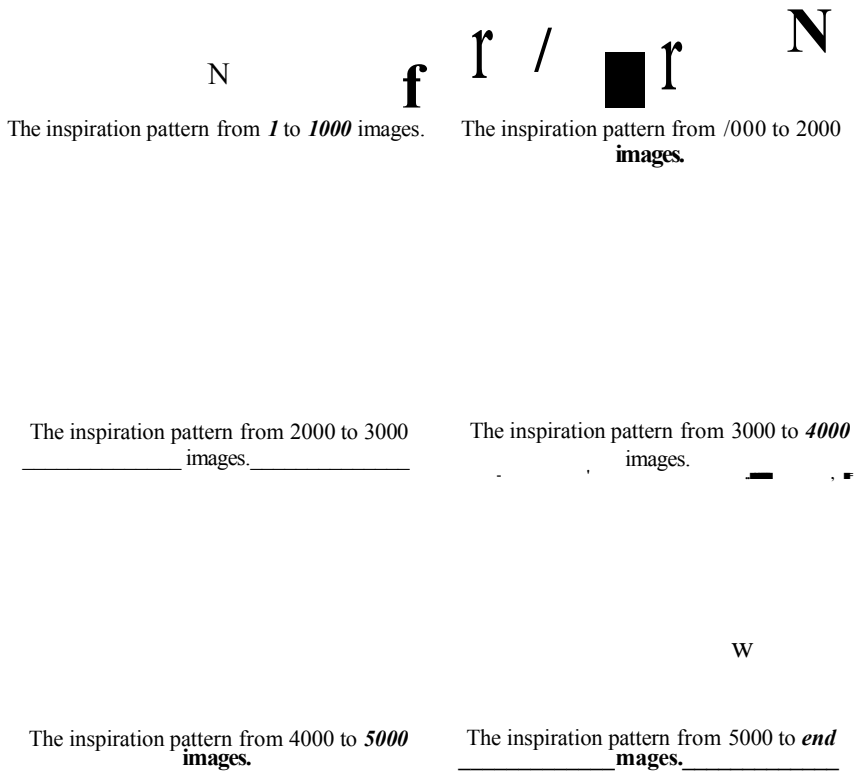

Fig.5.34: The different patterns of the inspiration operation in the same recording.

To obtain a respiration rate from respiration signals, several methods were investigated. These methods are explained below:

Method one (Fast Fourier Transform (FFT) method): the thermal breathing signal is quasi-periodic in nature despite irregularities in the amplitude and shape, as shown in Figs 5.33 and 5.34. For this reason it can be analysed through the FFT. As discussed in Chapter 3, FFT can be used to convert a digital signal from the time domain to a set of frequency harmonics in the frequency domain. FFT was applied to the respiration signals after they were lowpass filtered with the Butterworth filter (order=5, cutoff frequency=l .5 Hz).

Fig 5.35 illustrates the magnitude frequency spectrum of the respiration signal for a subject who was asked not make head movements during recording.

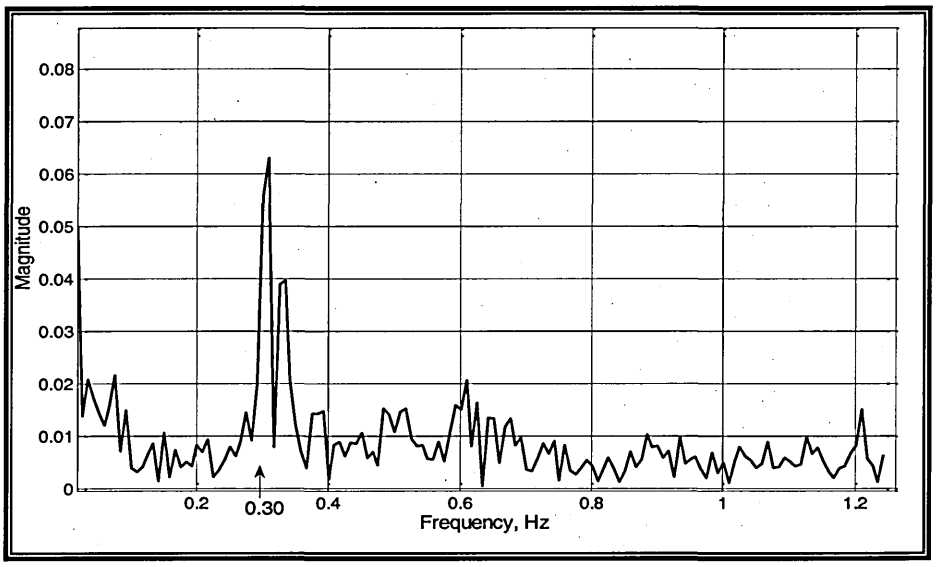

Fig.5.35: The magnitude frequency spectrum of the respiratory for the clearest respiration signal in the ROI .

Fig.5.35 shows the maximum peak *is 0.30*, which represents the number of cycles per second. The respiration rate (cycles per minute) is calculated by multiplying the number of cycles per second by *60*. Therefore the breathing rate is 18 cycles per minute.

The same process was applied to the recording with large head movements. Fig.5.36 shows typical results obtained. The maximum peak is *0.4* therefore the breathing rate is 24 cycles per minute.

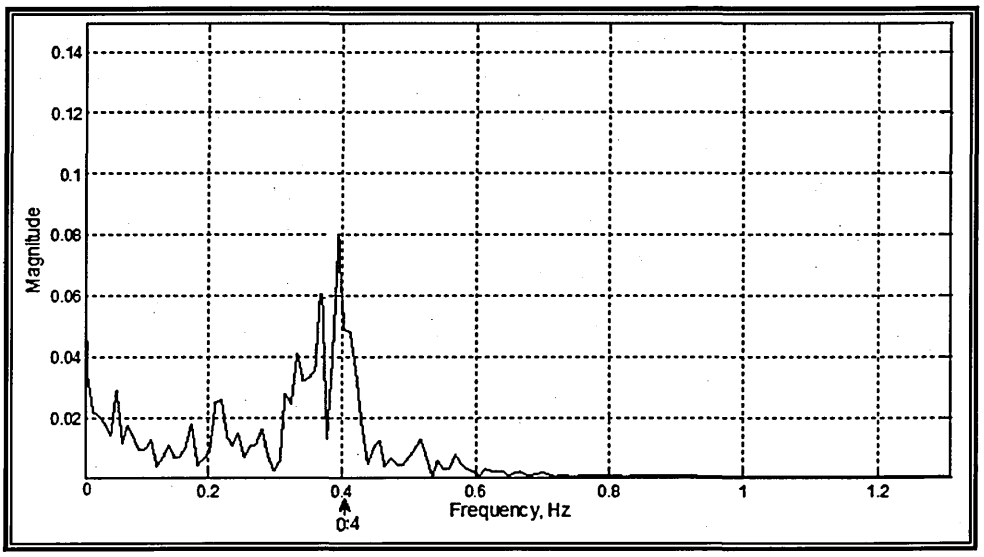

Fig.5.36: The magnitude frequency spectrum of the respiratory for the clearest respiration signal in the ROI for the video with large head movements.

Method two (Windowing method): In this method, the number of respiration cycles in a fixed time interval was calculated. After a number of experiments, the window size was chosen to be 20 seconds, with a 10 second gap to the start of the next 20 second window. This process was repeated for the complete signal The respiration rate in cycles per minute was then calculated by averaging the number of cycles over the selected windows and then multiplying the results by 3.

Fig 5.37 illustrates the application of this method to calculate the respiration rate.

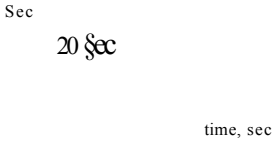

Fig.5.37: Windowing method of determining respiration rate.

Fig.5.38 shows an example of the result obtained. The subject has an average of 8 respiration cycles for every 20 seconds; proving a respiration rate of 24 cycles per minute.

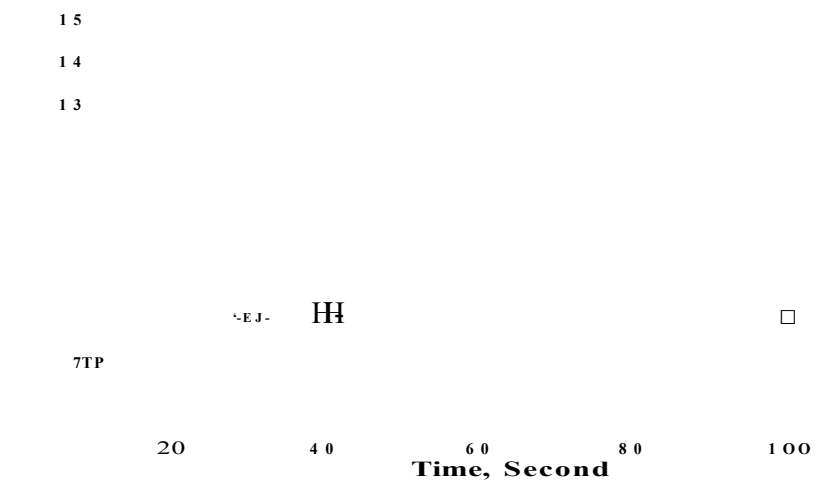

Fig.5.38: Respiration rate monitored over time in a case with no head movement.

The same process was applied to the recording with large head movements. Fig.5.39 shows typical results obtained. For this case, the average respiration rate is 27 cycles per minute.

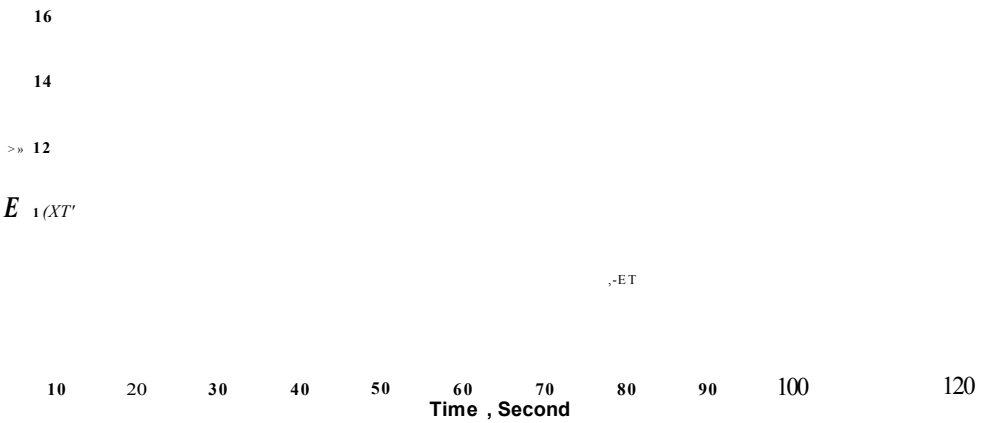

Fig.5.39: Respiration rate monitored over time in a case with large head movements.

The main limitation of this method is that it cannot accurately deal with fractions of a cycle within each window considered. For example, it treated a half cycle as a complete cycle, as in Fig.5.40.

Fig.5.40: Error produced as a result of rounding the fraction of cycle to full cycle.

In order to improve respiration rate calculation, the computation was instead based on respiration cycles. In this method the time duration of five complete successive cycles was determined. The average respiration rate was then calculated as

$$R = (5 \times 60) / T_i \qquad i = 1 \ldots end\ of\ cycles-1 \qquad (5.3)$$

Where R is the number of cycles in 60 seconds and T_t is the time duration of five complete successive cycles. The process was repeated by moving forward by one cycle. Fig.5.41 illustrates the application of this method to the signal in order to compute the respiration rate.

Fig.5.41: Respiration rate obtained by considering five complete respiration cycles.

Fig.5.42 illustrates the results of applying this method to the respiration signal for an adult without head movements. The figure indicates that respiration rate varies over time. The amount of the fluctuations could hold useful clinical information. For this recording the respiration rate is 79 cycles per minute.

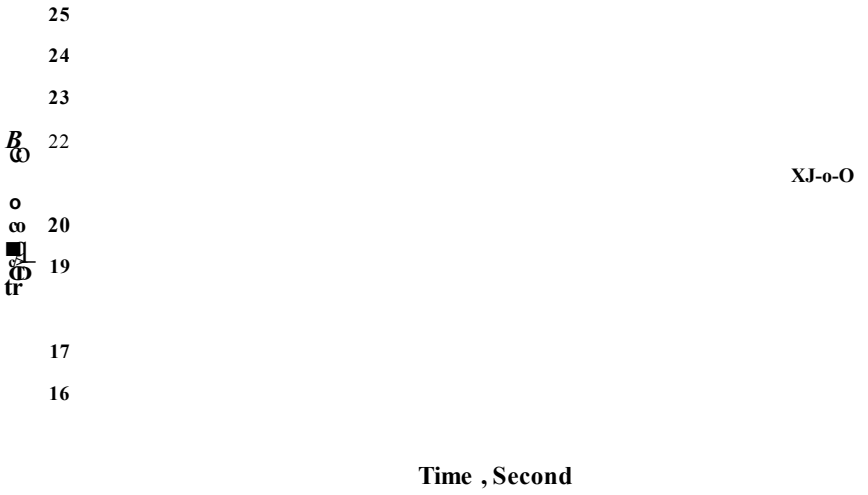

Fig.5.42: Average respiration rate plotted against time.

Fig. 5.43 illustrates the results of applying this method to the respiration signal for an adult with large head movements. The figure also indicates that respiration rate varies with time. For this case the respiration rate is 26 cycles per minute.

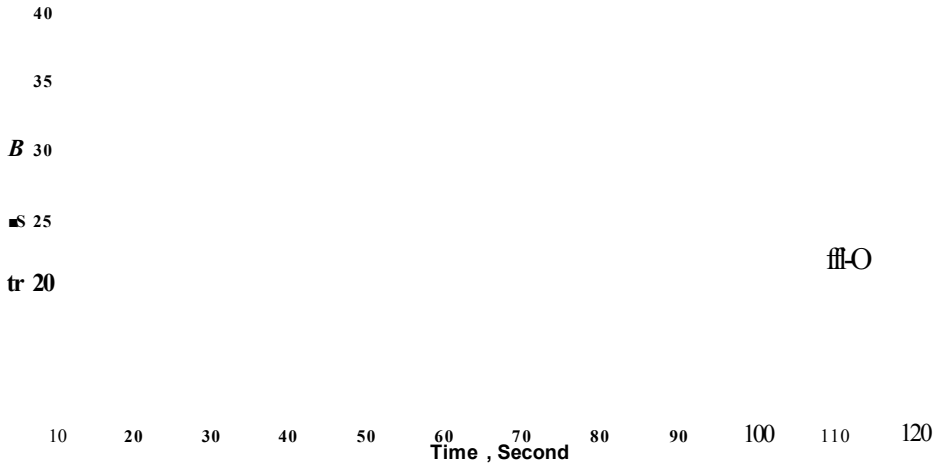

Fig.5.43: Average respiration rate for a case with large head movements.

Method three (Individual Cycle method): The third method of calculating the respiration rate was based on the analysis of the pattern of the respiration signal Zooming the signal showed that the respiration signal was longer in duration when representing breathing out and shorter for breathing in, as shown in Fig.5.44(a). The cycle is best represented as breathing out followed by breathing in The respiration signal was digitally filtered with the 5 order Butterworth filter (cutoff frequency of 0.5 Hz). Then, the peak to peak value of each was calculated. This represented the respiration period (T). This process is illustrated in Fig.5.44(b). The respiration rate (in cycles per minute) was then determined by obtaining an average of the values over a time interval

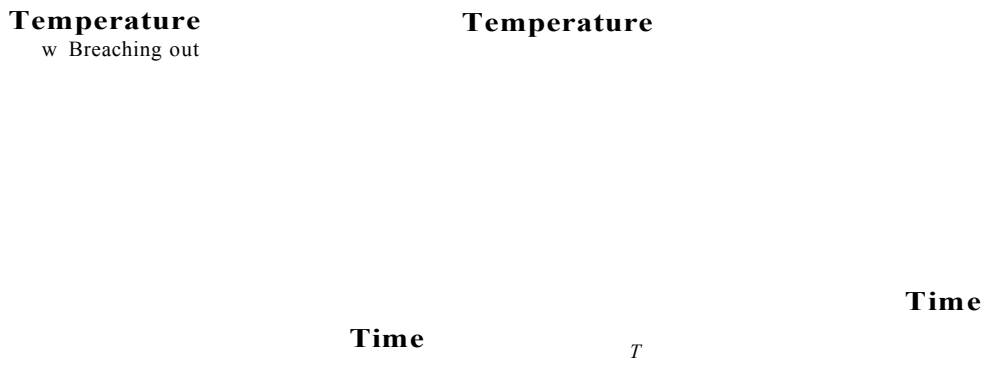

Fig.5.44: The respiration signal, (a) The fluctuations immediately after the signal level changes are consistent in pattern in different respiration cycles, (b) Its filtered signal indicating the respiration (7).

This method was applied after segmenting the ROI into eight parts. The respiration rate was calculated for each segment separately. An example of the results was obtained for when it was applied to the respiration signal of Figs.5.27 and 5.28. The average respiration rate obtained from each segment of the ROI for the images recorded over two minutes without head movements was 26.0, 22.9, 23.1, 23.0, 23.4, 23.3, 22.9 and 22.9 cycles per minute for segments 1 to 8 respectively, while the average respiration rate obtained from the complete ROI was 25.5 cycles per minute. The average respiration rates obtained from segment 1 and the one from the complete ROI were significantly different from those obtained from segments 2 to 8, and appear to be less

accurate. Therefore the respiration rate was approximately 23 cycles per minute in the video without head movements.

The same process was applied to the respiration plots of Figs.5.30 and 5.31 respectively to extract the respiration rate. The average respiration rates obtained from each segment of the ROI for the images recorded over the two minutes was 21.9, 21.8, 23.4, 22.7, 21.8, 22.8, 22.7and 21.8 cycles per minute from segments 1 to 8 respectively, while the average respiration rate obtained from the complete ROI was 21.8 cycles per minute.

5.3. Discussion of findings

The technique described in Section 5.2.2.2 was effective in removing unwanted noise. The technique was applied to thirty videos, each video containing 6000 images. The role of the LPFs in enhancing these images was more significant than HPFs. The median LPF filter was more useful than other filters in removing noise.

Detecting the ROI from the facial thermal image was achieved by using several techniques. These techniques will be explained in the following chapter.

In Section 5.2.3, four features from the ROI to obtain the respiration signal were described. The practical work shows that the respiration signals were obtained clearly by partitioning the ROI centred on the tip of the nose into eight equal parts; the pixel values of each of these segments were averaged. This process was repeated for all the images recorded from each subject. The resulting values were plotted against time to produce the respiration signal. This process provided an opportunity to analysis each part of the ROI separately and to detect the relationship between the signals from different segments.

The study demonstrated that the temperature profiles of some segments in some subjects were out of phase with the other segments (see Fig.5.45 for an example of this effect).

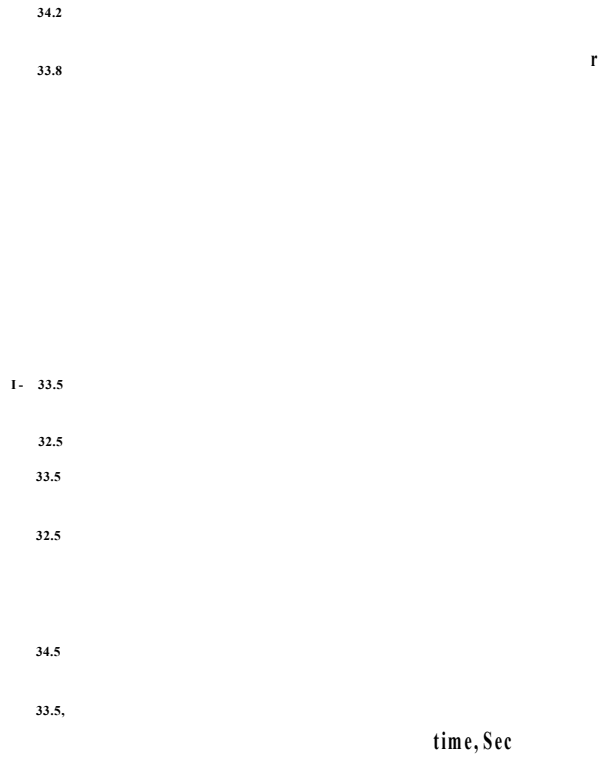

Fig.5.45: Respiration signal from segments 1 to 8 (from top to bottom respectively).

A comparison of the respiration signals from the eight segments indicates that the respiration signals from segments 2, 3 and 4 are the inverse of those in segments 5, 6, 7 and 8. That is, the respiration signals from segments 5, 6, 7 and 8 are delayed in time as compared with those from segments 2, 3 and 4, as shows in Fig.5.46.

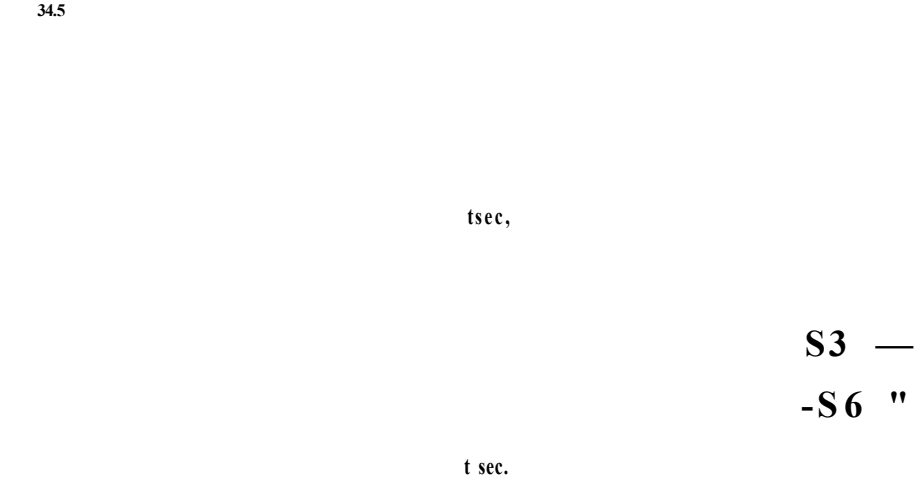

Fig.5.46: Respiration signals, (a) Respiration signals in segments 2 and 7. (b) Respiration signals in segments 3 and 6 respectively.

The cause of this effect could not be established. Three methods were suggested to determine the respiration rate. During the sleep unit studies these methods were tested and compared. The results are explained in the following chapters.

5.4. Conclusion

In this chapter a number of methods to calculate respiration rate were developed. In all these methods, a region centred on the tip of the nose was identified and then divided into eight segments. The respiration signal was obtained by averaging the pixel values in each segment and plotting the result against time. It was established that improved results could be obtained by dividing the respiration region into multiple parts and obtaining the respiration signal from each part. The respiration rate was obtained either by using a FFT method, or by determining the time duration of five cycles (windowing method) or time duration of individual cycles (individual cycle method). An analysis of the effectiveness of respiration rate measurement methods is provided in the following section.

Chapter Six

6. Techniques to Segment the Region of Interest (ROI)

6.1. Introduction

In this chapter the techniques developed to segment the region of interest (ROI) are described. The ROI represents the facial affected area most affected by exhaled air temperature changes. This area is the tip of the nose and the upper lip. Segmenting the ROI was considered an important task in monitoring respiration by thermal imaging.

6.2. Segmenting the ROI

Segmenting the ROI required a procedure to identify the location of the region in the thermal image and then to extract it in a suitable manner. Segmentation was carried out after the images were enhanced by the median LPF (the filtering operation is explained in Chapter 5). The segmentation process was performed either through a manual process or automatically. The descriptions of both are included in the following sections.

6.2.1. Manual Segmentation of the ROI

Initially several thermal videos were recorded with subjects not making any head movements. The ROI was manually identified in the first image and was highlighted by a rectangle. The same region was then automatically extracted from the remaining images of the video, as described in Section 3.5.3.1(Chapter

3). This manual technique was effective when dealing with cases in which there were no significant head movements by the subject, as head movements caused misalignment of the selected region.

To deal with image misalignment caused by small head movements, an image registration (alignment) technique was applied. This technique was effective in correcting the differences in the location of the ROI in successive images due to head movements. The approach is described in Section 3.5.7 (Chapter 3). Through a number of iterations it produced an optimal affine transformation which made the alignment of images as close as possible by considering the maximum correlations.

The alignment process was applied to the all images in the video recording using the reference image (the first image in the video), and then the correlation technique was applied to measure the similarity between the alignment images.

Figs. 6.1, 6.2 and 6.3 show examples of this alignment for different types of head movements. The correlation values between the alignment images and the reference images were calculated as 0.61, 0.79 and 0.72 respectively.

(a) **(b)** **(c)**

Fig.6.1: **Alignment of two images (a) The reference image, (b) The image to be aligned with the reference image, (c) The aligned image (correlation value** =0.61).

(b) (c)

Fig.6.2: Alignment of two images(a) The reference image, (b) The image to be aligned with the reference image (c) The aligned image (correlation value = 0.79).

1A

(a)

Fig.6.3: Alignment of two images (a) The reference image, (b) The image to be aligned with the reference image (c) The aligned image (correlation value =0.72).

As shown in these figures, the alignment technique managed to align the images and the effectiveness of the operation was quantified by calculating correlation technique.

In some cases, despite a large correlation value, the alignment of the images and the reference image was not successful because the subject's head in the reference image was not centred on the image, the effect of which was to corrupt the correct images (see Fig. 6.4 for an example). Also this technique was very time-consuming; therefore it is inefficient for processing 6000 images. In addition, this technique could not deal with large head movements.

(a) (b) (c)

Fig.6.4: Alignment of two images (a) The reference image, (b) The image to be aligned with the reference image (c) The aligned image (correlation value =0.82).

6.2.2. Automatic Segmentation of the ROI

Automatic segmentation the ROI from the images was based on first identifying the region and then tracking it. Three methods were developed for this purpose. In these methods the identification of the ROI required determining the salient features of the human face physiology, consisting of the warmest and coolest regions.

The images were initially enhanced using the median LPF, as described in Chapter 5. An edge detection algorithm was required to extract the subject from the image background. It detected the subject's boundary in the image. Edge detection operators are based on the concept that the edge information in an image is found by looking at the relationship a pixel has with its neighbours.
The effectiveness of the Prewitt, Sobel and Laplacian edge detection operators was investigated.

The $Prewitt$ operator is basically a neighbourhood-based gradient operator, as described in Section 3.5.3.2.I. It searches the edges in both the horizontal and vertical directions. Two convolution masks, Gvand G in the horizontal and vertical direction, are applied separately on the enhanced facial image by using Equations 3.8 and 3.9 respectively. These masks are convolved with each image to determine the edges at those points where the gradient of the image is at its

maximum. A typical result produced by applying the Prewitt segmentation to the thermal images is shown in Fig.6.5 (a).

The *Sobel* operator also uses two convolutions masks, G_x and G_y. They are applied in the horizontal and vertical directions of the image. The masks are shown in Equations 3.13 and 3.14. These masks were convolved with each image to return the edges at those points where the gradient of the image is at its maximum. A typical result obtained when applying the Sobel segmentation to the thermal images is shown in Fig.6.5 (b).

Laplacian is another operator that can be used to determine edges in an image. It uses Equation 3.15. A typical result produced when applying this operator is shown in Fig.6.5 (c).

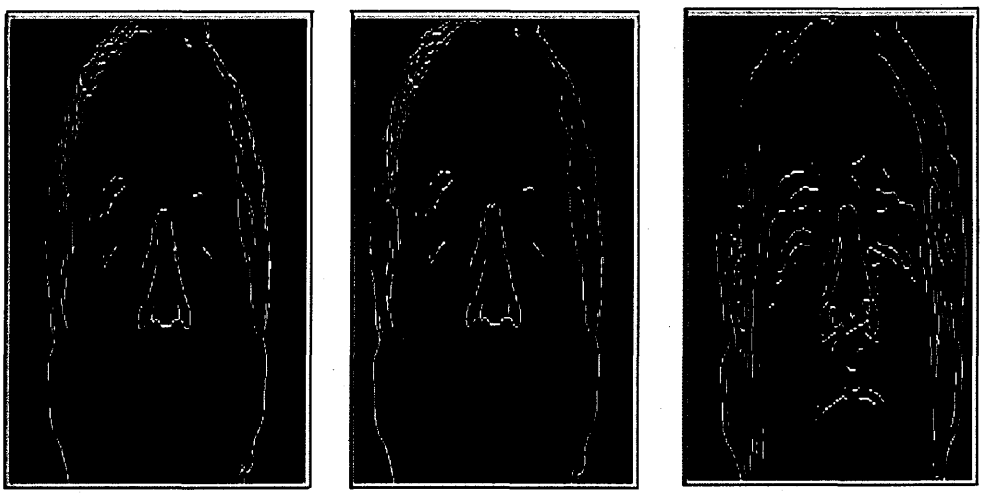

(a) (b) (c)

Fig.6.5: Identifying the subject's boundary from the image background; (a) Result produced when applying the Prewitt operator; (b) Result produced when applying the Sobel operator; (c) Result produced when applying the Laplacian operator.

In this study the Prewitt operator was used, as it best identified the boundary of the subject in the image than other details.

The ROI was determined as a circle centred on the tip of the nose. The radius of this circle is $1/16^{th}$ of the image rows. In order to identify and track the ROI a

number of methods were explored. These are described in the following sections.

6.2.2.I. First ROI Tracking Method

This method was applied to the images following the application of the Prewitt operator. The vertical highest *(Xmax)* and lowest *(Xmin)* and the horizontal highest *(Ymax)* and lowest pixel locations of the detected edges were determined, as shown in Fig.6.6.

m ax

Fig.6.6 **: Determined the vertical and the horizontal pixel locations of the detected edges.**

The centre (X0, F0) was identified by using Equations 6.1.

$$\_ \quad X_{min} + X_{max} \qquad y \quad \_ \quad V_{min} - \backslash - Y_{max} \qquad (6\ 1)$$

max and ^min »^max represents the outermost pixels in the *X* and the *Y* directions respectively.

The circle radius *(R)* was calculated using Equation 6.2

$$R = Y0 - Y\ ain \qquad (6.2)$$

This enables the face to be enclosed in a circle with radius R.

The coldest temperature region in the circle was identified. Practically, the corresponding location of this region represents the tip of the nose. A second circle was placed around the identified tip of the nose; the radius of this circle was $1/16^{th}$ of the number of image rows. This circle represented the ROI and was used to obtain the breathing rate.

Figs.6.7 shows an application of this method to track the ROI for the recording with no significant head movements.

Fig.6.7: Examples of Locating the ROI using the first method.

The first tracking method worked well in cases in which there were no significant head movements. It failed when there were significant head movements, as shown in Fig.6.8.

Fig.6.8: Failure in locating the ROI using the first method.

Therefore, a second tracking method to overcome the limitation of the first method was developed, as explained in the following section

6.2.2.2. Second ROI Tracking Method

To deal with head movements in tracking the ROI, a modification to the first method was carried out. Initially the subject's boundary in the image was determined using the Prewitt operator, then the warmest region within the boundary was determined. This area represents one of two areas between the bridge of the nose and the inner comer of an eye, as shown in Fig.6.9.

Fig.6.9: The warmest area in the human face.

The identified region was marked. In order to extract the second warmest region the pixels associated with the first area were set to zero. The process was repeated to identify the second warmest region associated with the symmetrical region, as shown in Fig 6.10.

Fig.6.10: The second warmest area in the human face.

The coolest region underneath the warmest region was also determined, as shown in Fig.6.11. The lowest value within this region corresponded to the tip of the nose. A circle was placed around the identified tip of the nose; the circle represented the ROI and was used to monitor respiration rate.

Fig.6.11: The coldest region in the human face.

Fig.6.12 shows examples of applying this approach.

Fig.6.12: Examples of tracking the ROI using the second method.

This method worked well when the subject breathed through the nose (not mouth) and the mouth remained closed. An open mouth became the warmest facial region, causing the method to fai

Fig.6.13 shows the warmest region (represented by white pixels) in a thermal facial image for a subject with his mouth open.

Fig.6.13: Highlighting the two warmest areas in the human face when the mouth is open, the first, warmest, region as a white colour and the second warm region as a blue colour.

In order to deal with cases when the subject's mouth was open, the images were classified as an open or closed mouth. In cases where the subject was breathing through the nose and the mouth was closed, the warmest facial regions corresponded to the regions between the comer of each eye and the bridge of the nose. In cases where the subject had opened the mouth, the warmest facial regions corresponded to the mouth and one of the areas associated with the comer of an eye and the bridge of the nose. The magnitude of the distance between these two warmest regions indicated whether the image corresponded to an open or closed mouth.

A rectangular area was selected which included the nose, in order to identify the minimum region within this area. The left and the right limits of this rectangle represented the horizontal lowest (Tw/«) of the first region and the horizontal highest $(Ymax)$ of the second region. The upper limit of the rectangle represented the vertical bwest $(Xmin)$ ofthe second warmest region.

The identification of the bottom limit of the rectangular area was based on the classification of the image as either an open or closed mouth. When the image was classified as a closed mouth, the bottom limit of the rectangular area represented the vertical highest $(Xmax)$ of the first region +100, as shown in Fig.6.14 (b). However, when the image was classified as an open mouth the bottom limit of the rectangular area represented the vertical highest $(Xmax)$ of the first region, as shown in Fig.6.14 (a).

(a) (b)

Fig.6.14: Detenriining the search area from the warmest regions,
(a) When the mouth is open; (b) when the mouth is closed.

The lowest facial temperature region was identified in the rectangular area. Fig.6.15 highlights the lowest facial temperature region when the mouth was open.

Fig.6.15: Highlighting the coldest region in the human face when the mouth was open.

The lowest temperature value within this region was identified; it corresponded to the tip of the nose. A circle was placed centred on the tip of the nose, as shown in Fig.6.16.

This ROI represents the region of best facial temperature changes affected by breathing and was used to determine respiration rate.

Fig.6.16: Tracking the ROI using the second method when the mouth was open.

The second method albwed successful tracking of the ROI with significant head movements, that is with either regular or random head movements, as well as solving the problem of an open mouth. On the other hand, this method of tracking sometimes failed during some types of random head movements because a wrong warmest regbn was identified, as shown in Fig.6.17.

Fig.6.17: Failure of the tracking algorithm to locate the correct warmest areas due to a large head movement.

As this method was based on determining the two wannest regions in order to find the coldest region, the error in identifying the second region during significant head movements led to the failure of this method, as shown in Fig.6.16. To overcome the limitation of this method, changes were made in order to improve this tracking algorithm, as shown in the following section.

6.2.2.3. Third ROI Tracking Method

To deal with limitations of the first two ROI tracking methods the following improvements were made. The images were initially enhanced by the Median LPF and then thresholded. Thresholding was needed to separate the head from the image background. This technique was performed by considering the facial temperature distribution. The temperature of the image background was relatively lower than the temperature of the subject's head. A suitable threshold to separate the background from the subject's face was 30°C. Thus the pixel values $f(x,y)$ in each image were thresholded according to Equation 3.17.
Figs 6.18 and 6.19 show a thermal image before and after the thresholding process respectively.

Fig.6.18: Thermal image before thresholding.

Fig.6.19: Thermal image after thresholding.

The Prewitt edge detection scheme was used to identify the boundary of the subjects' heads in the thresholded images. Detecting the boundary of the subject using the thresholding technique and the Prewitt operator aided removal of those pixels which were not necessary within the limits of the face boundary. These pixels were associated with hair, neck, clothes etc.

Fig.6.20 (a) shows the face boundary extracted from the image background by applying only the Prewitt operator. Fig.6.20 (b) shows the face boundary extracted from the image background by applying the thresholding technique and the Prewitt operator.

(a) (b)

Fig.6.20: Extraction of the subject from the image background: (a) results produced when only the Prewitt operator was applied; (b) Results produced when both thresholding and Prewittt operator were applied.

The outline of the human face can generally be described as being roughly elliptic in nature. Therefore the face boundary was extracted later from the image by selecting an elliptical area which fitted onto the selected boundary values. This ellipse enclosed the most important part of the image, i.e. the face. The edge map after the thresholding technique and Prewitt operator can give a good outline of the image containing the face region. The location and size of the ellipse were determined by performing the following tasks

- The highest (X_{max}) and lowest (X_{min}) pixel locations of the head boundary in the vertical direction were identified and the centre between these two locations (X_0) was determined.
- Centred at X_0, the head boundary points in the horizontal direction were identified, providing Y_{min} and Y_{max}. Then, the centre (Y_0) between Y_{min} and Y_{max} was calculated.
- The diagonals of the ellipse (i.e. $2a$ and $2b$) which represent the semi-major and the semi-minor axes respectively were determined, where a and b were calculated from X_0, and Y_0 to X_{min} and Y_{min} respectively.
- Since the aim was to fit an ellipse to the image outlined by its edges, the position of the ellipse on the filtered images was then determined by using the ellipse Equation 6.3 (Downing, 2003).

$$\frac{(X_i - X_0)^2}{a^2} + \frac{(Y_i - Y_0)^2}{b^2} = 1 \qquad (6.3)$$

This operation kept the elliptical region containing the human face and segmented it from the rest of the image, as shown in Fig 6.21.

Fig.6.21: The position of the ellipse superimposed on the filtered thermal image.

Once the subject's face was enclosed by an ellipse, the remaining parts of the image were removed.

The next task was to identify and track a circular region centred on the tip of the nose (i.e. the respiration region of interest, ROI). To achieve this, initially the image area enclosed by the ellipse was scanned to identify the warmest region.

A scanning operation was carried out inside the selected ellipse. This consisted of starting from its top-left corner and averaging the values of the pixels in an area of 5 x 5 pixels. This process continued till the scanning operation reached the far right corner of the boundary. Then the scanning process was repeated to the far-left corner of the image until the full selected area was scanned. During each scan, the most recently calculated average pixel value was compared with the previous largest average pixel value.

This process allowed the location of one of the two warmest facial regions to be detected. This area represented one of the two areas between the bridge of the nose and the inner corners of the eyes, as shown in Fig.6.22

Fig.6.22: The warmest facial area.

The procedure described above was repeated in the image section enclosed within the ellipse to locate the coolest region, but this time the scanning was performed beneath the identified warmest area so that the coldest area could be located. The reason for first identifying the warmest region and then the coolest region underneath it was to reduce thepossibility of a wrong region being chosen, especially when there were large head movements. The lowest value within this region was identified; it corresponded to the tipof the nose. The circle was centred on the tip of the nose, as shown in Fig.6.23.

Fig.6.23: ROI represented by a circle (mouth closed).

In this method respiration through the nose with the mouth open was dealt by looking for the warmest region on the upper part of the ellipse only, thus excluding the mouth region. The scanning was performed beneath the identified warmest area and the coldest area was located. The bwest value within this region was identified. This corresponded to the tip of the nose. The circle was centred on the tip of the nose, as shown in Fig.6.24.

Fig.6.24: ROI represented by a circle (mouth open).

Fig.6.25 shows the flowchart of the third ROI tracking method.

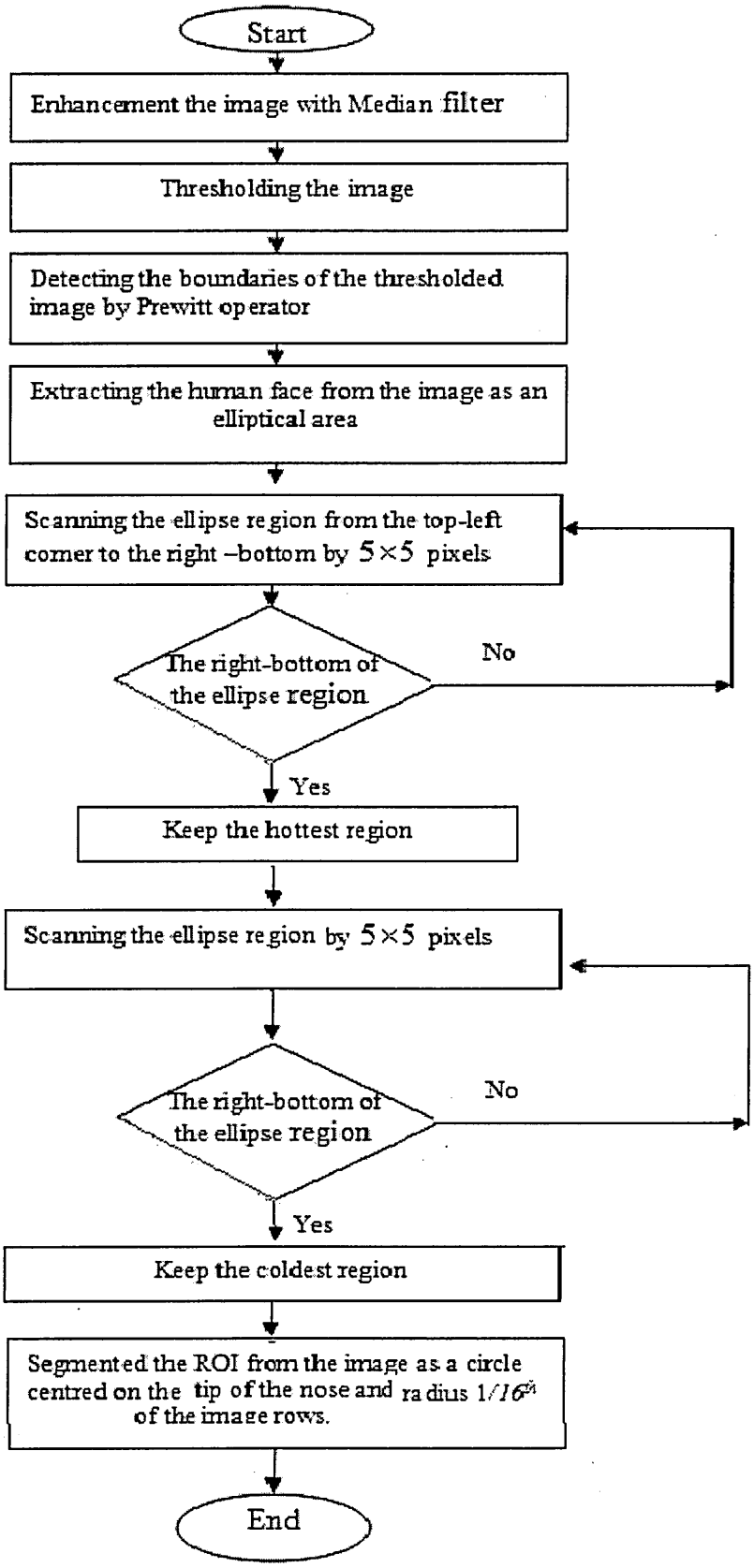

Fig.6.25: The flowchart of the third ROI tracking method.

This method was successful in tracking the ROI with different head movements (regular and random head movements), as shown in Fig 6.26 (a) and (b).

The process was repeated for each of the 6000 images (Le. 120 seconds recordingx 50 images per second) to determine the ROI as well as calculate the respiration rate.

(b)

Fig.6.26: (a) and (b) Examples of third method in tracking the ROI during different head movements.

6.3. Results and Discussion

In order to determine the effectiveness of the tracking methods for the ROI, two types of head movements were considered: regular movements and random movements.

1- Regular movements involved the head turning to the left and right less than 45°, as shown in Fig.6.27.

2

Mid-left Centre Mid-Right

Fig.6.27: Regular Movements.

2- Random movements involved the head turning to random positions to the left, right, up and down, as shown in Fig.6.28.

Fig.6.28: Random Movements.

6.3.1. Analysis of the effect of the shape of the ROI

Initially the ROI was represented as a rectangle. However, this shape proved to be unsuitable to allow successful tracking. For the images that had large diagonal head movements, the rectangular ROI provided inaccurate information, as shown in Fig.6.29.

Fig.6.29: The rectangular representation of the ROI with large diagonal head movements.

Also, in some images the nose appeared too close to the edge of the image, as shown in Fig.6.30. Therefore, the rectangular area fell outside the boundary of the image.

Fig.6.30: A head movement highlighting the nose very close to the edge of the image.

To deal with the above issues, the ROI was represented by a circle. This dealt with the problems of large diagonal head movements as well as the nose appearing too close to the edge of the image. Fig.6.31 shows the ROI being represented by a circle.

Fig.6.31: **The** ROI **highlighted by a circle.**

6.3.2. Hie Size of the ROI

To investigate the accuracy of the respiration rate measurement according to the size of the ROI, the circle radius was initially set to

$$*** = 1_{16}^{7} * AT \qquad (6\text{-}4>$$

Where **TV** is the number of image rows. *Rcircle* value was reduced by increasing the value in Equation 6.4 from *16* to *17,* and increased by decreasing the value in Equation 6.4, from *16 to 15.*

In each case the average pixel value within each circle was plotted against image number (see Fig.6.32). The results indicated changing the ROI by the specified amounts does not make a significant change to plots produced as they cover the nostrils.

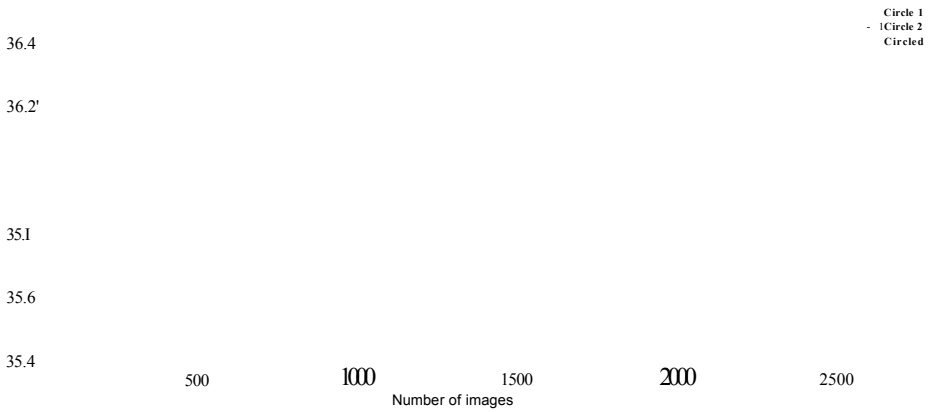

Fig.6.32: **Average pixel value within** ROI **represented by different circle sizes.**

Table 6.1 provides an evaluation of the third tracking method. The number of images that the ROI had not successfully tracked was visually determined. The accuracy of the tracking methods was calculated by determining the percentages of images that had not successfully tracked the ROI.

TABLE 6.1: Tracking Analysis Results for Different Head Movements

Subject	Number of images	% Failure (method one)	% Failure (method two)	% Failure (method three)	Video type
SO1	6000	28	2.63	0	Random movements
SO2	6004	17.4	4.98	0	Random movements
SO3	6000	35	5.35	0.08	Random movements
SO4	5991	1.67	0	0	Regular movements
SO5	5995	0	0	0	Regular movements
SO6	6000	21.3	0.69	0	Random movements
SO7	6010	15.8	0.2	0.02	Random movements
SO8	5999	2.2	0	0	Regular movements
SO9	6000	49	0.16	0	Random movements
SO10	6010	42	1.73	0	Random movements
SO11	5999	0.16	0	0	Regular movements
SO12	1148	4.6	0.17	0	Random movements
SO13	1150	6.7	0.53	0.17	Random movements
SO14	1150	0.6	0.13	0	Random movements
SO15	2580	0.34	0.19	0.03	Regular movements
SO16	550	6.7	2	0	Random movements
SO17	50	14	4	0	Random movements
SO18	50	8	8.0	4	Random movements
SO20	39	15	0	0	Random movements
SO22	28	0	0	0	Regular movements
SO23	35	51	11.4	0	Random movements

The tracking was considered as a failure when the ROI had not been located successfully for an image. The proportion of tracking failure was calculated as the total number of failures divided by the total number of images in a recorded video. Failed tracking was caused either by the subjects in the ROI extending too far from the image or by the effect of the environment on body temperature. There were some other limitations which will be explained in the following chapter.

6.4. Conclusion

A method to track the human face automatically in thermal images was developed. The method robustly dealt with static, regular and random head movements. During recordings under different head movement types it was possible to successfully detect the ROI associated with the respiration process.

Chapter Seven

7. Thermal Imaging Based Respiration Rate Monitoring in Children.

7.1. Introduction

In this chapter the investigation of thermal imaging for respiration rate monitoring is described. The method was evaluated on twenty children admitted to the sleep unit of Sheffield Children's Hospital.

All thermal image recordings were carried out in parallel with a number of conventional contact-based respiration monitoring methods which already exist in the hospital. This enabled a comparison to be carried out between the approaches.

7.2. Description of Existing Contact-Based Respiration Monitoring Systems

The existing instruments for respiration monitoring were:

A. Respiration belt transducer: A band should be tight enough to detect the chest and abdominal movements.
B. Nasal Pressure transducer: Dual nasal cannulas are used to measure nasal pressure. A sensor is used to measure the airflow based on the actual volume of the air exhaled.
C. Thermistor pod; sensors used to measure the temperature from the nose or mouth.

D. Transcutaneous CO_2 transducer: A sensor relies on the diffusion of gas to the skin and provides an overall estimate of changes in CO_2. It is applied to the skin, usually the earlobe.

E. Respiratory sounds transducer (microphone): A sensor is placed either close to the respiratory airways or over the throat to detect variation of sound.

F. Oximetry Probe (Sp02): A sensor is placed on the forehead, big toe, fingertip or bridge of the nose to detect the saturation of oxygen changes in blood (Sp_{0_2}).

G. Electrocardiogram derived respiration probes: four leads are attached to the chest and the ribs of the patent to provide the heart pattern (ECG). The respiration signal rate can be extracted from the ECG leads.

These instruments have been explained in Section 2.2.2 of Chapter 2.

Figs.7.1 and 7.2 show the various contact devices used in Sheffield Children's Hospital and their respective placement on a child's body.

Fig.7.1 : The standard contact respiration rate monitoring devices. (A) Respiration belt transducer; (B) Nasal Pressure transducer; (C) Thermistor pod; (D) Transcutaneous Co2 transducer; (E) Respiratory sounds transducer (microphone); (F) Oximetry Probe (Sp02);(G) Electrocardiogram derived respiration probes.

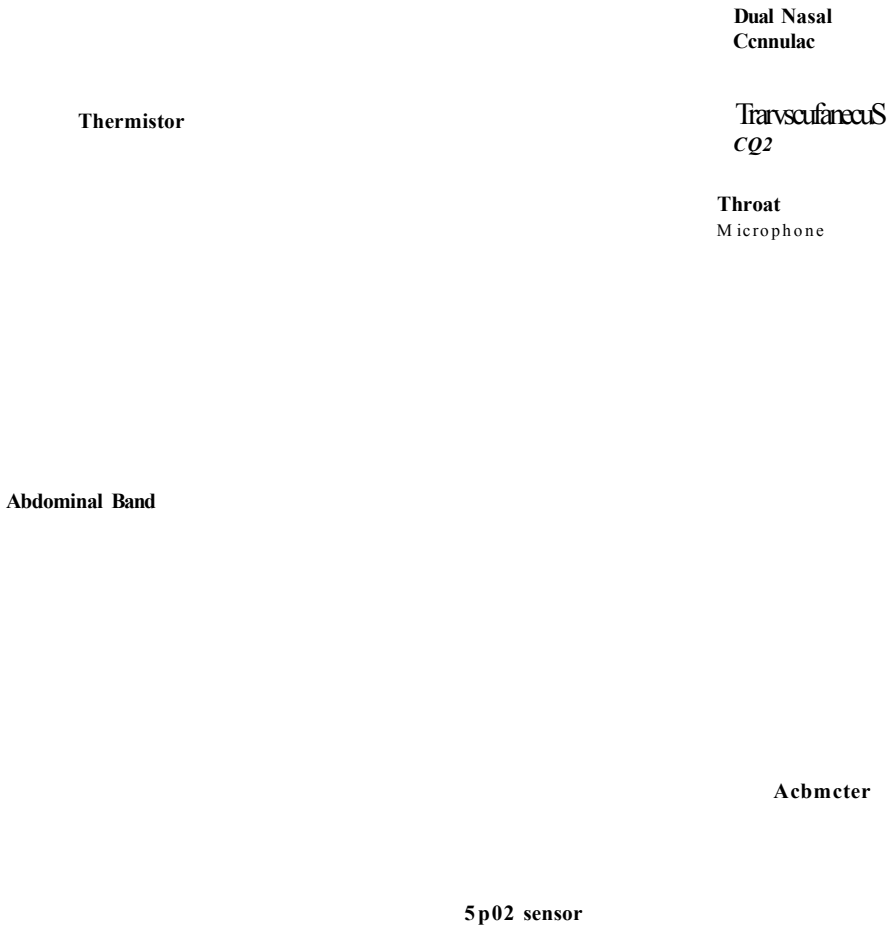

Fig.7.2 : Placement positions of contact devices on a child's body (The diagram was supplied by Sheffield Children's Hospital).

73. Patients' Details and Recording Procedure

The thermal imaging system is discussed in Section 5.2. The recordings took place in a room in the Sleep Unit of Sheffield Children's Hospital. Twenty infants and children (seven females, thirteen males) were enrolled. The age range was six months to seventeen years. Relevant details of the subjects included in the study are provided in Table 7.1.

TABLE: 7.1: Details of subjects included in the study.

Gender	Number	Age			
		Minimum	Maximum	Mean	Standard deviation
Female	7	1 year	17 years	8	5.59
Male	13	6 months	15 years	7.19	4.64

The patients were appropriately informed of the nature of the study and their parents consented for the data to be used in the study. All thermal recordings were carried out in parallel with conventional contact-based respiration monitoring methods to allow comparisons to be made.

The thermal recordings were performed with the subjects resting comfortably on a bed. The recordings did not cause any form of distress or discomfort to the subjects. Some patients were awake during the recordings while others were sleeping. The recording room temperature was at about 30°C.

The thermal images were recorded using a FLIR A40 thermal camera. The camera was fixed on a tripod in front of the subject at a distance of about one metre. The camera's emissivity setting was 0.92°. Its thermal sensitivity was 0.08 degrees Kelvin.

The duration of each data recording was two minutes. This produced 6000 thermal images (i.e. 120 seconds × 50 images). Therefore, the image capture rate was adequate for the variations in the images being recorded.

The thermal images were filtered and segmented as described in Chapter 5. The respiration ROI in sixteen children was automatically tracked using the procedure described in Section 6.2.2.3. The remaining four subjects either breathed through the nasal area covered by attached medical instruments or

breathed through the mouth. A different tracking algorithm (described in a later part of this chapter) was used for these four subjects.

The region was partitioned into eight equal segments. This enabled the respiration rate from each section to be examined separately. The pixel values within each segment were averaged to produce a single thermal feature for that segment. A respiration signal was then produced by plotting each segment's feature against time. Respiration rate was automatically calculated by determining the number of oscillations in the respiration signals(individual cycle method), as described in Section 5.2.2.5 of Chapter 5.

The clarity (i.e. the ease with which the respiratory cycles could be visually observed in the respiration signal) produced by each contact method varied in different children and therefore the specific method that provided the clearest respiration signal for each child was visually selected and used. The contact methods only produced a respiration signal (not a respiration rate). In order to determine the respiration rate, the number of visually-observed respiration cycles had to be manually counted.

7.3.1. Results and Discussion

The results of applying the thermal imaging based respiration rate monitoring method for twenty infants and children are explained in this section. Eighteen children breathed through the nose while the other two had mouth breathing. For the sixteen children who had nasal breathing the ROI was tracked automatically by the method described in Section 6.2.2.3. A different tracking algorithm (described in the next section of this chapter) was used for the two subjects who breathed through the nasal area covered by attached medical instruments.

7.3.1.1. Nasal Breathing

An example of a recording was taken of a child, aged 13 years, who was awake and who breathed through his nose. The ROI was tracked automatically by the method explained in Section 6.2.2.3 and selected as a circle centred on the tip of

the nose. The ROI was segmented into eight equal segments centred on the tip of the nose, as shown in Fig.7.3.

Fig.7.3: Respiration region of interest, its position centred on the tip of the nose.

Fig.7.4 illustrates the plots of the respiration signals obtained by averaging the pixel values of each segment of the ROI indicated in Fig.7.3. This figure shows the respiration signal after bw pass filtering with a 5th order Butterworth filter with cutoff frequency of 1.5 Hz The respiratbn cycles from segments 1, 2, 3, 4 and 5 are more identifiable than those from the other segments. This is because the areas related to these segments were affected by respiration more than the other areas. The respiratbn rate was calculated by the individual cycle method (method 3) described in Section 5.2.2.5. The process involved determining the peak-to-peak duration of each respiration cycle (T, in seconds). The respiratbn rate (in cycles per minute) was determined by first producing the average of all respiratbn cycles. The reciprocal of this value was divided by 60 to obtain the respiration rate in cycles per minute. The respiration rate from segments 1 to 5 was approximately 17.5 cycles per minute.

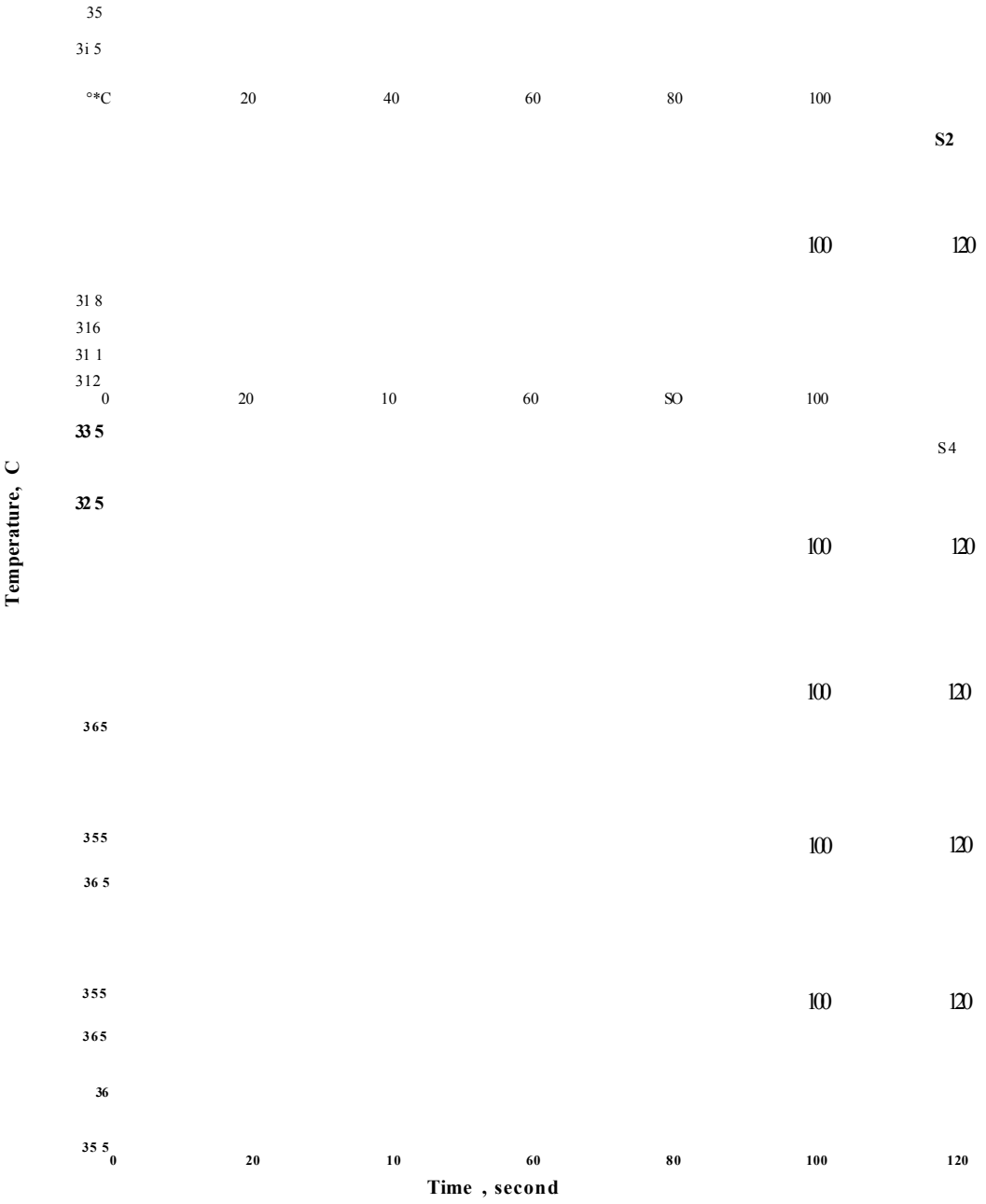

Fig.7.4: Respiration signals obtained using thermal imaging. The signals obtained from segments 1 to 8 are shown from top to bottom respectively.

The same process was applied for the sixteen children and infants. The respiratbn rates were 23.3, 17.5, 22, 22, 16.8, 15, 15.3, 20.6, 19.5, 18, 19, 34, 15.5, 27, 24 and 22 cycles per minute respectively.

In order to show the variatbns of respiration rate over time, a moving average of respiration rate was also produced using the windowing method (method 2)

in Section 5.2.2.5 to the clearest signal of the ROI. This involved determining the average respiration rate within a window containing five successive respiration cycles, and then repeating this calculation by moving the window forward by one cycle. The average of the respiration signal (fifth segment) by this method was calculated to be 17.4 cycles per minute.

Fig.7.5 shows this windowing operation performed on the clearest signals of the ROI for sixteen children. The average of the respiration rate for each child was 23.3, 17.4, 21.6, 22, 16.7, 15, 15, 20, 18.9, 17.9, 19, 33, 15.4, 26.7, 24, 22 cycles per minute respectively. The figure also indicates that the respiration rate varies with time. The amount of the fluctuations is useful in monitoring the pattern of respiration rate.

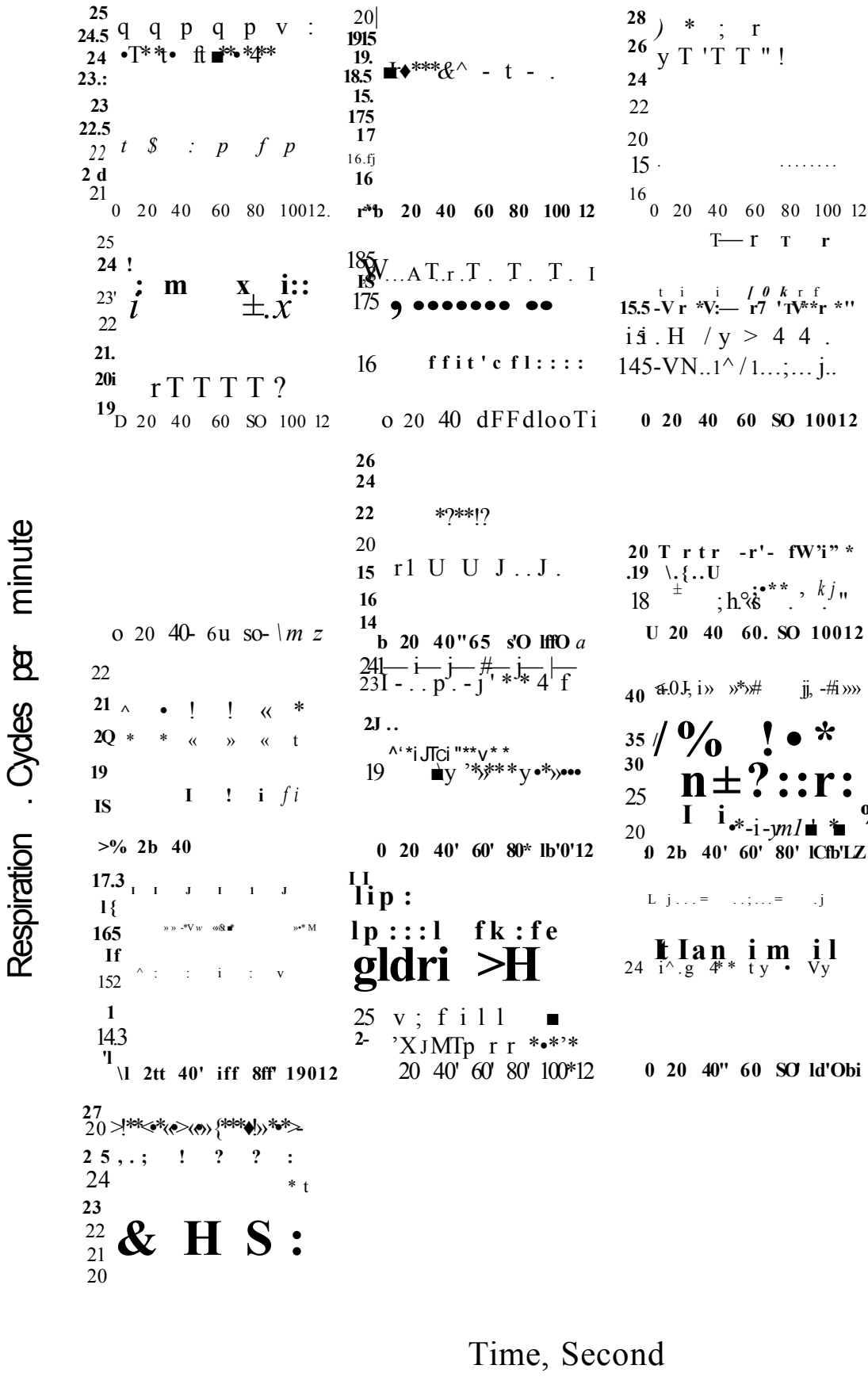

Fig.7.5:Respiration rates running average for the clearest respiration signals of the ROI for the sixteen children respectively .

The magnitude frequency spectrum of the respiration signal shown in Fig.7.4 (fifth segment) was also produced. This was obtained using the FFT (method 1) described in Section 5.2.2.5. The highest peak in the frequency spectrum (i.e. the component that contains most energy) occurs at 0.3 Hz. This corresponds to a respiration rate of 0.3 cycles per second, or 18 cycles per minute. This value is close to the value obtained directly from the respiration signal by determining the number of cycles per seconds.

The same method (the FFT method in Section 5.2.2.5) was applied to sixteen children. The highest peak in the frequency spectrum for the clearest signal occurred at 0.39, 0.3, 0.35, 0.38, 0.28, 0.25, 0.25, 0.3, 0.31, 0.3 , 0.316, 0.64, 0.26, 0.44, 0.40 and 0.37 cycles per second respectively (see Fig.7.6). This corresponds to respiration rates of 23.4, 18, 21.4, 22.8, 16.8, 15, 15, 18, 18.6, 18, 19, 38, 15.6, 26.4, 24 and 22 cycles per minute.

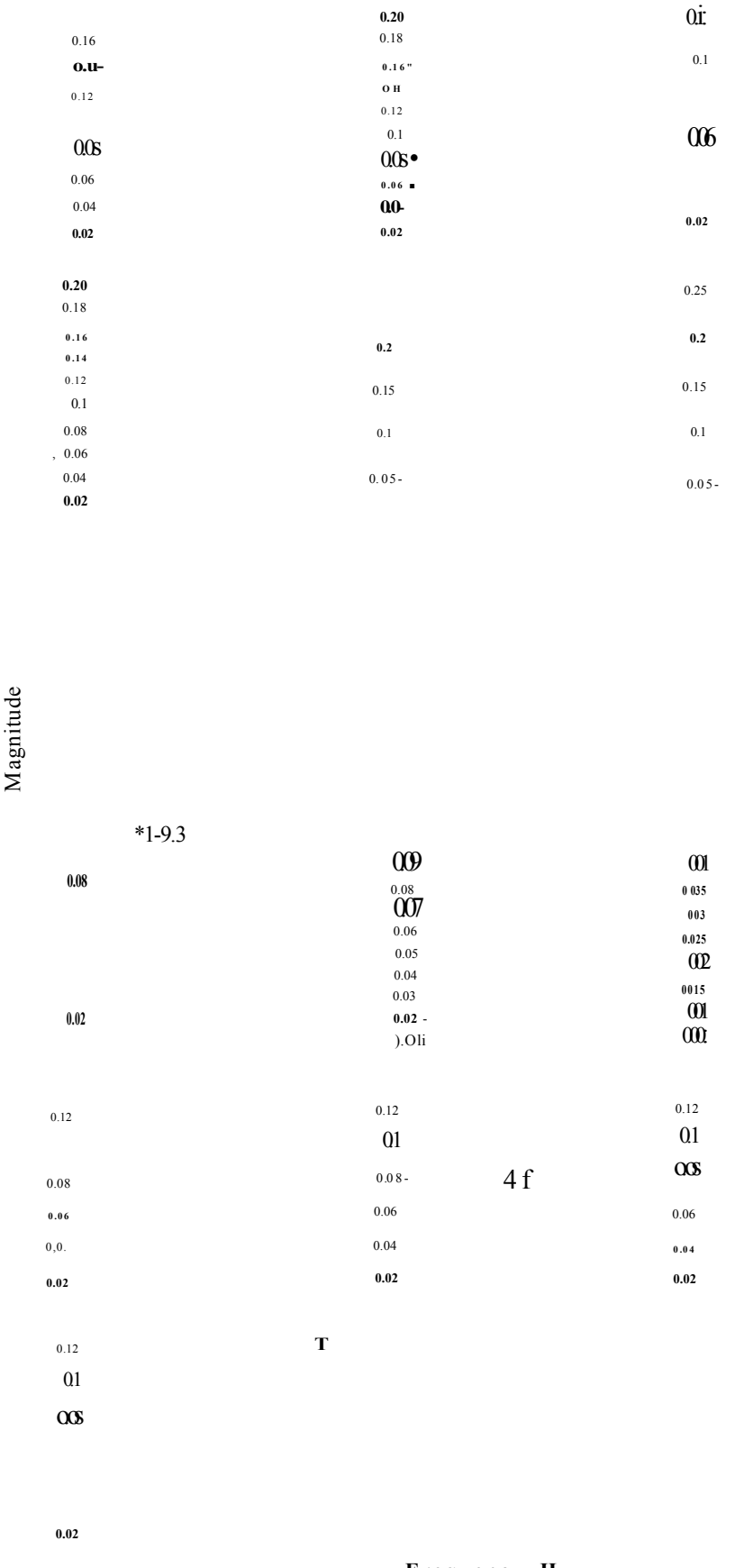

Fig.7.6 : The magnitude frequency spectrum of the respiratory signal for the clearest segments of the ROI of the sixteen children.

The performance of the thermal imaging respiration rate monitoring method was evaluated by comparing it against the values obtained using conventional contact-based methods. The clarity of the respiratbn signal obtained using contact methods varied in different children; therefore, the clearest signal (Le. the signal with best identifiable respiration cycles) was selected visually. Fig.7.7 shows the respiratory signals obtained using a nasal pressure probe, thoracic belt and transcutaneous CO_2 for the child in Fig.7.3. The value of the respiratbn rate was determined from these signals by manually counting the number of cycles. For the signals shown in Fig.7.7, this was 17.5 cycles per minute.

Fig.7.7: Respiration signals obtained using Nasal pressure, thoracic belt and C02probe.

The clarity of respiration signals obtained for the sixteen children using contact methods was visually selected. The number of manually-counted respiration cycles was 23.5, 17.5, 22, 22, 16.5, 15.5, 15, 19, 18, 18, 18.75, 34, 15.25, 27, 23.75, 21.75 cycles per minute respectively.

The remaining two subjects breathed through a nasal area covered by attached medical instruments. A different tracking algorithm was used for these two subjects (described in the following section). The ROI was selected as a circle centred on the tip of the nose and the ROI was segmented into 8 parts. The pixel values of each segment of the ROI were indicated. Then the respiration rate was calculated for each segment by using the three methods in Sectbn 5.2.2.5.

Examples of recordings were taken for children, aged two and eleven years, while asleep and awake. The respiration signals were extracted from the clearest segment of the ROI. The respiration rate was calculated from the clearest signals by using the Individual cycle method (method3) in Sectbn 5.2.2.5; it was 26.8 and 21 cycles per minute respectively.

In order to show the variations of respiration rate over time, the windows cycle method (method 2) described in Sectbn 5.2.2.5 of the clearest signals of the ROI was produced, as shown in Figs. 7.8(a) and 7.8(b). The average of the respiration signals (clearest signals in the ROI) by this method was calculated; it was 26.8 and 21 cycles per minute respectively.

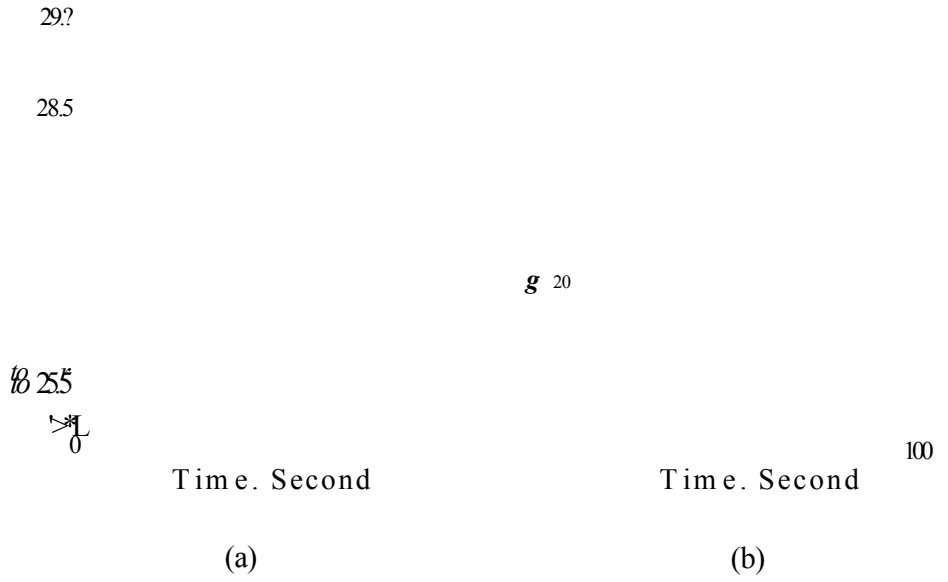

(a) (b)

Fig.7.8: Respiration rates running average for the clearest respiration signal of the ROI for the two children breathing through a nasal area covered by attached medical instruments.

The magnitude frequency spectrum of the respiration signals for the clearest respiration signal for the two children breathing through a nasal area covered by attached medical instruments is shown in Fig.7.9 (a) and (b). This was obtained using the Individual cycle method described in Sectbn 5.2.2.5. The highest peaks in the frequency spectrum are at 0.45 and 0.37 Hz respectively. This corresponds to a respiration rate of 0.45 and 0.37 cycles per second or 27 and 22 cycles per minute.

(a) (b)

Fig.7.9 : The magnitude frequency spectrum of the respiratory signals for the clearest segments of the ROI of the two children breathing through a nasal area covered by attached medical instruments.

The respiration rate values obtained using thermal imaging was compared with those obtained using conventional contact-based devices. The respiration rate obtained from the conventional methods was 26.5 and 21 cycles per minute respectively.

7.3.I.2. Respiration Monitoring in Subjects Breathing Through the Mouth

The current tracking method to determine the ROI has assumed that respiration is performed via the nose. Optimal breathing is achieved via the nose (Janssen and Rechelbacher, 2009; Friedman, 2009 and Shneerson, 2005). However, in some cases a subject's respiration is through the mouth. Examples of recordings were taken for children aged ten years shown in Fig.7.10 (a) and (b) who had mouth breathing.

The method described in this study did not identify the mouth region as the area for respiration rate analysis. This is because the algorithm used in this study to find the tip of the nose (coolest facial area) first detected the warmest facial area and then scanned for the coolest area beneath it. Therefore, in these subjects the mouth region was initially tracked manually by using the method described in

Sectbn 6.2.1 of Chapter 6. However, practical observatbns showed that this method was not robust when there were head movements. Therefore, this tracking algorithm was modified to deal with its limitatbns

(a) (b)

Fig.7.10: Segmenting the ROI into eight parts for a sleeping child. The ROI is centred on the mouth.

The procedure to track the mouth region manually started by identifying the subject's boundaiy in each image as an ellipse by using thresholding technique and Prewitt operator as described in Sectbn 6.2.2.3. The centre of the mouth was determined manually in the elliptical area of the reference image and then the distance from this centre to the outermost edge pixel in both the X and Y directions of the elliptic was determined.

The mouth region was extracted from the outermost edge pixel for each image. This process was applied to patients of seven and eight who breathed via the mouth. A circle was placed centred on the mouth, as shown in Fig.7.10 (a) and (b). The circled area represents the ROI for extracting the respiratory signal This area was divided into eight equal segments and the signal was extracted for each part. Then the respiration rate was calculated for each segment by using the three methods in Section 5.2.2.5.

Typical respiration signals obtained from the mouth regbn (ROI) for the children in Figs. 7.10(a) and 7.10(b) were extracted. The respiration rates were extracted from the clearest signals in the ROI segments by the Individual cycle

method in Section 5.2.2.5. These were 20 and 20.5 cycles per minute respectively.

Figs.7.11(a) and 7.11(b) show the variations of respiration rate over time for the clearest respiratbn signals for the children shown in Figs.7.10(a) and 7.10(b). This was obtained by employing the windows cycle method in Section 5.2.2.5. The average of the respiration rates to the respiration signals (clearest signals in the ROI) by this method were calculated to be 19.5 and 20.4 respectively.

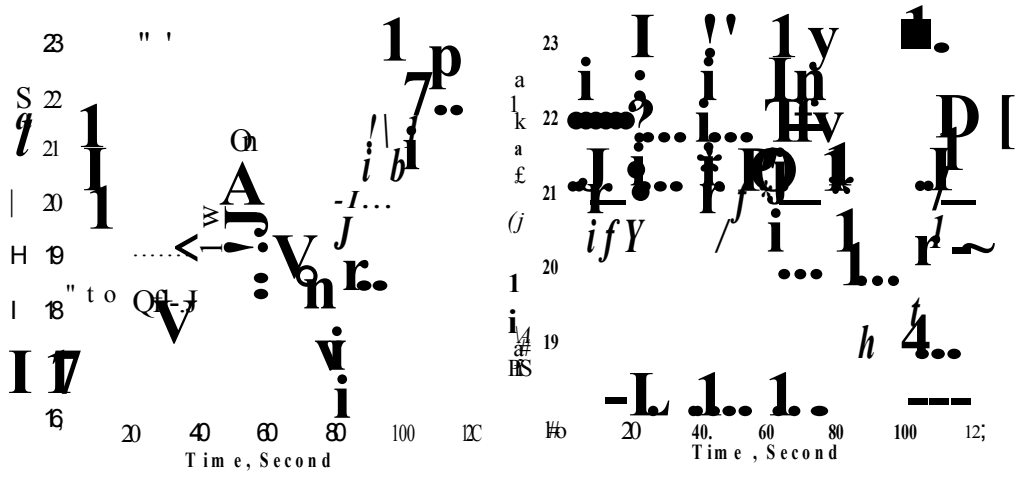

(a) (b)

Fig.7.11: An examples of respiration rate running average of clearest segments during mouth breathing for the children in Fig.7.10(a) and (b).

The magnitude frequency spectrum of the respiratbn signals for both children shown in Figs.7.10 (a) and 7.10(b) is shown in Figs.7.12 (a) and 7.12(b). This was obtained using the FFT method described in Sectbn 5.2.2.5. The highest peaks in the frequency spectrum were at 0.308 and 0.35 Hz respectively. This corresponded to respiration rate of 0.308 and 0.35 cycles per second, or 18.5 and 21 cycles per minute.

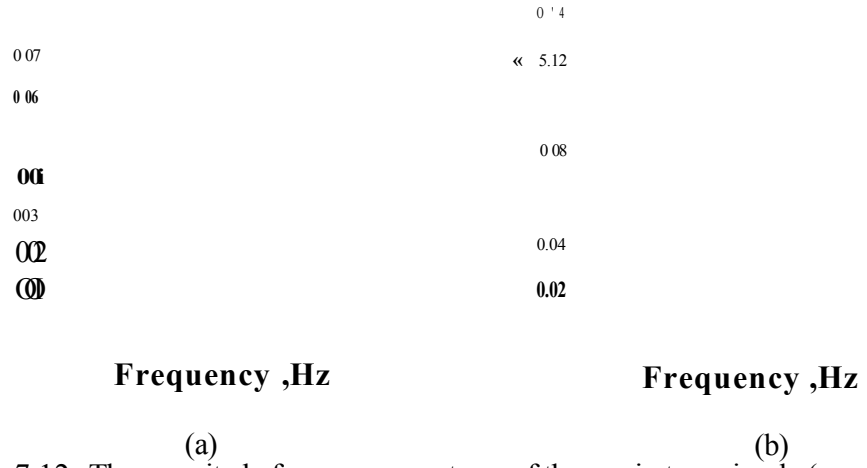

(a) (b)

Fig.7.12: The magnitude frequency spectrum of the respiratory signals (corresponding to the clearest segment of the ROI) for the children in Fig.7.10(a) and (b).

The respiratbn rate values obtained using thermal imaging were compared with those obtained using conventional contact-based devices. The respiration rates obtamed from the conventional methods were 19.75 and 20.5 cycles per minute respectively.

7.3.I.3. Detecting Respiration-Related Illnesses

Conditions such as apnea can be detected by analysing respiration signals. Fig. 7.13 illustrates an example of the respiration signal for a child who had apnea. The clearest signals were obtained from the ROI segments 1, 2, 7 and 8. The average respiratbn rate was 34 cycles per minute.

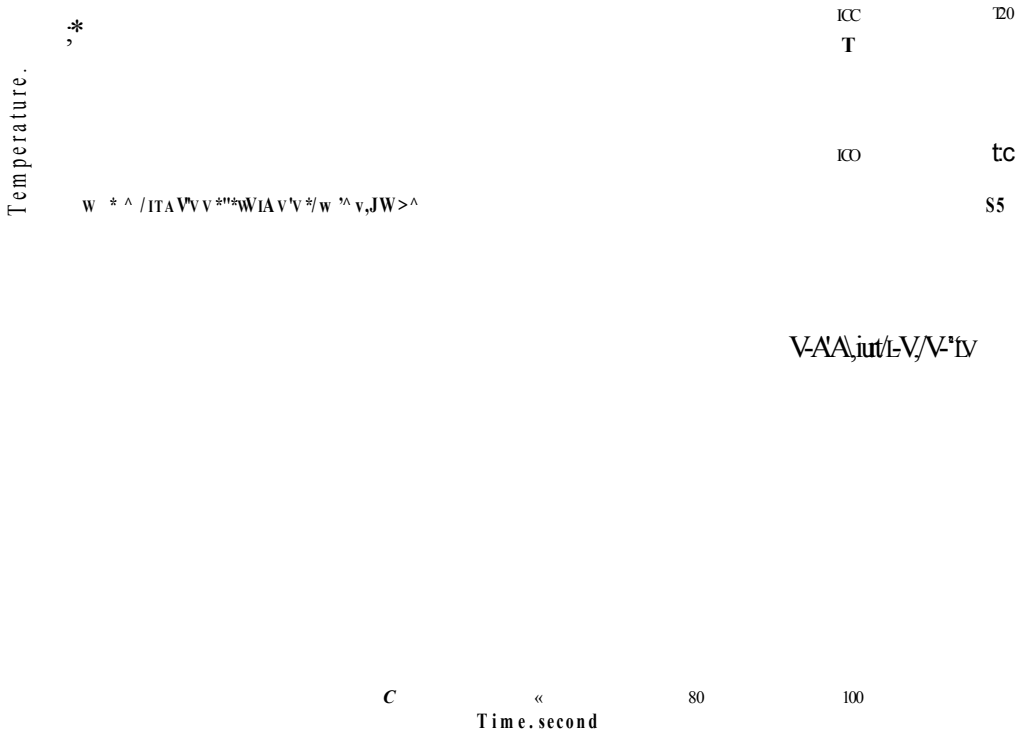

Fig.7.13: Respiration signals obtained using thermal imaging. The signals obtained from segments 1 to 8 are shown from top to bottom respectively.

Fig.7.14 shows the variations of respiration rate over time for the respiration signals of Fig 7.13(Individual cycle method). The average respiratbn rate obtained from segment 1 was 33 cycles per minute.

Fig.7.14: An example of respiration rate running average of segment 1 shown in Fig.7.13 for a child who had apnea.

The respiration signals obtained using thermal imaging and those obtained using contact methods showed that there was a breathing problem for this child that was visible in the signals (between 66 and 79 seconds). The clearest respiration signals for contact-based approaches were obtained using the transcutaneous CO_2, thoracic belt, and nasal pressure and thermistor methods, as shown in Fig 7.15. The respiration rate obtained from these conventional methods was 34 cycles per minute.

Fig.7.15: Detection of apnea in the respiration signal obtained using transcutaneous CO_2, thoracic belt, and nasal pressure.

Twenty children were included in this study. The three methods described in Section 5.2.2.5 were applied for all the children to extract the respiration rate from the respiration signal.

Table 7.2 shows the respiration rate values for these children. The ROI in sixteen children was tracked automatically, while the ROI in the remaining children was selected manually. The table compares the respiration rates obtained using the thermal imaging method against those obtained using contact methods for each child. The mean respiration values across all children using the thermal imaging method (BR_t) and the contact methods (BR_c) were 20.9 and 20.7 cycles per second respectively.

The correlation coefficients (ρ) for respiration values obtained using the thermal imaging methods and contact methods (using Equation 3.27) were 0.97, 0.92 and 0.99 for methods1, 2 and 3 respectively. These results indicate method 3 provided a closer correlation to the contact methods.

TABLE: 7.2 Summary of respiration rate analysis.

Patient No	**Gender**	**State of Patient**	**Age in years**	**The most effective contact Methods**	**Respiration rate in cycles per minute using the selected contact method BR_c**	**Respiration rate in cycles per minute using thermal imaging methods BR_t**		
						FFT method	*Windows cycle method*	*Individual cycle method*
P1	Male	asleep	4	Abdominal belt & transcutaneous Co2	23.5	23.4	32.3	23.3
P2	Male	awake	13	Thoracic belt & Nasal Pressure & transcutaneous Co2	17.5	18	17.4	17.5
P3	Female	asleep	6	Transcutaneous Co2	22	21.4	21.6	22
P4	Female	asleep	1	Transcutaneous Co2	22.	22.8	22	22.

TABLE: 7.2 Summary of respiration rate analysis (continue).

Patient No	Gender	State of Patient	Age in years	The most effective contact Methods	Respiration rate in cycles per minute using the selected contact method	Respiration rate in cycles per minute using thermal imaging methods ^{DR} *1*		
						FFT method	*Windows cycle method*	*Individual cycle method*
p5	Male	asleep	2	Abdominal belt	26.5	27	26.8	26.8
P6	Male	asleep	12	Thermistor & transcutaneous Co2	16.5	16.8	16.7	16.8
P7	Male	awake & Oral breathing	10	Abdominal belt	19.75	18.5	19.5	20
P8	Male	awake & Oral breathing	10	Abdominal belt	20.5	21	20.4	20.5
P9	Female	asleep	2	Thermistor Abdominal & Thoracic belts & transcutaneous Co2	15.5	15	15	15
P10	Female	asleep	11	Thermistor Abdominal & Thoracic belts & transcutaneous Co2	15	15	15	15
P II	Female	awake	17	Thermistor	19	18	20	20.6
P12	Male	asleep	5	Abdominal & Thoracic belts	18.	18.6	18.9	19.5
P13	Female	asleep	8	Thoracic belts & transcutaneous Co2	18	18	17.9	18
P14	Male	asleep	7	Thoracic belts	18.75	19	19	19
P15	Male	asleep	0.5	Thermistor & Abdominal & Thoracic belts & transcutaneous Co2	34	38	33	34

TABLE: 7.2 Summary of respiration rate analysis (continue).

Patient No	Gender	State of Patient	kge in years	The most effective contact Methods	Respiration rate in cycles per minute using the selected contact method BR_C	Respiration rate in cycles per minute using thermal imaging methods BR		
						FFT method	*Windows cycle method*	*'ndividual cycle method*
P16	Male	asleep	9	Thermistor & Thoracic belts & Nasal Pressure	15.25	15.6	15.4	15.5
P17	Female	awake	11	Abdominal belts & rranscutaneous Co2	21	22	21	21
P18	Male	awake	15	Abdominal & Thoracic belts	27	26.4	26.7	27
P19	Male	asleep	3	Thoracic belts & Nasal Pressure	23.75	24	24	24
P20	Male	asleep	3	Abdominal & Thoracic belts	21.75	22	22	22
Correlation with conventional methods						0.97	0.92	0.99

A Paired Student's t-test was used to establish whether a significant difference existed between the respiration values obtained using thermal imaging (method 3) and the selected contact methods. The probability value obtained from the test was 0.87, indicating that there was not a significant difference between the two sets of values. Fig.7.16 shows a plot of respiration rate values obtained by using the thermal imaging method against those obtained from the most effective contact respiration rate monitoring method. A close correlation between the thermal imaging and contact based respiration rate measurements is evident.

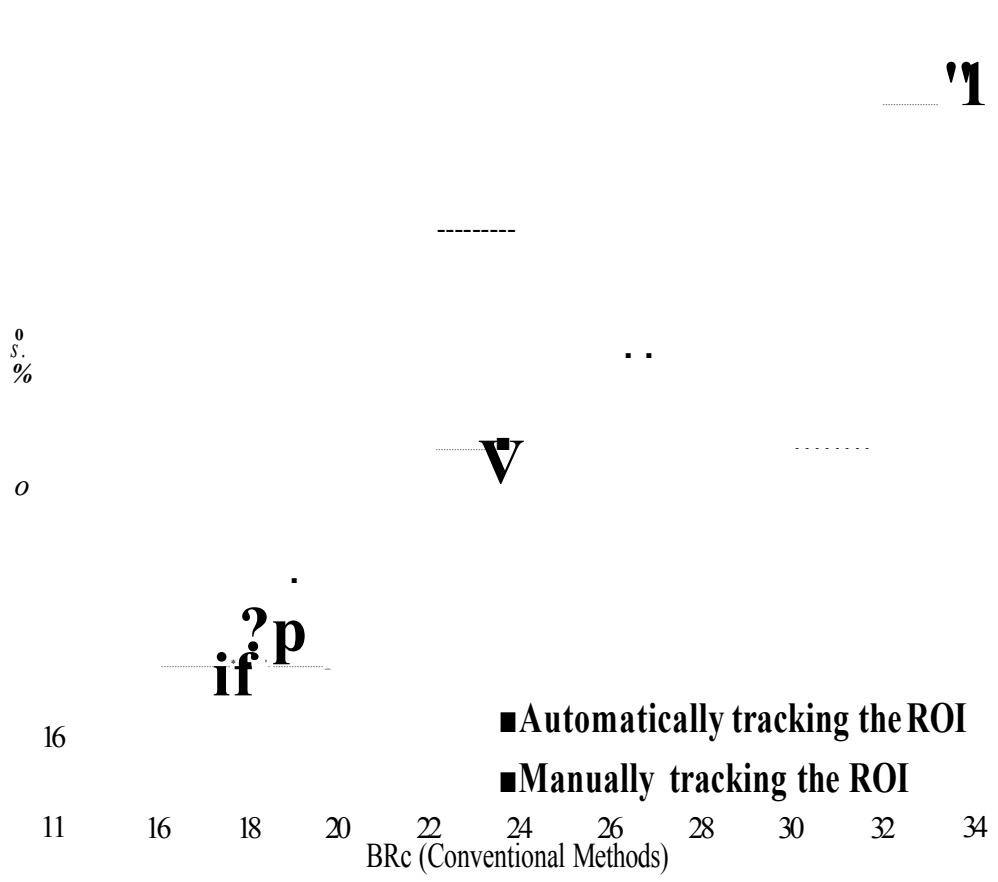

Fig.7.16: A plot of respiration rate values obtained using thermal imaging against values obtained using a convention methods.

73.2. Discussion of Respiration Rate Monitoring Issues

A number of issues were encountered in tracking the ROI in children suffering from respiratory problems. In some thermal image recordings, the child was lying on his/her tummy instead of his back; thus the extraction of the facial boundary became inpossible.

Another complication was respiration via the mouth. Most children who had a respiration problem breathed through their mouth. These issues were dealt with using the method described in Section 7.3.1.2.

The sensors attached to subjects' feces to monitor respiration affected the local skin temperature. For example, the transcutaneous CO_2 sensor, which is placed in a child's ear, causes an increase in skin temperature to more than 39.7°C, which means the local skin temperature is higher than the normal skin temperature of 37°C. Fig.7.17 illustrates the effect on extracted facial features of attaching

sensors to the face. Therefore, the procedure to identify and track the ROI of Sectbn *6.2.23* was developed. This involved using a reduced elliptical area to identify the face and remove the ear regbns. Then the same procedure was applied to identify and track the ROI to extract the respiratbn rate.

Fig.7.17: The effect of the conventional measurement methods on the child's skin temperature.

Another limitation was when the nasal area was blocked by a blanket, toy or the child's hands, as shown in Fig.7.18. In this situation the ROI was not visible. Hence, the respiration signal could not be obtained. In these cases recording started when the ROI became visible.

Fig.7.18: **The child covers the nasal area and oral area with his /her hand.**

Putting a mask on the child's face to provide oxygen obscured the ROI. Glasses worn by some children also hindered the tracking algorithm operatbn. In these

cases the procedure to identify and track the ROI was performed manually as described in Sectbn 7.3.1.2.

In some children the respiratbn signals obtained from the eight segments of the ROI were not in phase. Fig.7.19 illustrates the segmentation of the ROI for a child eight years old. As shown in this figure, the lower part of the ROI represented segments 1, 2, and 3. The upper part represented the other segments of the ROI.

Fig.7.19: Illustrating the segmented parts of the ROI.

Out of phase relationship of the respiratbn signals between the lower and the upper lips is visible in the plots shown in Fig 7.20.

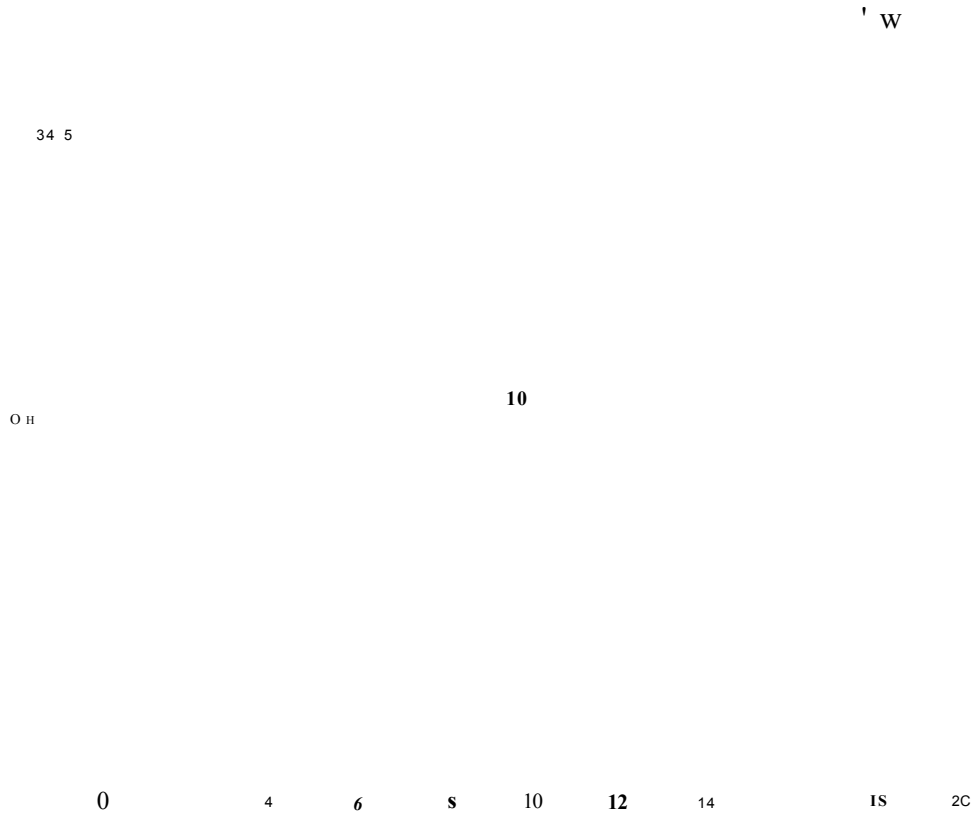

Fig.7.20: **Shows the inverse situation between signals, (a) Illustrates the inverse between S2 and S7. (b) Illustrates the inverse between S3 and S6. (c) Illustrates the inverse between SI and S8. (d) Illustrates the inverse between S2 and S4.**

7.4 Conclusions

In this study a non-contact method to monitor respiration rate was developed and its effectiveness was evaluated by applying it to twenty children. In sixteen children the ROI was tracked automatically while for the remaining four the ROI was tracked manually. A close correlation existed between the respiration rate values obtained using the thermal imaging methods and those obtained using contact methods. The study indicated that thermal imaging is valuable for monitoring breathing as well as for detecting breathing problems such as apnea.

Chapter Eight

8. Conclusions and Future Work

8.1. Introduction

Thermal imaging is a means for non-contact respiration monitoring. Respiration monitoring is important in order to monitor health and to diagnose various medical conditions.

This study provided an investigation into approaches to facilitate respiration monitoring using thermal imaging.

8.2. Conclusions

The methods developed to monitor respiration rate involved identifying the facial ROI most affected by breathing and then determining variations in its skin surface temperature. The ROI was the tip of the nose and the upper lip. The ROI was identified and tracked in thermal images using a number of methods.

Initially a number of thermal video recordings were carried out on healthy adult volunteers from Sheffield Hallam University. These allowed the processing methods to be developed and optimised. The developed method was later applied to thermal videos of twenty children recorded at Sheffield Children's Hospital.

The developed methods allowed the ROI to be automatically identified and tracked in sixteen children. Manual tracking was used for the remaining four children as in these children the ROI was either obscured by medical instruments, the child's sleeping position made it difficult to record the complete facial area, or they breathed via the mouth. The automatic tracking method could not operate well when a child breathed via the mouth. When a child wore glasses, the automatic tracking method did not function correctly as glass appears as the coldest area in a thermal image.

Respiration rate was determined by enhancing the thermal images to reduce their unwanted aspects (noise). This was achieved using suitable LPFs. The effectiveness of the median LPF to remove thermal noise, as well as smoothing the thermal imaging, was investigated. Then the subject boundary was identified from the image background. This was achieved by employing thresholding using Prewitt edge detection. The ROI was identified and tracked in each image. This was achieved by developing tracking algorithms which were based on identifying the physical features of the face.

In order to separate the subject boundary from the face, a procedure was developed that enclosed the face by an ellipse. The area in this ellipse was scanned initially to locate the warmest region. This region corresponded to a small area between the bridge of the nose and the inner corner of the eye. The coolest region beneath the identified warmest areas corresponded to the tip of the nose. A circle was placed around the identified tip of the nose. The circle represented the ROI and was processed to determine respiration rate.

In order to examine the different parts of the ROI for respiration rate monitoring, the ROI was divided into eight equal segments centred on the tip of the nose. The pixel values within each segment of the ROI were averaged for each image. This provided the respiration rate feature. The number of images recorded for each subject was 6000. The respiration feature for each segment of each image was plotted against the time to obtain a respiration signal.

The respiration signals were digitally filtered using a 5th-order Butterworth filter with a cut-off frequency of 1.5 Hz. The filter smoothed the respiration signal, making it ready for determining respiration rate. Respiration rate was automatically calculated by individual cycle method to the clearest respiration signals.

A window cycle method was used to show the variations of respiration against time. This involved determining the average respiration rate within a window containing five successive respiration cycles, and then repeating this calculation by moving the window forward by one cycle. The results indicated that respiration rate varies significantly with time.

The magnitude frequency spectrum of the respiration signals was also produced by using FFT method. The highest peak in the frequency spectrum corresponds to a number of cycles per second. The results indicated that this value is close to the value obtained directly from the respiration signal by determining the number of cycles per second.

Three methods were employed to extract the respiration rate from the respiration signals. These were applied to all the subjects and the results were compared against the values obtained using contact methods for determining respiration rate, using a correlation coefficient. These results indicated that the respiration rate values from the three developed thermal methods closely matched those obtained using contact methods. The third method gave the closest correlation to the contact methods.

The study indicated that thermal imaging is a means for monitoring respiration rates in a non-contact manner. The process requires accurate localisation and tracking of the respiration region of interest. The existing contact methods of monitoring respiration rate are contact-based and thus require a sensing device to be attached to a subject's body, causing them discomfort. These methods only produce a respiration signal. The respiration rate needs to be calculated manually by counting the number of cycles.

Nevertheless, the thermal imaging method used in this study had a number of limitations:

- The processing was off-line due to the extent of processing required. It is advantageous for the respiration rate to be obtained in real time.

- The thermal imager should be operated in a stable indoor environment with a stable operating ambient.

- The current method cannot handle large head movements. When there is a large head movement the region associated with respiration moves very close to the edge of the image. Therefore, the respiration rate is not determined accurately.

8.3. Scope of Future Work

Improvements can focus on further developments of the tracking algorithms, ROI segmentation, and analysing the respiration signal.

- Developing an improved tracking algorithm to handle the images that have failed by using our tracking method and deal with cases when the subject breathes via the mouth is a further development consideration.

- Developing improved image processing techniques to facilitate on-line processing of images and generation of respiration rates is an essential part of future development. The current method produces the respiration rate by processing the images off-line.

- Developing a thermal camera to monitor the respiration rate for children and infants in hospitals. This can be achieved by installing a thermal camera on the flexible stand that is installed in the ceiling above the bed to be able to obtain more accurate video recordings of a child during sleep.

- Currently a sophisticated thermal camera is used for the data recordings. The camera has numerous advanced features that are not needed for respiration monitoring (such as a temperature range that exceeds 1000° Celsius). Replacing the thermal camera with a cheaper, more customised device is a significant advantage.

- The effect of environmental conditions while recording (such as recording room temperature, air circulation effect etc.) on the accuracy of the results should be investigated.

- Twenty children and some adults were enrolled in this study. It would be helpful to validate the methods on a larger number of children and adults.

- More extensive digital signal processing could be performed on the respiration signals to diagnose respiration-related illnesses, such as apnea, pneumonia and asthma.

References:

Adamson T., Crange S., Maloney J., Wilkinson H.M., Wilson E.F., and Yu H.Y. (1981), "***The Maturation of Respiratory Patterns in Normal Full Term Infants during the First Six Postnatal Month: Sleep States and Respiratory Variability***". Australian Journal of Paediatrics and Child Health. No.4, Vol. 17, pp(s):250-256.

Al-Azzawi A. (2007), ***Photonic: principles and practices***, Handbook, ISBN: 0-8493-8290-4, CRC Press Taylor & Francis Group.

Alobasis I.F. (2008), "***Pattern Recognition of thermal Images to monitor breathing***". MSc. Thesis in Computer and Network Engineering, Sheffield Hallam University.

Aoki H., Takemura Y., Mimura K. and Nakajima M. (2001). "***Development of Non-restrictive Sensing System for Sleeping Person Using Fiber Grating Vision Sensor***". Proceedings of 2001 International Symposium on Micromechatronics and Human Science, Nagoya, Japan. pp(s):155 – 160.

Banik S., Rangayyan M. and Boag G. (2009), ***Landmarking and Segmentation of 3D CT Images***. Handbook by Morgan & Claypool publishers.

Bankman N.S. (2000), ***Handbook of Medical Image Processing and Analysis (Biomedical Engineering),*** Academic Press a Harcourt Science and Technology Company, USA.

Bankman N.S. (2009), ***Handbook of Medical Image Processing and Analysis (Biomedical Engineering).*** 2nd Edition, Academic Press a Harcourt Science and Technology Company, USA.

Baxes A.G. (1994), ***Digital Image Processing: Principles and Applications*** Handbook, John Wiley, New York.

Bhuiyan M., Ampornaramveth V., Muto S. and Ueno H. (2001), ***"Face detection and facial feature extraction"***.International Conference. on Computer and Information Technology, No.5, pp (s): 270-274.

Bianchi G. and Sorrentino R. (2007).***Electronic filter simulation & design***. [Online] last accessed on 9th of February 2010. Available at: http://books.google.com/books?id=5S3LCIxnYCcC&pg=PT32&dq=Butterworth-approximation+maximally-flat&lr=&as_brr=3&ei=SiyWSt_yH5jGM5TdidcH#v=onepage&q=Butterworth-approximation%20maximally-flat&f=false .

Blom A J. (2004), ***Monitoring of Respiration and Circulation***, Handbook published by CRC Press LLC, Boca Raton London New York Washington, D.C.

Bovik C.A. (2000), ***Handbook of Image and Video Processing.*** ISBN: 0-12-119790-5.Communications, Networking, and Multimedia. San Diego, CA: Academic Press. A Harcourt Science and Technology Company.

Bovik C.A. (2009), ***The Essential Guide to Image Processing***. Handbook Communications, Networking, and Multimedia. 2nd Edition, Elsevier Inc USA.

Bronzino D.J. (2006), ***The Biomedical Engineering Handbook: Medical Devices and Systems.*** 3rd Edition, Published by CRC Press Taylor & Francis Group.

Brunelli R. and Poggio T. (1993), ***"Face Recognition: Features Versus Templates"***. Pattern Analysis and Machine Intelligence, IEEE Transactions. Vol. 15, No. 10, pp(s):1042 – 1052.

Buddharaju P., Manohar C., Pavlidis I. and Tsiamyrtzis P. (2006), ***Biometrics: Face Recognition in Thermal Infrared***. Handbook, 3rd Edition, Chapter 29, CRC Press.

Burnary S.G., Williams L.T. and Jones H.C. (1988), ***Applications of thermal imaging***, Handbook, ISBN: 9780852744215, Adam Hilger. Institute of Physics Publishing, Taylor & Francis Group.

Butkov N. and lee-Chiong L.T. (2007), ***Fundamentals of Sleep Technology: Endorsed by the American Association of Sleep Technologists.*** [Online] last accessed on 10th July 2009, Available at: http://www.amazon.co.uk/gp/reader/0781792878/ref=sib_rdr_prev2_toc1?ie=UTF8&p=S00B&j=1&ns=1#reader-page .

Cacioppo T.J., Tassinary G.L. and Berntson G.G. (2007), ***Handbook of Psychophysiology.*** 3rd Edition, Published in Cambridge University Press.

Chan S.L. (2008), ***"Development of an ultrasound system to monitor breathing in infants"***. MSc. Thesis, Faculty of Arts Computer, Engineering and Science in Materials and Engineering Research Institute (MERI) of Sheffield Hallam University, UK.

Chekmenev Y. and Rara H. and Farag A. (2006), ***"Non-contact, Wavelet-based Measurement of Vital Signs using Thermal Imaging"***. ICGST International Journal on Graphics, Vision and Image Processing (GVIP). Vol.6, No.2, pp(s):25-30.

Clarke L.P., Velthuizen R.P., Camacho M.A., Heine J.J., Vaidyanathan M., Hall L.O., Thatcher R.W. and Silbiger M.L. (1995), ***"MRI Segmentation: Methods and Applications"***. Magnetic Resonance Imaging, Vol. 13, No. 3, pp(s):343-368.

Corbishley P. and Rodriguez-Villegas (2008), *"Breathing detection: toward a miniaturised, wearable, battery-operated monitoring system"*, IEEE Transactions on Biomedical Engineering, Vol.55, No.1, pp(s):196-204.

Cretikos M., Chen J., Hillman K., Bellomo R. , Finfer S., Flabouris A. (2007). *"The Objective Medical Emergency Team Activation Criteria: a case-control study"*. Resuscitation; Vol.73, No.1, pp(s):62-72.

David C. D. (2009), Medlineplus Medical Encyclopaedia. U.S. National Library of Medicine and National Institutes of Health, last accessed on 2nd January 2010 available [online] at: http://www.nlm.nih.gov/medlineplus/ency/article/002341.htm.

DeCusatis C. (1997). ***Handbook of applied photometry***, ISBN: 1-5639-416-3, Optical Society of America USA and Spring-Verlag New York.

Dhawan P. A., Huang K. H. and Kim S. D. (2008), ***Principles and Advances Methods in Medical Imaging and Analysis.*** Handbook ISBN: 9789812705341, Published by World Scientific Publishing Co. Pte. Ltd.

Downing D. (2003), ***"Algebra the Easy Way "***, 4th Edition, Handbook [online] last accessed on 23rd of October 2010; available at: http://books.google.co.uk/books?id=RiX-TJLiQv0C&pg=PA199&dq=ellipse+equation&hl=en&ei=CSrETJinIZCSOtPkna0M&sa=X&oi=book_result&ct=result&resnum=2&ved=0CDAQ6AEwAQ#v=onepage&q=ellipse%20equation&f=false.

Diakides A. N. and Bronzino D. J. (2008), ***Medical Infrared Imaging,*** Handbook, CRC Press, published by Taylor & Francis Group.

Diakides N., Diakides M., Lupo J. and Paul L. J. (2006), ***Biomedical Engineering Handbook: Biometrics: Advances in Medical Infrared Imaging,*** 3rd Edition, Chapter 19, CRC Press.

Dorf C. R. (2006), ***The Biomedical Engineering Handbook: Medical Devices and Systems.*** Handbook 3rd Edition, published by Taylor & Francis Group, LLC.

Drury A. S. (2001), ***Image interpretation in geology.*** 3rd Edition, published on U.K London in Nelson Thomes Ltd., Last accessed on 2nd of January 2010. Available at: http://books.google.co.uk/books?id=LjptxU-4VjMC&printsec=frontcover&dq=Image+interpretation+in+geology&lr=&cd=1#v=onepage&q=&f=false .

Fei J., Zhu Z. and Pavlidis I. (2005)." ***Imaging Breathing Rate in the CO_2 Absorption Band***". 27th Annual International Conference of the IEEE Engineering in Medicine and Biology - Proceedings 2005, No. 1616510 , Vol. 7 , pp(s):700-705.

Feing K. (2008), "***Infrared Based Quantification OF Breathing Rate*** ". MSC Thesis, Faculty of Arts Computer, Engineering and Science in Materials and Engineering Research Institute (MERI) of Sheffield Hallam University, UK.

Fieselmann J. F., Hendryx M.S., Helms C. M., Wakefield, D.S. (1993), "***Respiratory rate predicts cardiopulmonary arrest for internal medicine patients***". Journal of General Internal Medicine, Vol.8, pp(s).354-360.

Friedman M. (2009) "***Sleep apnea and snoring: surgical and non-surgical therapy***". Handbook 2nd Edition USA . ISBN: 141603112X.

"***FLIR Systems: FLIR Infrared Cameras Help the Search for Swine Flu and other Viral Diseases***" (2009). [Online] last accessed on 8th of November 2009 at: http://www.flir.com/thermography/eurasia/en/content/?id=18420.

Folke M., Cernerud L. , Ekstro¨ M. and Hok B. (2002) , "***Comparative provocation test of respiratory monitoring methods***". Journal of Clinical

Monitoring and Computing. Publisher Springer Netherlands. Vol.17, No.2, pp(s):97-103.

Folke M., Cernerud L., Ekstro¨ M. and Hok B. (2003), " ***Critical review of non-invasive respiratory monitoring in medical care***". Medical and Biological Engineering and Computing, Vol. 41, No.4, pp (s):377-383.

Fonseca L. and Manjunath S. B. (1996), ***"Registration Techniques for Multisensor Remotely Sensed Imagery".*** Photogrammetric Engineering & Remote Sensing, Vol. 62, No. 9, pp(s):1049-1056.

Gabbott p. (2008), ***Principles and Applications of Thermal Analysis***. Published in Wiley-Blackwell Ltd.

Gonzalez C. R. and Wood E. R. (1992), ***Digital Image Processing,*** Addison–Wesley, Reading, MA. Pearson Education, the USA.

Gonzalez C. R. and Wood E. R. (2002), ***Digital Image Processing***, 2nd Edition, ISBN number 0201180758. Addison–Wesley, Reading, MA. Pearson Education, the USA

Gonzalez C. R. and Woods E. R.; Eddins L.S. (2004), ***Digital Image Processing Using MATLAB,*** 1st Edition ,Gatesmark Publishing, Knoxville, TN. USA.

Gonzalez C.R. and Wintz P. (1987), ***Digital Image Processing,*** 2nd Edition, ISBN: 9780201110265 Addison-Wesley USA.

Goshtasby A. (2005), ***2-D and 3-D Image Registration: for Medical, Remote Sensing, and Industrial Applications***, Print ISBN: 9780471649540, A John Wiley & Sons, Inc., Publication.

Grau V., Mewes A., Alcañiz M., Kikinis R., Warfield S. K. (2004)," ***Improved Watershed Transform for Medical Image Segmentation Using***

Prior Information", IEEE Transactions on Medical Imaging, No. 4, Vol. 23, pp(s) 447-458.

Greneker E. F. (1997), "***Radar sensing of Heartbeat and Respiration at a Distance with Applications of the Technology***". Radar, Vol. 97, No. 449, pp(s): 150-154.

Guo G., Li Z. and Chan. K. (2000),"***Face Recognition by Support Vector Machines***". Proceeding Fourth IEEE International Conference on Automatic Face and Gesture Recognition, pp(s). 196-201.

Hajnal J. V., Hill L.G. , Hawkes J. D. (2001), ***Medical Image Registration,*** ISBN: 0-8493-0064-9, CRC Press.

Haralick R. M, Shapiro L. G. (1985), ***Survey: Image segmentation techniques.*** Comp Vision Graph Image Proc.; Issue 1, Vol. 29, pp(s): 100–132.

Harris J. F. (1978), "***On the Use of Windows for Harmonic Analysis with the Discrete Fourier Transform***", Proceeding Of the IEEE, No. 1, Vol. 66, pp(s): 51- 83.

Hashim H., Jailani R. and Nasir M. (2002), "***A Visual Record of Medical Skin Disease Imaging using Matlab tools***", IEEE Student Conference on Research and Development proceeding, Biomedical Engineering-Malaysia. pp(s):40-44.

Head F. J., Wang F., lipari A. C., Elliott L. R. (2000) ," ***The important Role of Infrared Imaging in Breast Cancer***", in Proc. IEEE 2000 engineering in medical and Biology, pp(s) :52–57.

Hjelmas E., Low K. B. (2001),"***Face detection: A survey***". Computer Vision and Image Understanding, Vol. 83, No.3, pp(s): 236-274.

Hoppenbrouwers T., Hodgman J., Harper R., Steman M., (1980), *"Respiration During the First Six Months of Life in Normal Infants: IV. Gender Differences"*. Early human development journal in Ireland, Vol.4, No.2, pp(s) :167-77.

Houdas Y. and Ring E. F. (1982) ***Human Body Temperature — Its Measurement and Regulation.*** Plenum Press, New York.

Hsu C. H. and Chow C. J. (2005)*"Design And Clinic Monitoring of Monitoring Of A newly Developed Non –Attached Infant Apnea Monitor"* . Center for Biomedical Engineering, Taiwan, Province De Chine Vol. 17, No. 3, pp (s) :126-133.

Jahne B. and Haubecker H. (2000), ***Handbook of Computer Vision and Applications. Volume I: Sensors and Imaging. Volume II: Signal processing and Pattern recognition Volume III: Systems and Applications.*** A Guide for Students and Practitionersg , Academic Press. San Diego.

James J., Tiwari L., Upadhyay P., Sreenivas V., Bhambhani V. and Puliyel M J. (2006), " ***Evaluation of pulse-oximetry oxygen saturation taken through skin protective covering***", publisher BioMed Central Ltd. http://www.pubmedcentral.nih.gov/articlerender.fcgi?artid=1523331.

Janssen B. M. and Rechelbacher M. H. (2009) ,*"Pleasure health: Mindful Practices & Sacred Spa Rituals for Self-nurturing"*. Handbook. [Online] last accessed on 25th of October 2010 at: http://books.google.co.uk/books?id=wf90rI0QopUC&pg=PA219&dq=the+optimal+breathing+through+the+nose&hl=en&ei=igjxTNaNE4OWhQfv9eWyBA&sa=X&oi=book_result&ct=result&resnum=3&ved=0CDUQ6AEwAg#v=onepage&q=the%20optimal%20breathing%20through%20the%20nose&f=false .

Jones D. W., (2006),*"Safer Driving in The Dead of Night* ". IEEE Spectrum. [Online] last accessed on 28th of February 2010 at: http://spectrum.ieee.org/maro6/3043.

Kaplan H., (2007), *"Practical Applications of Infrared Thermal Sensing and Imaging Equipment"*.3rd Edition, published by SPIE The Society of Photo – Optical Instrumentation Engineers, USA.

Konno K.; Mead J., (1967), *"Measurement of the separate volume changes of rib cage and abdomen during breathing*", Jappl Physiol , No.3, Vol. 22, pp (s): 407–422. Publication by Am Physiological Soc.

Konica Minolta Sensing Americas, Inc. (2006), *"Basic understanding of the pulse oximeter"*.

Kruse W. P. and Skatrude D. D. (1997), ***Uncooled Infrared Imaging: Arrays and Systems, Semiconductors and Semimetals***. Handbook, Academic Press USA.

Larsson C. and Staun P. (1999): *"Evaluation of a new fibre-optic monitor for respiratory rate monitoring* ".Journal of Clinical Monitoring and Computing, Vol. 15, No. 5 , pp(s) :295-298.

Lausted C. G. and Jonston A. T.(2006), ***Respiratory system***. Chapter Seven, In: Bronzino J.D., Editor. ***Biomedical engineering fundamentals.*** Handbook 3rd Edition, CRC Press.

Lee-Chiong L. T. (2006), ***Sleep: a comprehensive handbook,*** publication Wiley.

Levi H. (2007), *"Thermal Imaging Survey Specialists"*, [online] Last accessed on 19th of September 2009 at: http://www.hortonlevi.co.uk/welcome/default.htm.

Linh D. T., Linh Q.H. (2003), *"Medical Image Registration in Matlab* ", the Department of Biomedical Engineering- Faculty of Applied Science HCMC University of Technology, Vietnam. Vol. 7, No. (8). pp(s): 1224-1229.

Madisetti K. V., Madisetti V., Williams B. D. (1999), ***Digital Signal Processing Handbook: Crcnetbase 1999.*** Published by CRC Press LLC.

Mazzanti, B., Lamberti, C. and de Bie, J. (2003), "***Validation of an ECG-drived respiration monitoring method***", Computers in Cardiology, Vol.30, pp(s) :613-616.

McAndrew M. A. (2004), ***An Introduction to Digital Image Processing With Matlab,*** School of Computer Science and Mathematics Victoria University of Technology Boston, MA, United States.

Mehtre B. M. (1993), "***Fingerprint image analysis for automatic identification***". Machine Vision and Applications Vol. 6, No. 2, pp(s):124–139.

"***Medical Thermal Imaging*** ". [Online] last accessed on 14th of September 2009 at: http://www.medicalti.com/4.html.

Merchant J. and Manager S. (2009), "***Infrared Temperature Measurement Theory and Application".*** Mikron Instrument Company Inc. [Online], last accessed on 2nd of December 2009 at www.omega.com/techref/iredtempmeasur.html .

Moody G., Mark R., Bump M., Weinstein J., Berman A., Mietus J. and Goldberger, A. (1986), "***Clinical validation of ECG-derived respiration (EDR) technique***" ,Computers in Cardiology, Vol.13, pp(s) :507- 510.

Morley J. C., Thornton J. A., Fowler A. M., Cole J. T. and Hewson H. P. (1990), "***Respiratory rate and severity of illness in babies under 6 months old***". Department of Paediatrics, University of Cambridge., August; Vol. 65, No. 8, pp(s):834–837.

Mollmann K., Karstadt D. , Pinno F., Vollmer M. (2006),"***Thermal image quality –Visualization of spatial and thermal resolution in thermal imaging***". Vol. 7, pp(s): 79 – 91.

Murthy R., Pavlidis I. and Tsiamyrtzis P. (2004), "***Touchless monitoring of breathing function***". Engineering in Medicine and Biology Society, 2004. IEMBS apos; 04. 26th Annual International Conference of the IEEE. Vol.2, No.1, pp(s):1196 – 1199.

Murthy R., Pavlidis I.(2006), "***Non-Contact Monitoring of Breathing Function Using Infrared Image",*** in Proc. IEEE 2006 Engineering in Medicine and Biology Magazine, Vol. 25, No. 3, pp (s) :57-67.

Nakai H., Komukai T., Saiwai-ku K. (2000), "***Non-restrictive Visual Respiration Monitoring***". Pattern Recognition, IEEE 2000. Proceedings. 15th International Conference on in Barcelona, Spain Vol. 4, pp(s): 647-651.

NASA official: Sharon sample, (2007), " ***The Electromagnetic Spectrum: The_infrared***". [Online] last accessed on 5th of March 2009 at: http://science.hq.nasa.gov/kids/imagers/ems/index.html.

Nakajima K., Matsumoto Y. and Tamura T. (2001), "***Development of real time image sequence analysis for evaluating posture change and respiratory rate of a subject in bed***", Physiological Measurement, Vol.22, No.3, pp(s).21-28.

Nam H. , Yim G. , Ryu Y. , Shin C. , Kang J. , Kim S. (2005), "***The Preliminary Study of Unobtrusive respiratory monitoring for e-health***" . Proceedings of the 2005 IEEE Engineering in Medicine and Biology 27th Annual Conference Shanghai, China, Vol.4, pp(s): 3796 -3798.

Nepal K., Biegeleisen E. and Ning T. (2002), "***Apnea Detection and Respiration rate Estimation through Parametric Modeling***", Proceedings of

the 28th IEEE Annual Northeast Bioengineering Conference, Philadelphia, Pennsylvania. pp(s) 277-278.

Ng E. Y. and Sudharsan N. M. (2000), "***Can numerical simulation adjunct to thermography be an early detection tool***". Journal of Thermology International No. 10: pp(s): 119–127.

Ng E.Y. and Sudharsan N.M. (2001), "***Numerical computation as a tool to aid thermographic interpretation***". Journal of Medical Engineering and Technology, No.2, Vol.25 pp(s):53-60.

Nixon S. M. and Aguado S. A. (2002), ***Feature Extraction and Image Processing.*** Handbook 1st Edition, Academic Press is an imprint of Elsevier.

Nixon S. M. And Aguado S. A., (2008). ***Feature Extraction and Image Processing.*** Handbook, 2nd Edition, ISBN: 07506 5078 8, Academic Press is an imprint of Elsevier,

Ochi S., Lizuk T. ,Sato Y. , Hamasaki M., Narabu T., Kato K., Kagawa Y. , (1997),"***signal processing***".[Online]Last accessed on 10th July 2008 , Available from at : http://books.google.com.my/books .

Otsuka K., Okada S., Hassan M., Togawa T. (2002). "***Imaging of skin thermal properties with estimation of ambient radiation Temperature***". *IEEE Engineering in Medicine and Biology.* No. 6, Vol. 21, pp(s):49-55.

Pai P., Mishra B., Tejasvi T. and Bhat D. (2009), "***A Prototype for Non-Intrusive Respiratory Monitoring and Apnea Detection***". The ICEDSP International Conference on Electronic Design and Signal processing n India.

Park S., Noh Y., Parks. and Yoon H. (2008), "***An improved algorithm for respiration signal extraction from electrocardiogram measured by Conductive Textile Electrodes Using Instantaneous Frequency***

Estimation". Medical & Biological Engineering & Computing, Vol.46, No.2, pp (s): 147-158.

Pandya S. (2009), "***Thermal image diagnostics*** ". [Online] last accessed on 5th of March 2009 at: http://serc-plasma09.pssi.in/documents/DT-20_IR_imaging.pdf , DST-SERC School on Plasma Diagnostics.

Pavlidis I., Levine J., Bukol P. (2000), "***Thermal Imaging for Anxiety Detection***" Proceeding . IEEE 2000 workshop on computer vision beyond the visible spectrum : Methods and Applications, publisher on IEEE Computer Society Washington, DC, USA , pp(s) 104–109.

Penzel T., McNames J., deChazal P. , Raymond B., Murray A. ,Moody G., (2002), "***Systematic Comparison of Different Algorithms for Apnoea Detection Based on Electrocardiogram Recordings***". Medical & Biological Engineering & Computing, Vol. 40.

"***Physics of Electro-optic Detector***", (1998). [Online] last accessed on 14th of November 2009, available at: http://www.everettinfrared.com/detectors.htm.

Pratt K. W.(2007), ***Digital Image Processing*** . Handbook 4th Edition, A Wiley-Interscience publication in Canada.

Richard F. and Cohen L. (2003), "***A New Image Registration Technique with Free Boundary Constraints: Application to Mammography***". Computer Vision and Image Understanding, Elsevier Science (USA). Vol. 89, pp(s) 166-196.

Richmond C. J., DeWitt P. D. (1985), ***Applications of radiation thermometry: a symposium.*** American Society for Testing and Materials. [Online] last accessed on 7th of December 2009 at: http://books.google.co.uk/books?id=h9DV8MEM630C&pg=PA86&dq=advantage+of+thermal+imaging+measurement&cd=2#v=onepage&q=&f=false.

Rowley H., Baluja V., Kanade T. (1998), *"Neural Network-based face detection"*. IEEE: Pattern Recognition, and Machine intelligence Proceedings. Vol. 20, No. 1, pp(s): 23-38.

Ruiz R. (2008), *"Sensor Design for Range Measurement"*, Thesis, Microsystems and Machine Vision Laboratory (MMVL) research group in Materials and Engineering Research Institute (MERI) of Sheffield Hallam University, UK.

Russ C. J. (2007). ***The Image Processing Handbook.*** 5th Edition, CRC Press Taylor & Francis Group.

Sadeh A. , Acebo C., Seifer R., Aytur S. and Carskadon M.A. (1995)," ***Carskadon Activity-Based Assessment of Sleep-Wake Patterns During the 1st Year of Life"*** .Infant Behavior and Development, Publisher: Elsevier, Vol. 18, No. 3, pp(s): 329-337.

Sato I. and Nakajima M. (2005),*"Non-contact Breath Motion Monitoring System in Full Automation"*. Proceedings of the 2005 IEEE Engineering in Medicine and Biology 27th Annual Conference, Shanghai, China, pp(s):3448-3451.

Scribner D., Warren P. and Schuler J. (2000), *"Extending Color Vision Methods to Bands Beyond the Visible"*. Machine Vision and Applications, Publisher Springer Berlin / Heidelberg. No. 6, Vol. 11, pp(s): 306-312.

Semmes B. J., Tobin M. J., Snyder V., and Grenvik A. (1985), *"Subjective and Objective measurement of Tidal Volume in Critically Ill Patients."* Vol.78, pp (s): 577–579.

Semmlow L. J. (2004), ***Biosignal and Biomedical Image Processing: MATLAB –Based Applications***. Handbook Printed in the United States of America.

Sheskin D. (2004), ***Handbook of Parametric and Nonparametric Statistical Procedures.*** 3rd Edition, by Chapman &Hail /CRC Press.

Shiavi R. (2007), ***Introduction to Applied Statistical Signal Analysis: Guide to Biomedical and Electrical Engineering Applications.*** Academic Press in Elsevier USA.

Shneerson M. J.(2005) , ***Sleep Medicine: A Guide to Sleep and its Disorders,*** Handbook 2nd Edition, Published by Blackwell Publishing Ltd UK.

"Sleep apnea"(1995), Department of Health and Human Services, National Heart, Lung, and Blood Institute. [Online] last accessed on 25th of February 2010, Available at: http://www.nlm.nih.gov/.

Smith O. J.(2008), ***Mathematics of the Discrete Fourier Transform (DFT) With Audio Applications***, 2nd Edition, Center for Computer Research in Music and Acoustics (CCRMA) USA.[Online], Last accessed on 2nd of January 2010. Available at: https://ccrma.stanford.edu/~jos/dft.

Smith W. S. (2003), ***Digital signal processing: a practical guide for engineers and scientists.*** ISBN 075067444X, Academic Press in Elsevier USA.

Sonka M., Hlavac V. , and Boyle R. (1993), ***Image processing, analysis, and machine vision. ,*** Handbook 1st Edition, Chapman & Hall computing series, Chapman and Hall computing series.

Storck K., Karlsson M., Ask P. and Loyed D. (1996), ***"Heat transfer evaluation of the nasal thermistor technique"***, IEEE Transactions on Biomedical Engineering, Vol.43, No.12, and pp(s): 1187-1191.

Stranneby D. and Walker W. (2004)," ***Digital Signal Processing and Applications***". Handbook, Amsterdam; London. 2nd Edition. ISBN:0750663448, Elsevier.

Subbe C.P., Davies R.G., Williams E., Rutherford P. and Gemmell L. (2003), *"Effect of introducing the Modified Early Warning score on clinical outcomes, cardiopulmonary arrests and intensive care utilisation in acute medical admissions"*. Anaesthesia; Vol.58 No.22, pp(s:)1314-1316.

Tarassenko L., Mason L. and Townsend N., (2002), *"Multi-sensor fusion for robust computation of breathing rate"*. IEEE Society, Vol.38, No.22, pp(s): 1314-1316.

Tan K., Saatchi R., Elphick H. and Burke D. (2010). *"Real-time vision based respiration monitoring system"*. Submitted to IEEE, IET International Symposium on Communication Systems, Networks and Digital Signal Processing, 21-23rd of July 2010, Northumbria University, United Kingdom.

Technical information SD-12 Characteristics and use of infrared detectors (2004), Hamamatsu Japan. [Online] last accessed on 2nd of December 2009 at: http://sales.hamamatsu.com/assets/applications/SSD/Characteristics_and_use_of_infrared_detectors.pdf.

"Temperature"(2009).Integrated publishing: Fire Controlman. [Online] last accessed on 9th of November 2009 at: http://www.tpub.com/content/fc/14104/css/14104_48.htm.

The Pennsylvania Child Walfare Training Program, [online] last accessed on 10th of October 2009. Available at: http://www.pacwcbt.pitt.edu/Curriculum/.

"Thermal imaging"(2009). [Online], last accessed on 5th of November 2009 at: http://www.tpub.com/content/aviation/14030.

"ThermoVision™ A40 M: operator's manual", (2004) Manual, FLIR Systems, Pub No. 1557813, Rev A72, Issued October 29, 2004.

"ThermoVision™ Researcher: Professional Edition. Version 2.9", (2007) Manual, FLIR Systems, Pub No. T559009, Rev A249, Issued November 1, 2007.

Tian Y. and Bolle M.R. (2008) ***"Automatic Detection Neutral Face for Face Authentication and Facial Expression Analysis"***. Exploratory Computer Vision Group, In AAAI-03 Spring Symposium on Intelligent Multimedia Knowledge Management. [Online] last accessed on 2nd of April 2008 at: http://www.research.ibm.com/peoplevision/Neutralface.pdf.

Tobin M. J. (1988), ***"Respiratory Monitoring in the Intensive Care Unit"***. Division of Pulmonary and Critical Care Medicine, Mayo Clinic, Rochester, Minnesota 55905, USA. Vol. 6, No. 138, pp(s):1625–1642.

Travaglini A., Lamberti C., DeBie J. and Ferri M.(1998). ***"Respiratory of signal derived from eight-lead ECG"***. IEEE Proceedings of Computers in Cardiology Vol. 25, No. 2: pp(s): 65-68. 1998.

Tsiamyrtzis P., Dowdall J., Shastri D., Pavlidis I., Frank M. and Ekman P. (2005), ***"Lie detection—Recovery of the Periorbital Signal through Tandem Tracking and Noise Suppression in Thermal Facial Video"***. The 22nd Annual Houston Conference on Biomedical Engineering Research, Houston, TX, Vol. 5778, pp(s): 213-225.

Turk M. and Pentland, A. (1991), ***"Eigenfaces for recognition"***. Journal of cognitive neuroscience, Vol. 3, No.1, pp(s):71-86.

Turkan M., Dulek B., Omaran I. and Cetin E. (2006), ***"Human Face Detection in Video Using Edge Projections"***, in Proceeding of the SPIE –the international society for optical Engineering: Visual Information Processing XV, Vol. 6246, No.1.

"Understanding Infrared Camera Thermal Image Quality" (2008) published by Electrophysics Resource Center: Infrared Imaging, [online], last

accessed on 5th of November 2009 at:
http://www.articlesbase.com/electronics-articles/understanding-infrared-camera-thermal-image-quality-670826.html.

Wang W. C., Ahmed A. and Hunter A. (2006), "***Vision Analysis in Detecting Abnormal Breathing Activity in Application to Diagnosis of Obstructive Sleep Apnoea***", Proceedings of the 28th IEEE EMBS Annual International Conference. Institute of Electrical and Electronics Engineers, Inc, New York, USA, pp(s): 4469-4473.

Wel C. C. (2008), "***Development of Stereo Vision Based Respiration Rate Measuring System***". MSc. Thesis in Computer and Network Engineering, Faculty of Arts, Computing, Engineering and Sciences, Sheffield Hallam University.

Werthammer J., Krasner J., DiBenedetto J. and Stark R. A.(1983), "***Apnea Monitoring by Acoustic Detection of Airflow***", Pediatrics , No.1,.Vol.71, pp(s):53-55.

Weszka J. S. (1978), "***A survey of threshold selection techniques, Computer Graphics and Images***". Proc. Computer Graphics and Image Processing No. 2, Vol. 7, pp(s): 259-265.

Williams L. T. (2009). ***Thermal imaging Cameras: Characteristics and Performance***. CRC Press Taylor & Francis Group an information business, USA.

Wong W. K., Lam M. K. and Siu C. W.(2001),"***An Efficient Algorithm for Human Face Detection and Facial Feature Extraction under Different Condition.***", Pattern Recognition, Department of Electrical and information, the Hong Kong University. Pattern Recognition, Vol. 34, No. 10, pp(s): 1993-2004.

Ye A. and Yuji M. (1997), "***Respiration Rate Measuring Apparatus***", US Assignee: Colin Corporation No. 423448 filed. Last accessed on 7th of august 2009 [online] available at: http://www.patentstorm.us/patents/5682898/fulltext.html.

Zaitova B. and Flusser J. (2003), "***Image Registration methods: a Survey***". Image and Vision Computing, Vol. 21, No. 11, pp(s):977-1000.

Zhao Y., Zhao J., and Li O. (2008),"***Derivation of Respiratory Signals from Single-Lead ECG***". ISBN: 978-0-7695-3561-6, International Seminar on Future BioMedical Information Engineering, pp(s):15-18.

Zhu Z., Fei J. and Pavlidis I. (2005), "***Tracking Human Breath in Infrared Imaging***". Proceeding of the 5th IEEE, Symposium on Bioinformatics and Bioengineering (BIBE'05). Organization IEEE Computer Society Washington, DC, USA, Vol. 19, Issue. 21, pp(s): 227—231.